

**WCAP-16996-P, “Realistic LOCA Evaluation Methodology Applied to the Full Spectrum of Break Sizes  
(FULL SPECTRUM LOCA Methodology)”  
Request for Additional Information – (Non-Proprietary)  
RAIs 36-39**

**March 2014**

Westinghouse Electric Company LLC  
1000 Westinghouse Drive  
Cranberry Township, PA 16066

©2014 Westinghouse Electric Company LLC  
All Rights Reserved

## 1 Background

This document provides an overview of the responses to Requests for Additional Information (RAIs) 36-39 [1] on the **FULL SPECTRUM™** LOCA (**FSLOCA™**) Methodology [2] and the updates to the **FSLOCA** methodology related to fuel pellet thermal conductivity degradation (TCD) [

]<sup>a,c</sup> Along with this overview, the following materials are also provided:

- Responses to RAIs 36-39
- Updates to Sections 2, 8, 11, 25, 26, 29, 30, and 32 of the **FSLOCA** topical report

In RAIs 36-39 [1], further information was requested regarding:

- RAI 36: the modeling of fuel TCD in WCOBRA/TRAC-TF2 (WCT-TF2),
- RAI 37: the effects of TCD on initial stored energy and the modeling of fuel rod burnup,
- RAI 38: the treatment of fuel rod related parameters that are burnup dependent, and
- RAI 39: the fuel burnup sampling approach in the **FSLOCA** methodology.

[

]<sup>a,c</sup>

Westinghouse has recently submitted the PAD5 fuel rod design methodology [4] that includes explicit treatment of fuel TCD. In conjunction with responding to RAIs 36-39, [

]<sup>a,c</sup>

The following sections provide a high level summary of the updates made to the **FSLOCA** methodology in each of these categories. The final section provides a summary of the updates made in each of the **FSLOCA** topical sections.

Throughout this overview, items in (*italics*) refer to further detail provided in the attached RAI responses and updated **FSLOCA** topical sections.

*ZIRLO is a registered trademark and Optimized ZIRLO, FULL SPECTRUM and FSLOCA are trademarks of Westinghouse Electric Company LLC, its affiliates and/or its subsidiaries in the United States of America and may be registered in other countries throughout the world. All rights reserved. Unauthorized use is strictly prohibited. Other names may be trademarks of their respective owners.*

2 [ ]<sup>a,c</sup>

The Modified Nuclear Fuels Industries (NFI) fuel thermal conductivity model, as included in FRAPCON 3.3 [5], includes explicit treatment of fuel TCD. The FSLOCA methodology has been updated to use the Modified NFI model in all analyses with nuclear fuel, including plant analyses. PAD5 calculations are used in initializing WCT-TF2 fuel rods in plant analyses; PAD5 also explicitly accounts for TCD and includes detailed fuel rod models important for predicting initial fuel pellet temperatures and rod internal pressures over the life of the fuel. [

]<sup>a,c</sup> (Section 11.4, RAI

36, RAI 37)

The consideration of fuel TCD [

]<sup>a,c</sup>

3 [ ]<sup>a,c</sup>

[

] <sup>a,c</sup> The calculation of MLO includes both pre-accident corrosion and the oxidation occurring during the LOCA, consistent with NRC Information Notice 98-29 [7]. [

] <sup>a,c</sup> The NRC has initiated the formal process to revise 10 CFR 50.46, and it is anticipated that the MLO criterion will be replaced with an Equivalent Cladding Reacted (ECR) limit based on cladding hydrogen content (along with other considerations). A submittal (Appendix A) will be provided at a later date that describes how the **FSLOCA** evaluation model (EM) will comply with the known elements of the 10 CFR 50.46c rulemaking when the rulemaking process is complete. (*RAIs 38 and 39, Sections 29.4, 30.1, and 32*)

[

] <sup>a,c</sup>

4 [

] <sup>a,c</sup>

Because [

] <sup>a,c</sup>

[

] <sup>a,c</sup>

## 5 Summary

The updates to the **FSLOCA** methodology to explicitly consider TCD have prompted a set of closely related updates and improvements. The updates to the **FSLOCA** topical sections included in this response package are as follows:

Section 2: (Section 2.3.2.1)

- Updates to [

] <sup>a,c</sup>

Section 8: (Sections 8.4, 8.4.1, and 8.6)

- Updates related to [

] <sup>a,c</sup>

Section 11: (Section 11.4)

- Update to identify the use of the Modified NFI fuel thermal conductivity model.

Section 25: (Introduction, Sections 25.1, 25.2, 25.8)

- Updates related to [

] <sup>a,c</sup>

Section 26: (Sections 26.4, 26.5)

- Updates for [

] <sup>a,c</sup>

Section 29: (Introduction, Sections 29.4.1, 29.4.2, 29.5.1, and 29.7)

- Updates for [

] <sup>a,c</sup>

[

] <sup>a,c</sup>Section 30: (Sections 30.1, 30.4, 30.5, 30.6, and 30.7)

- Updates to identify that MLO is calculated as the sum of pre-accident oxidation and the oxidation occurring during the LOCA.
- Updates to [

] <sup>a,c</sup>Section 32: (Sections 32.1, 32.2, and 32.4)

- Updates to identify that MLO is the sum of pre-accident oxidation and the oxidation occurring during the LOCA.

**References:**

1. Letter from E. Lenning to J. Gresham, "Request for Additional Information Re: Westinghouse Electric Company Topical Report WCAP-16996-P Volumes I, II, and III, Revision 0/WCAP-16996-NP, Volumes I, II, and III, Revision 0, 'Realistic LOCA Evaluation Methodology Applied to the Full Spectrum of Break Sizes (FULL SPECTRUM™ LOCA Methodology),' – FOURTH SET (TAC No. ME5244)," August 15, 2012.
2. WCAP-16996-P (Proprietary), WCAP-16996-NP (Non-Proprietary), "Realistic LOCA Evaluation Methodology Applied to the Full Spectrum of Break Sizes (FULL SPECTRUM LOCA Methodology)," November 2010.
3. WCAP-15063-P, Revision 1 (Proprietary), WCAP-15064-NP, Revision 1 (Non-Proprietary), "Westinghouse Improved Performance Analysis and Design Model (PAD 4.0)," 1999.
4. WCAP-17642-P (Proprietary), WCAP-17642-NP (Non-Proprietary), "Westinghouse Performance Analysis and Design Model (PAD5)," 2013.
5. NUREG/CR-6534, Volume 4, "FRAPCON-3 Updates, Including Mixed-Oxide Fuel Properties," Pacific Northwest National Laboratory, 2005.
6. LTR-NRC-13-37, "Submittal of Westinghouse Responses to "WCAP-16996-P, 'Realistic LOCA Evaluation Methodology Applied to the Full Spectrum of Break Sizes (FULL SPECTRUM LOCA Methodology)' Request for Additional Information" (Proprietary/Non-Proprietary), Project 700, TAC No. ME5244." June 5, 2013.
7. Roe, J., "NRC Information Notice 98-29: Predicted Increase in Fuel Rod Cladding Oxidation," August 3, 1998.

**Question #36: Fuel Thermal Conductivity Model**

WCAP-16996-P/WCAP-16996-NP, Volumes I, II and III, Revision 0, Section 11.4, "Thermal Properties of Nuclear Fuel Rod Materials," explains that the COBRA/TRAC-TF2 default nuclear fuel rod model computes the  $UO_2$  thermal conductivity from a MATPRO-9 correlation to reduce computer time. It is also explained that this correlation has the same error band of 0.2 W/(m-K) and gives very nearly the same conductivity over the expected operating range of 500 K to 3,000 K when compared to the more complex version in MATPRO-11. Section 11.4 also states that an additional optional model is also provided in WCOBRA/TRAC-TF2 to account for the effects of burnup on thermal conductivity. The model, referred to as "the modified Nuclear Fuel Industries (NFI) model," is described as based on the Nuclear Fuels Industries (NFI) model by Ohira and Itagaki, on pages 541-549 of "Thermal Conductivity Measurements of High Burnup  $UO_2$  Pellet and a Benchmark Calculation of Fuel Center Temperature," in Proceedings of the ANS international topical meeting on LWR Fuel Performance, Portland, Oregon, March 2-6, 1997. Section 11.4 also provides the range of applicability of the modified NFI correlation with regard to temperature, rod-average burnup and as-fabricated density in accordance with NUREG/CR-6534, "FRAPCON-3 Updates, Including Mixed-Oxide Fuel Properties," Vol. 4, 2005.

Please clarify the following items related to the default nuclear fuel rod model in WCOBRA/TRAC-TF2 and the modeling approach to account for the effects of burnup on fuel thermal conductivity in LOCA analyses.

- (1) The default thermal conductivity model in WCOBRA/TRAC-TF2, based on a MATPRO-9 correlation, does not explicitly account for fuel thermal conductivity degradation with burnup. Please describe the purpose of this model and state the conditions under which its application in LOCA analyses is considered acceptable and justify so. If overestimation of thermal conductivity can be associated with the application of the model for such analyses, are there any other code adjustments in WCOBRA/TRAC-TF2 to compensate for this limitation.
- (2) The additional optional model implemented in WCOBRA/TRAC-TF2 to account for the effects of burnup on thermal conductivity is based on a modification of the NFI correlation, which agrees with Equation (2.3-9) in NUREG/CR-7024, "Material Property Correlations: Comparisons between FRAPCON-3.4, FRAPTRAN 1.4, and MATPRO," March 2011. Such a burnup dependant model was not available in the previous ASTRUM LBLOCA methodology documented in WCAP-16009-P-A (Nissley, M. E., et al., 2005). Please describe the conditions under which this "additional optional model" is considered applicable in FSLOCA LOCA analyses and provide justification.
- (3) Please explain how the WCOBRA/TRAC-TF2 nuclear fuel rod model was evaluated for predicting degradation of fuel thermal conductivity with burnup. Describe how contributions from other processes and models such as gap conductance, fission gas release, and radial power profile were taken into consideration in the evaluation. Present analysis results, if available, and provide references to existing assessments that demonstrate the applicability of the model for the purposes of the FSLOCA methodology applications. Include findings from benchmarking against measured data, if available.

- (4) The current Westinghouse fuel rod design methodology (approved by NRC in July 2000) is based on the Performance Analysis and Design (PAD) 4.0 fuel performance code, “Westinghouse Improved Performance Analysis and Design Model (PAD 4.0),” WCAP-15063-P-A/WCAP-15064-NP-A, Revision 1. The PAD 4.0 code has a thermal conductivity model with no burnup dependence. Please explain if specialized fuel performance codes were used in support of the evaluation of the WCOBRA/TRAC-TF2 nuclear fuel rod model for predicting fuel thermal conductivity degradation with burnup. If this was the case, please present the assessment results and include comparison of prediction results for fuel temperatures and rod internal pressures obtained by the codes using the same input conditions. Provide references to the available assessment documentation.

**Response:**

In conjunction with the response to RAIs 36-39, the aspects of Section 11 and 29 of the FSLOCA Topical report [1] related to fuel rod burnup and pellet thermal conductivity have been updated. Along with those updates, the response to RAI 36 describes the updated fuel thermal conductivity treatment. When referring to the contents of Sections 11 and 29, this response is referring to the updated section.

Response to Parts (1) and (2) of the RAI

The revised Section 11.4.1 of WCAP-16996-P describes a version of the Nuclear Fuels Industries (NFI) thermal conductivity model as modified in FRAPCON 3.3 [2], which explicitly accounts for thermal conductivity degradation (TCD) with burnup. This modified NFI model will be used in FSLOCA plant analyses and in the simulation of validation tests (e.g. LOFT) involving UO<sub>2</sub> fuel pellets.

The MATPRO-9 correlation described in the original Section 11.4.1 of WCAP-16996-P is no longer included in the FSLOCA analysis methodology.

Response to Part (3) of the RAI

As stated in the revised Section 11.4.1, the modified NFI fuel thermal conductivity model is applicable over the following range of conditions (see also Section 2.4 of [2]):

Temperature	=	300 – 3000K
Rod-Average Burnup	=	0 – 62 GWD/MTU
As-fabricated Density	=	92 – 97% Theoretical Density

The above conditions cover the range expected for the FSLOCA EM.

The updated Figure 11-29 of WCAP-16996-P, taken from Figure 2.4 of [2], shows that the thermal conductivity model compares well to unirradiated pellet material data. Section 2.3 of [2] also shows that the model is adequate for predicting the conductivity of irradiated material.

Westinghouse has recently developed, and submitted to the USNRC, an updated version of the PAD fuel performance code, PAD5 [3]. The updated fuel performance code is designed to supersede PAD 4.0 and

FATES3B. Among other features, PAD5 includes an explicit treatment of burnup-related phenomena such as fuel TCD.

The final, approved version of PAD5 will be the fuel performance interface to the FSLOCA EM. As described in Section 4.3 of [3], the PAD5 code includes models for accurate prediction of fission gas release. Section 3.6.2 of [3] describes the PAD5 pellet radial power distribution model. [

] <sup>a,c</sup>

Figure RAI36-1 shows a comparison of the modified NFI conductivity model used in WCOBRA/TRAC-TF2 (WCT-TF2) and the model in PAD5 [3]. [

] <sup>a,c</sup>

As described in Section 11.4.4 of [1], the gas conductance is calculated based on the individual species' mole fractions and their respective thermal conductivity correlations. The thermal conductivity correlations for the fill and fission gases, taken from MATPRO-11 Rev.1 and shown in Section 11.4.4 of [1], [

] <sup>a,c</sup>

In WCT-TF2, a temperature jump distance is used in Equation 8-29 of [1] to compensate for the nonlinearity of the temperature gradient near the walls and the temperature discontinuities on the wall surface that result from incomplete thermal mixing of the gas molecules near the surface. Similarly, considerations are made in the PAD5 code as described in Sections 3.5.2 and 3.5.3 of [3], although this effect is neglected for all gases except Helium.

The pellet-cladding contact conductance model is described in Section 8.3.2 of [1], and was chosen based on its agreement with a wide range of contact conductance data. [

] <sup>a,c</sup>

Response to Part (4) of the RAI

[

] <sup>a,c</sup> The thermal conductivity model for the pellet in WCT-TF2 relies on an industry-accepted correlation that has been benchmarked to test data and has been found to be applicable over the range of conditions expected in the FSLOCA EM in [2]. Similarly, [

] <sup>a,c</sup>**References:**

1. WCAP-16996-P, "Realistic LOCA Evaluation Methodology Applied to the Full Spectrum of Break Sizes (FULL SPECTRUM LOCA Methodology)," November 2010.
2. NUREG/CR-6534, Volume 4, "FRAPCON-3 Updates, Including Mixed-Oxide Fuel Properties," Pacific Northwest national Laboratory, 2005.
3. WCAP-17642-P (Proprietary), WCAP-17642-NP (Non-Proprietary), "Westinghouse Performance Analysis and Design Model (PAD5)," 2013.
4. NUREG/CR-1845, "FRAPCON-2: A Computer Code for the Calculation of Steady State Thermal-Mechanical Behavior of Oxide Fuel Rods," January, 1981.

a,c

**Figure RAI36-1**

**Comparison of WCOBRA/TRAC-TF2 and PAD5 UO<sub>2</sub> Pellet Thermal Conductivity Models**

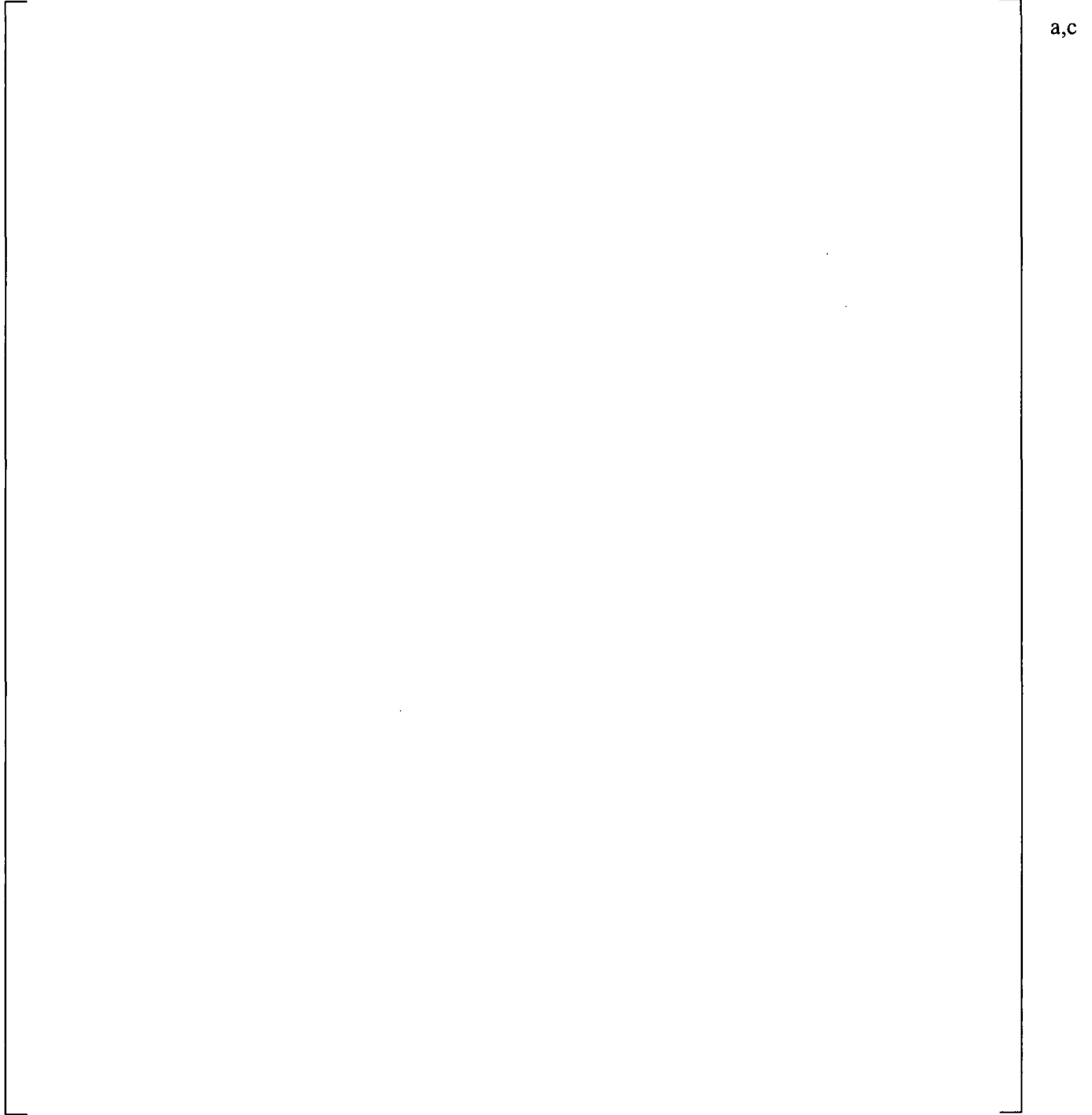


**Figure RAI36-2**

[

]a,c

**Question #37: Burnup Impact on Fuel Thermal Conductivity and Initial Stored Energy**

Concerned about the impact of irradiation on fuel thermal conductivity, the U.S. Nuclear Regulatory Commission (NRC) issued Information Notice (IN) 2009-23 dated October 8, 2009 (ML091550527). In particular, IN 2009-23 states that “safety analyses performed for reactors using pre-1999 methods may be less conservative than previously understood.” WCAP-16996-P/WCAP-16996-NP, Volumes I, II and III, Revision 0, Section 11.4, “Thermal Properties of Nuclear Fuel Rod Materials,” explains that the WCOBRA/TRAC-TF2 nuclear fuel rod model uses a default  $\text{UO}_2$  thermal conductivity model based on a MATPRO-9 correlation that does not account for the effect of degradation with burnup. An additional optional model based on the Nuclear Fuels Industries (NFI) model by Ohira and Itagaki (1997) is provided to account for the effects of burnup on thermal conductivity.

With regard to LOCA applications, WCAP-16996-P/WCAP-16996-NP, Volumes I, II and III, Revision 0, Section 8.6 explains that the steady state fuel temperature is calibrated against the PAD code and refers to WCAP-16996-P Section 29. Subsection 29.4.2.2, “Initial Calibration of the Steady-State Condition for the Nuclear Rods,” explains that the initial fuel temperature and rod internal pressure for Westinghouse pressurized water reactors (PWRs) are calibrated against the PAD 4.0 fuel performance code, “Westinghouse Improved Performance Analysis and Design Model (PAD 4.0),” WCAP-15063-P, Revision 1, 1999. The calibration for Combustion Engineering (CE) PWRs is performed against the FATES3B code, “Improvements to Fuel Evaluation Model,” CEN-161(B)-P, Supplement 1-P-A, CE, 1992. Subsection 29.4.2.2 of WCAP-16996-P/WCAP-16996-NP, Volumes I, II and III, Revision 0, Section 29, also states that “the initial fuel temperature is a function of the peak linear heat rate and burnup.”

Please clarify the following items related to the nuclear fuel rod model and modeling approach in WCOBRA/TRAC-TF2 with regard to accounting for the effects of fuel burnup in LOCA analyses.

- (1) Please explain how the FSLOCA methodology accounts for fuel burnup effects in obtaining core thermal-hydraulic parameters and fuel thermal response under steady state for the purpose of initialization of LOCA analyses. Include consideration of factors related to different reactor fuel cycles, reactor operation time in a cycle, and core nodalization. The FSLOCA methodology core nodalization scheme models a single hot rod and a hot assembly and represents the rest of the core by 3 separate assembly groupings: (1) low power assemblies on core periphery, (2) average power interior assemblies under guide tube structures, and (3) average power interior assemblies located under other structures. Please explain how WCOBRA/TRAC-TF2 accounts for individual fuel assembly burnup levels for each of the fuel rods that model the reactor core and justify any assumptions.
- (2) If results from any other codes are used in the FSLOCA methodology to initialize, calibrate, benchmark, match, or in other way alter WCOBRA/TRAC-TF2 calculated results that have an impact on the initial pellet stored energy, please identify these codes, the frozen code versions used, and their approval status with the NRC. In addition, please document in details and explain such calibrating techniques and describe related algorithms, expressions, criteria, limitations, and

assumptions. Justify the applicability and appropriateness of such techniques to account for the effects of fuel thermal conductivity degradation with burnup. Clearly explain how results from the PAD 4.0 or FATES3B codes are used if the code has a thermal conductivity model with no burnup dependence.

- (3) If the FSLOCA methodology employs initial calibration of the steady state condition for the nuclear rods by altering the initial fuel temperature and rod internal pressure, please explain why WCOBRA/TRAC-TF2 predictions results for LOCAs should be considered acceptable in terms of describing the core fuel transient responses. In this regard, please present any supporting analyses, if available.

**Response:**

In conjunction with the response to RAIs 36-39, the aspects of Section 11, 26, and 29 of the FSLOCA Topical report [1] related to fuel rod burnup, pellet thermal conductivity, and pellet average temperatures have been updated. Along with those updates, the response to RAI 37 describes the updated fuel thermal conductivity treatment and the initialization of the fuel rod in WCOBRA/TRAC-TF2 (WCT-TF2).

Response to Part (1) of the RAI

The response to RAI 39 describes the updated fuel burnup sampling methodology. Please see the response to RAI 39 and the updated Section 29.4.1.1 for a detailed description of how fuel burnup effects are considered in defining the various rods (hot rod, hot assembly rod, core balance rods, and low-power rod). [

] <sup>a,c</sup>

Response to Part (2) of the RAI

[ <sup>a,c</sup> PAD5 was recently submitted to the USNRC [2], and is designed to supersede PAD 4.0 and FATES3B. The fuel pellet thermal conductivity models in WCT-TF2 and PAD5 both explicitly account for the effects of fuel thermal conductivity degradation. [

] <sup>a,c</sup> The applicability of the pellet thermal conductivity model used in WCT-TF2 is established in [3], which has shown the model to be applicable within the range expected for the FSLOCA EM.

[

] <sup>a,c</sup>

[

] <sup>a,c</sup>

Response to Part (3) of the RAI

[

] <sup>a,c</sup>

[

] <sup>a,c</sup>**References:**

1. WCAP-16996-P, "Realistic LOCA Evaluation Methodology Applied to the Full Spectrum of Break Sizes (FULL SPECTRUM LOCA Methodology)," November 2010.
2. WCAP-17642-P (Proprietary), WCAP-17642-NP (Non-Proprietary), "Westinghouse Performance Analysis and Design Model (PAD5)," 2013.
3. NUREG/CR-6534, Volume 4, "FRAPCON-3 Updates, Including Mixed-Oxide Fuel Properties," Pacific Northwest National Laboratory, 2005.

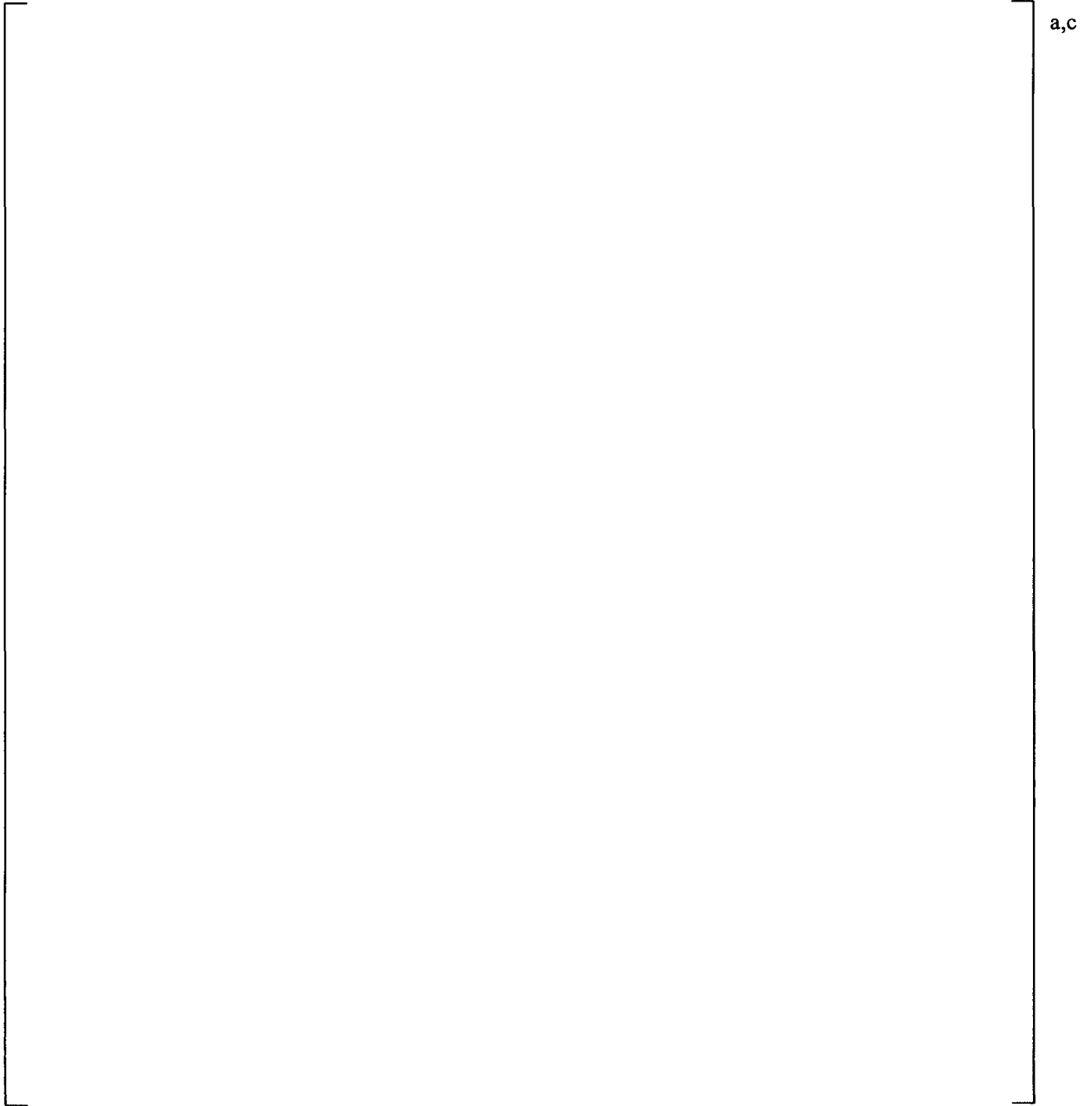
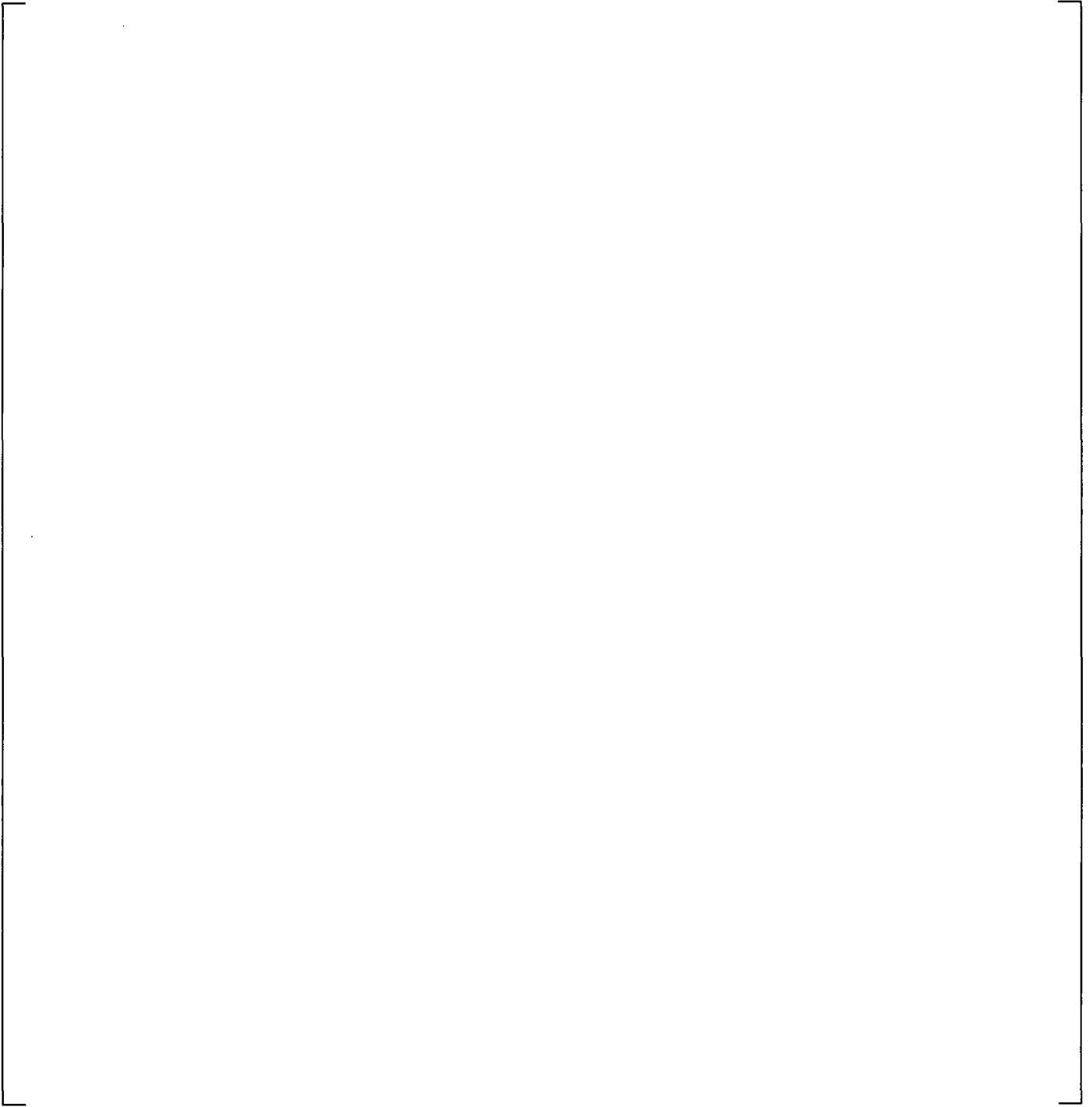


**Figure RAI37-1**

[

] <sup>a,c</sup>



a,c

**Figure RAI37-2**

[

]a,c

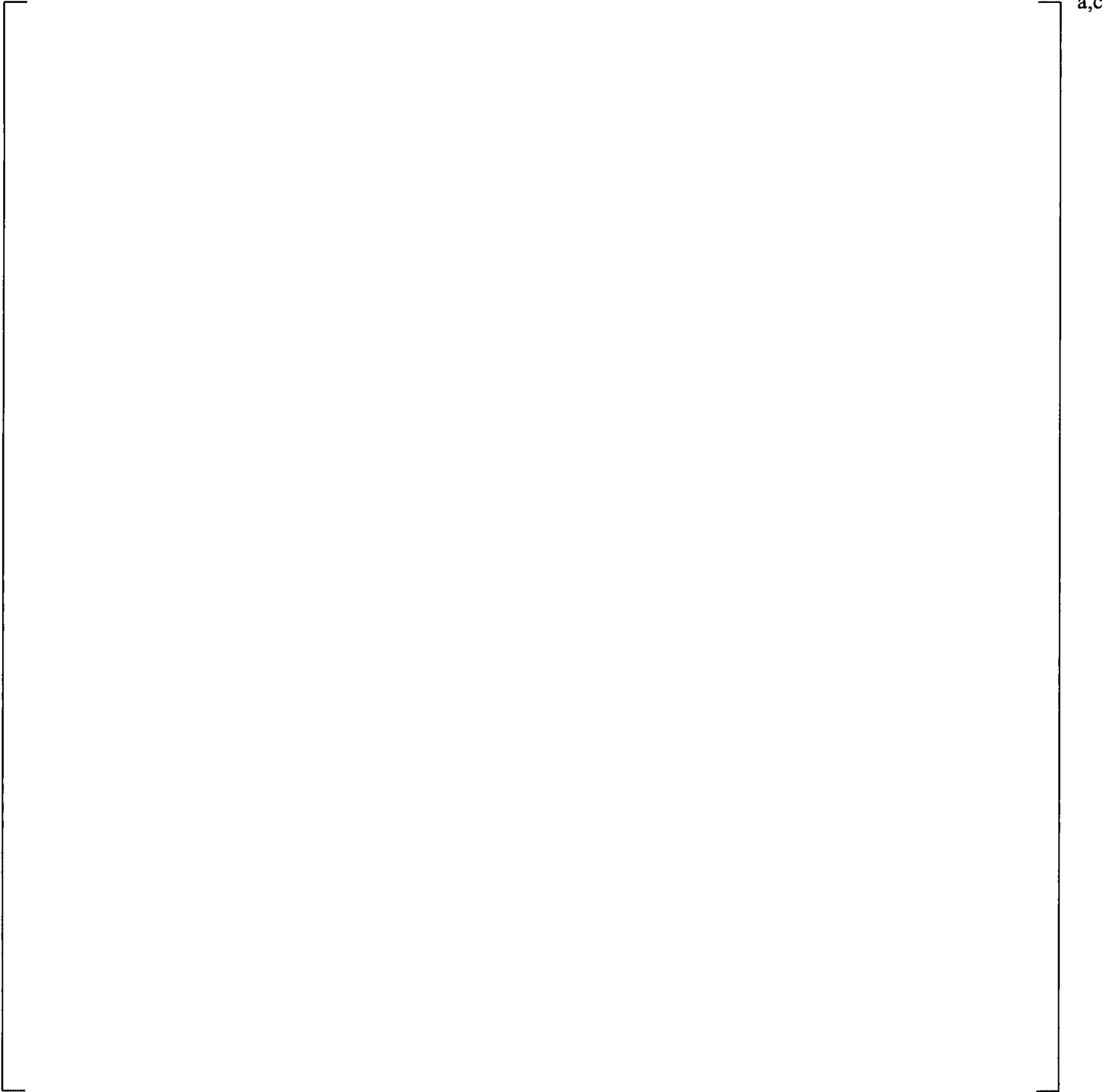


**Figure RAI37-3**

[

] <sup>a,c</sup>

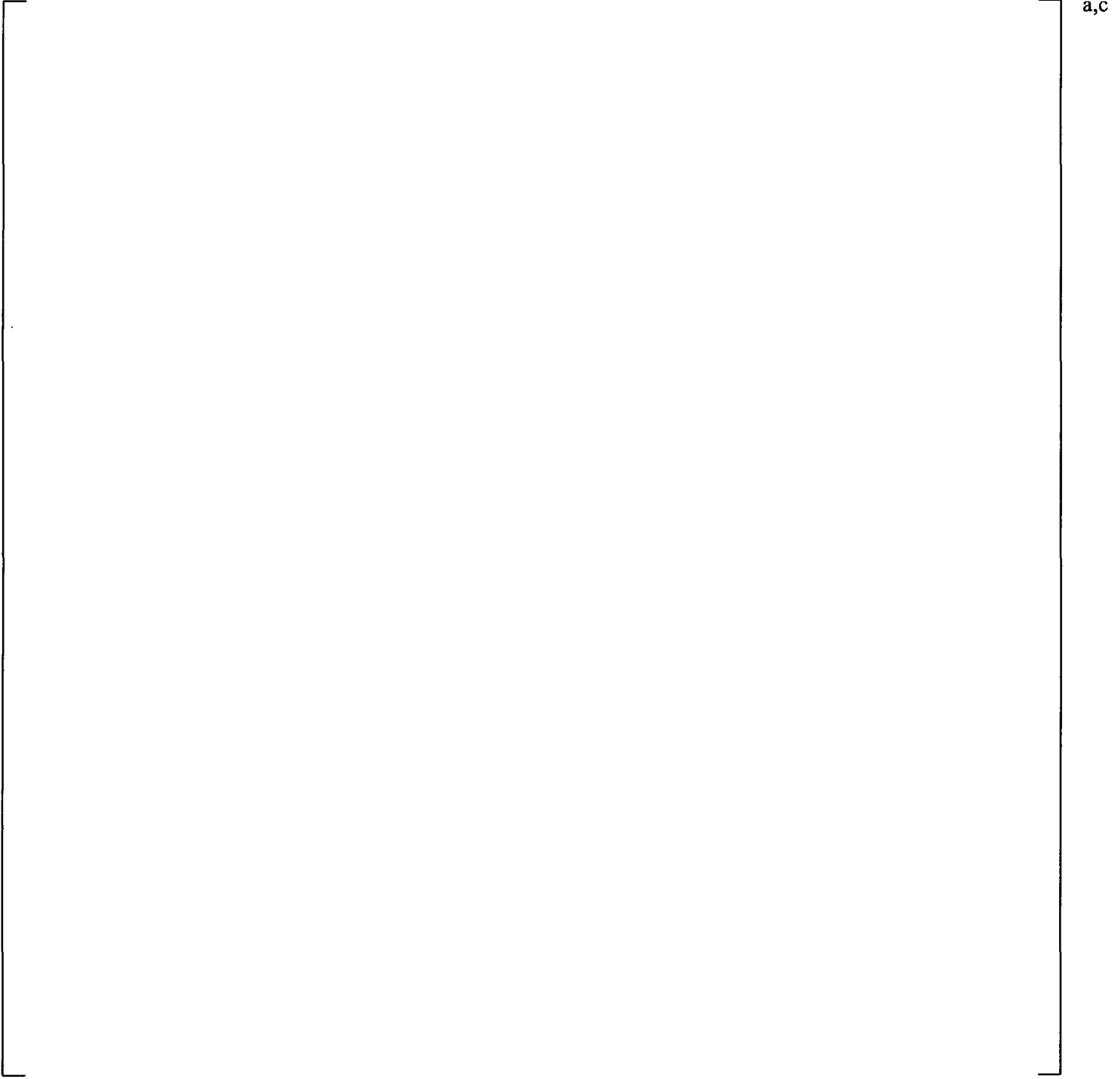


**Figure RAI37-4** [

] <sup>a,c</sup>



a,c

**Figure RAI37-5** [

] a,c



a,c

**Figure RAI37-6** [

] <sup>a,c</sup>

**Question #38: Treatment of Fuel Burnup Dependant Parameters**

WCAP-16996-P/WCAP-16996-NP, Volumes I, II, and III, Revision 0, Section 29, "Assessment of Uncertainty Elements," states that "many fuel related parameters are a function of burnup."

Please clarify the following items related to the consideration of burnup effects on nuclear fuel rod related parameters in the FSLOCA<sup>TM</sup> methodology and the accounting for such effects in LOCA analyses.

- (1) Please identify the parameters that have been identified as dependant on variability in the fuel burnup. Describe the importance of each parameter with regard to its possible impact on steady state initialization results and on LOCA transient predictions obtained by using the FSLOCA methodology.
- (2) Please explain how the functional dependence of each of the identified parameters on the fuel burnup accounts for variability in burnup and provide the burnup range that was considered. Describe how the burnup sampling process proposed for the FSLOCA methodology affects the treatment of each of these parameters.
- (3) From the list of parameters identified as burnup dependant, please identify those that are sampled on their own in the FSLOCA methodology. Explain how burnup is accounted for in the definition of the sampling ranges and sampling distributions for each of these burnup dependant parameters.
- (4) Please provide a table that summarizes the findings in response to the above identified items.

**Response:**

In conjunction with the response to requests for additional information (RAI) 36-39, the aspects of Section 29 of the FULL SPECTRUM LOCA Topical report [1] related to fuel rod burnup have been updated. Along with those updates, the response to RAI 39 describes the updated fuel burnup sampling methodology. Within that context, many fuel-related parameters remain a function of rod burnup, and so it is within that context that a response is provided here. When referring to the contents of Sections 25, 29 and 30, this response is referring to the updated section.

The treatment of the important burnup-related parameters is summarized in Table RAI38-1. The following discussion provides details specific to each of the listed parameters.

[

] <sup>a,c</sup>

[

]a,c

[

] <sup>a,c</sup>

As described in Section 30.1, the FSLOCA methodology demonstrates compliance with the 10 CFR 50.46(b)(2) oxidation criterion by showing that the sum of pre-accident oxidation and the oxidation occurring during the LOCA remains below the 17% limit. [

] <sup>a,c</sup>

Other nuclear fuel rod parameters are dependent upon the rod average burnup, but are of secondary importance for the steady-state and transient predictions. These parameters are included in the models to ensure reasonable agreement between WCOBRA/TRAC-TF2 (WCT-TF2) and PAD5 with respect to steady state initialization, and their uncertainty is not considered in the FSLOCA methodology.

- Pellet-Cladding Gap Gas Composition (Section 11.4.4): The gas composition as a function of rod average burnup [ ]<sup>a,c</sup>
- Pellet-Cladding Gap Conductance (Section 8.3.2): The gap conductance is the sum of thermal radiation conductance, conductance of the fill gas, and conductance due to pellet-clad contact pressure. It is calculated using the models in WCT-TF2 [ ]<sup>a,c</sup>
- Pellet-Cladding Gap Width: [ ]

] <sup>a,c</sup>

In summary, one independently sampled parameter in the FSLOCA uncertainty methodology is [ ]

] <sup>a,c</sup>

**Reference:**

1. WCAP-16996-P, "Realistic LOCA Evaluation Methodology Applied to the Full Spectrum of Break Sizes (FULL SPECTRUM LOCA Methodology)," November 2010.

**Table RAI38-1 Summary of Important Fuel-Burnup-Dependent Parameters**

Parameter	Sampling Approach	Basis
[		
		] <sup>a,c</sup>

**Question #39: Fuel Burnup Sampling**

Please describe the process of fuel burnup sampling as proposed in the FSLOCA methodology. Describe the sampling technique and explain how the proposed sampling approach accounts for fuel burnup variability with regard to space in consideration of fuel assemblies with different burnup in the core (e.g., fresh, once-burned, and twice-burned fuel) as well as for fuel burnup variability with regard to time in consideration of different fuel cycles (non-equilibrium and equilibrium) and reactor operation time in a cycle. In addition to the information in WCAP-16996-P/WCAP-16996-NP, Volumes I, II, and III, Revision 0, Subsection 29.4.1.1, "Time in Cycle," please explain if any such aspects due to burnup variability in space and time have been simplified or ignored in the proposed FSLOCA methodology fuel burnup sampling approach and provide justification.

**Response:**

In conjunction with the response to RAIs 36-39, the aspects of Section 29 of the FSLOCA Topical report [1] related to fuel rod burnup have been updated. Along with those updates, the response to RAI 39 describes the updated fuel burnup sampling methodology.

As described in the updated Section 29.4.1.1, and further in the response to RAI #38, one parameter that is independently sampled in the FSLOCA uncertainty methodology [

[

] <sup>a,c</sup> Regardless of its actual location, the hot assembly is always assumed to reside in the most limiting location relative to the upper internals such that blowdown cooling is minimized and the most limiting LOCA results are calculated. [

] <sup>a,c</sup>**Reference:**

1. WCAP-16996-P, "Realistic LOCA Evaluation Methodology Applied to the Full Spectrum of Break Sizes (FULL SPECTRUM LOCA Methodology)," November 2010.

**Updates to Section 2.3.2.1 of WCAP-16996-NP**

**“Realistic LOCA Evaluation Methodology Applied to the**

**Full Spectrum of Break Sizes**

**(FULL SPECTRUM LOCA Methodology)”**

## 2.3.2 Identification of System, Components, Processes and Ranking

### 2.3.2.1 Fuel Rod

#### Stored Energy

The stored energy is the total energy content of the fuel rods, and its spatial distribution, at the initiation of the transient. The stored energy is primarily a function of axial and radial power distributions throughout the core, pellet-clad gap conductance, and fuel thermal conductivity. The time in the fuel cycle at which the transient occurs affects the stored energy primarily through the [fuel thermal conductivity](#) and [the gap conductance](#). [

] <sup>a,c</sup>

#### Clad Oxidation

At high temperatures the zirconium base metal in the clad undergoes an exothermic reaction with the steam. [

] <sup>a,c</sup>

[

] <sup>a,c</sup>**Decay Heat**

Fission product decay heat is calculated using the American National Standards Institute/American Nuclear Society (ANSI/ANS) 5.1-1979 model. Implementation of the model includes consideration of the spatial distribution, and uncertainty of the decay heat itself. The power history during the transient is also considered in the Westinghouse analysis methodology. This affects the local power of all fuel rods included at the PCT location.

[

] <sup>a,c</sup>**Clad Deformation (Burst Strain, Relocation)**

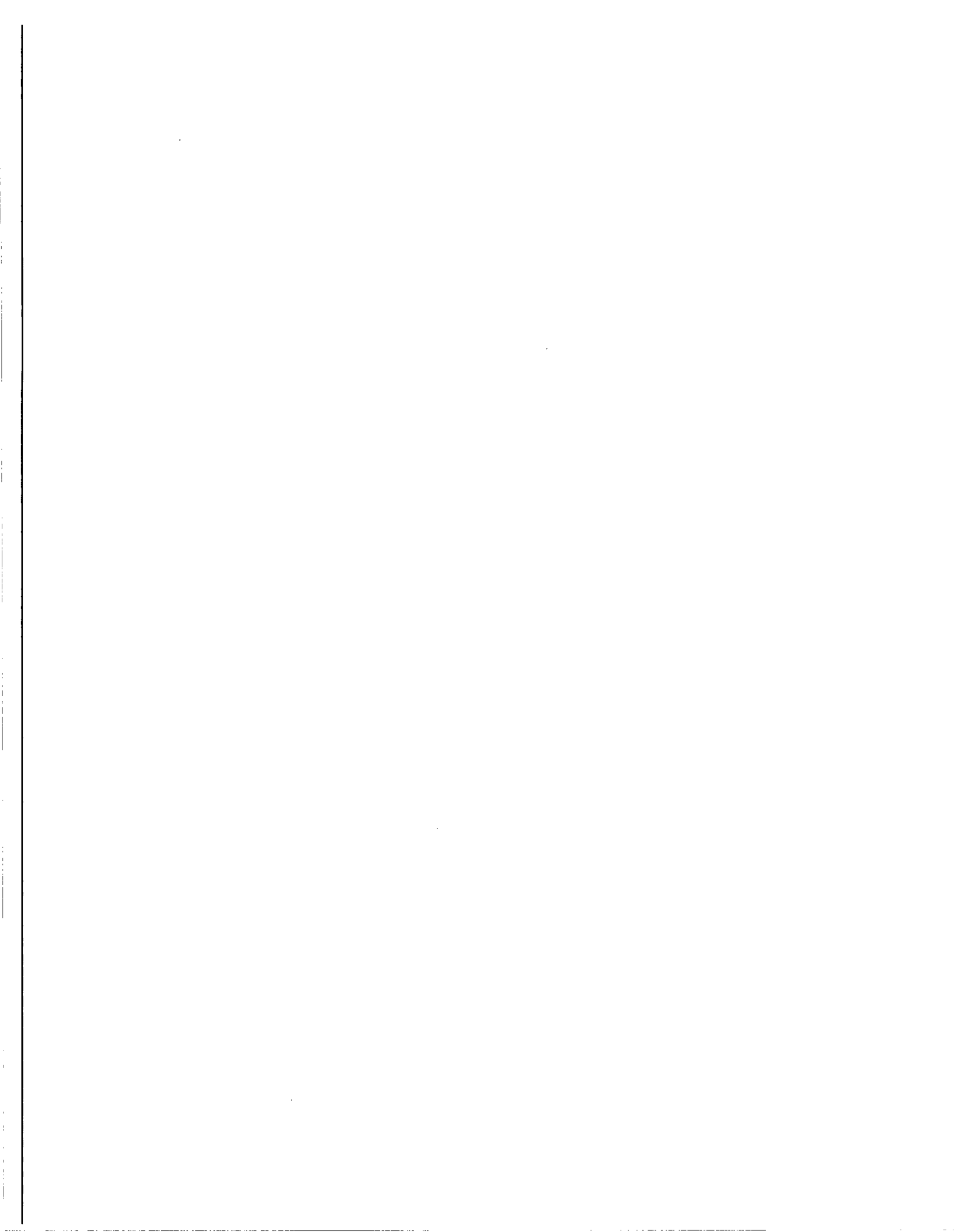
As the system depressurizes below the rod internal pressure, clad swelling and burst can occur. Fuel pellet fragments can relocate into the ballooned section of the clad at the burst location, thereby increasing the local heat generation rate. The clad burst temperature depends on the differential pressure across the clad. Burst strain depends on the metallurgical phase of the clad at the time of burst. [

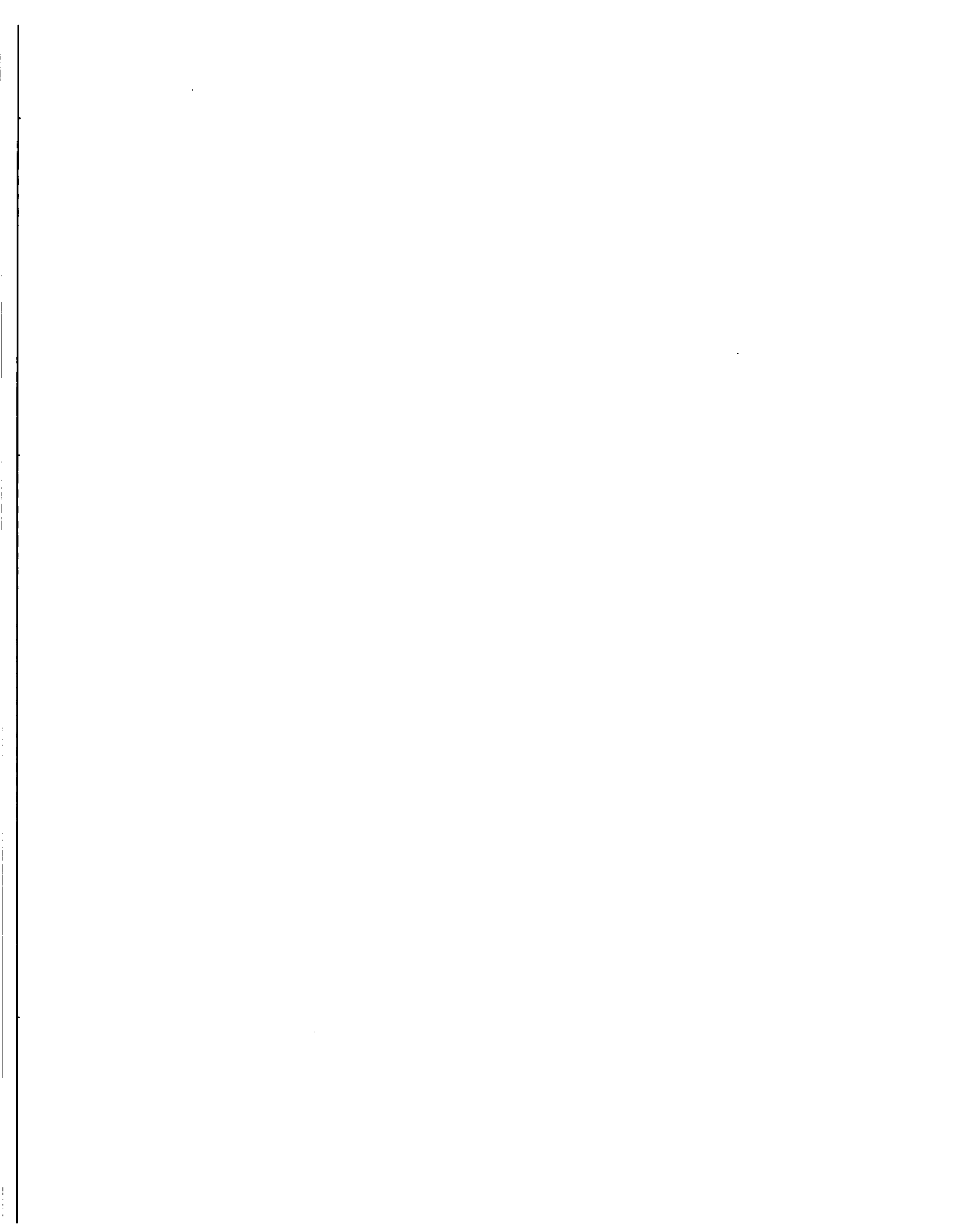
] <sup>a,c</sup>

[

] <sup>a,c</sup>







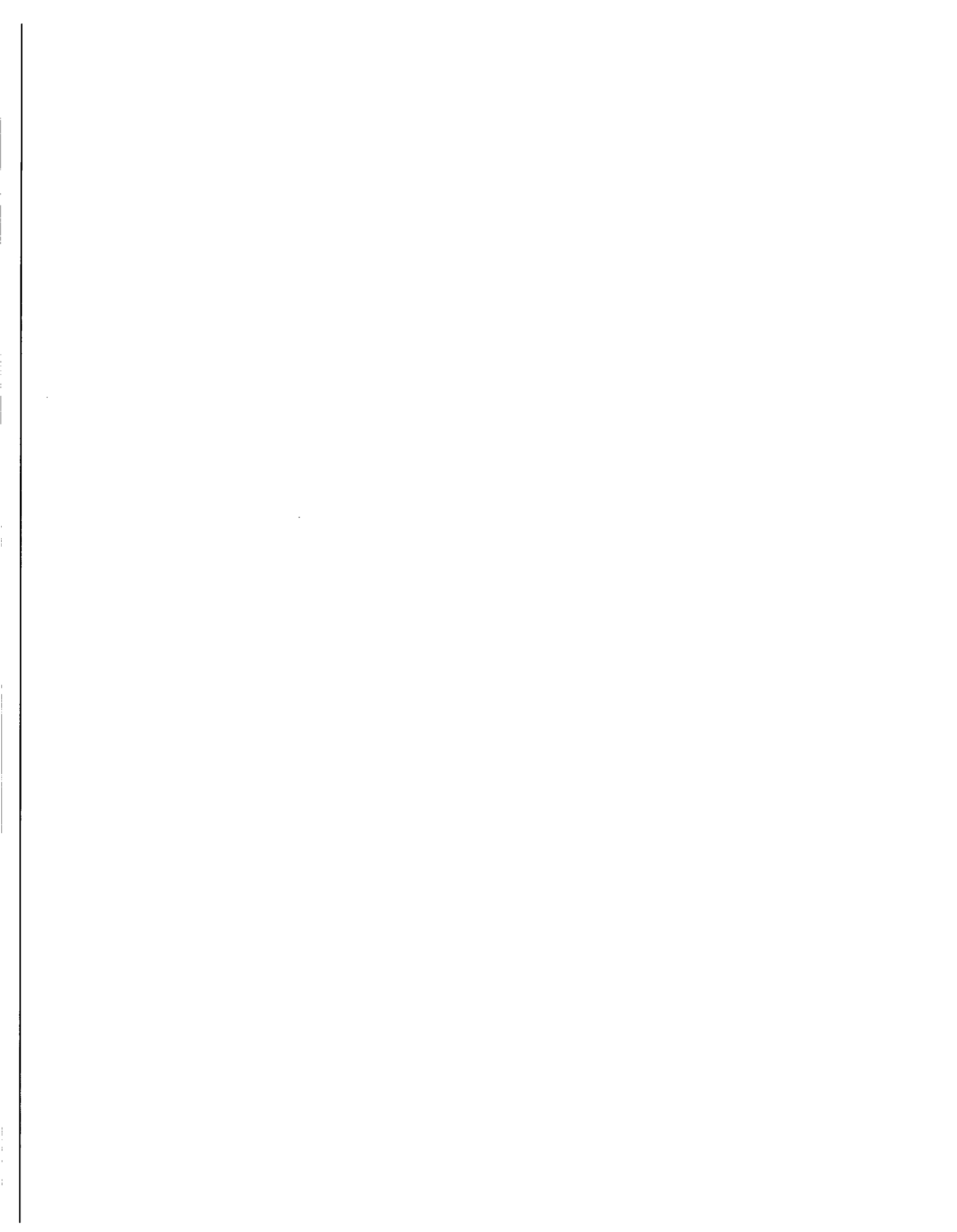


**Table 2-2 Requirement Assessment Against FSLOCA PIRT: Model Availability and Need**

a,c

**Table 2-2 Requirement Assessment Against FSLOCA PIRT: Model Availability and Need (cont.)**

a,c

**Table 2-2 Requirement Assessment Against FSLOCA PIRT: Model Availability and Need (cont.)**

a,c

**Table 2-2 Requirement Assessment Against FSLOCA PIRT: Model Availability and Need (cont.)**

a,c

**Table 2-2 Requirement Assessment Against FSLOCA PIRT: Model Availability and Need (cont.)**

a,c

**Table 2-2 Requirement Assessment Against FSLOCA PIRT: Model Availability and Need (cont.)**

a,c

**Table 2-2 Requirement Assessment Against FSLOCA PIRT: Model Availability and Need (cont.)**

a,c

**Table 2-2 Requirement Assessment Against FSLOCA PIRT: Model Availability and Need (cont.)**

a,c

**Table 2-2 Requirement Assessment Against FSLOCA PIRT: Model Availability and Need (cont.)**

a,c

**Table 2-2 Requirement Assessment Against FSLOCA PIRT: Model Availability and Need (cont.)**

a,c

**Table 2-2 Requirement Assessment Against FSLOCA PIRT: Model Availability and Need (cont.)**

a,c

**Table 2-2 Requirement Assessment Against FSLOCA PIRT: Model Availability and Need (cont.)**

a,c

**Table 2-2 Requirement Assessment Against FSLOCA PIRT: Model Availability and Need (cont.)**

a,c

**Updates to Sections 8.4, 8.4.1 and 8.6 of WCAP-16996-NP**

**“Realistic LOCA Evaluation Methodology Applied to the**

**Full Spectrum of Break Sizes**

**(FULL SPECTRUM LOCA Methodology)”**

## 8.4 FUEL ROD DEFORMATION MODEL

### Model Basis

Fuel pellet and cladding dimensional changes will occur during a loss-of-coolant accident, as a result of the thermal and mechanical stresses present in a nuclear fuel rod. The fuel rod deformation model calculates these changes and their effects on the core transient thermal-hydraulics. WCOBRA/TRAC-TF2 calculates the effects of fuel rod deformation on the pellet-cladding gap conductance, the cladding dimensions used in the conduction equation and the calculation of cladding oxidation, the cladding surface heat transfer area, and the continuity and momentum areas of the fluid cells associated with the fuel rods. The modeling of each of these effects is discussed in this section.

### Model as Coded

The fuel rod deformation mechanisms which are modeled in WCOBRA/TRAC-TF2 are described in Section 8.4.1. The effects of fuel rod deformation on the core transient thermal-hydraulics are discussed in Section 8.4.2.

### 8.4.1 Deformation Mechanisms

#### Fuel Pellet Thermal Expansion

The axial and diametral thermal expansion of the fuel is calculated using the MATPRO-11 (Revision 1) (Hagrman, Reymann, and Manson, 1980) FTHEXP subroutine correlation for thermally induced strain in  $UO_2$ . The correlation was simplified by omitting the corrections for molten fuel and mixed oxide (Pu). FTHEXP will return the same numerical value as the correlation in WCOBRA/TRAC-TF2, when FCOMP (weight percent  $PuO_2$ ) is equal to zero, and when T (fuel temperature) is less than FTMELT (fuel melting temperature). This is apparent by inspection of the subroutine listing in MATPRO.

In this model, the radial cracks in the fuel are assumed to relieve the hoop and radial stresses, allowing unrestrained radial movement of the fuel in each concentric radial node. The total radial movement at the fuel pellet surface is the sum of the expansion in all the fuel nodes.

$$(\Delta r_{th})_{fuel} = \sum_{i=1}^{NFUEL} \epsilon_r(T_i)_j \Delta r_i \quad (8-36)$$

where:

$$\begin{aligned} \epsilon_r(T_i)_j &= \text{thermal strain at axial node } j \text{ and radial node } i \\ &= 1 \times 10^{-5} T_i + 0.04 \exp(-5000/T_i) - 0.003 \\ T_i &= \text{node temperature (K)} \\ \Delta r_i &= \text{thickness of radial node } i \\ NFUEL &= \text{number of radial nodes in the fuel} \end{aligned}$$

The stress-free axial thermal expansion of the fuel pellet stack is calculated in an analogous manner. The fuel pellet stack length change due to the thermal expansion is:

$$(\Delta \ell_{th})_{fuel} = \sum_{j=1}^{NDX} \epsilon_z(\bar{T}_j) \Delta X_j \quad (8-37)$$

where:

$$\begin{aligned} \epsilon_z(\bar{T}_j) &= \text{thermal strain at axial node } j \text{ based on volume-averaged radial node} \\ &\quad \text{temperatures} \\ \Delta X_j &= \text{height of axial node } j \\ NDX &= \text{number of axial nodes} \end{aligned}$$

### Cladding Thermal Expansion

The axial and radial thermal expansion of the cladding are calculated using the CTHEXP subroutine correlations from Hagman, Reymann, and Manson (1980). The radial thermal expansion is calculated as:

$$(\Delta r_{th})_{clad} = \epsilon_r(\bar{T}_j) \bar{r} \quad (8-38)$$

where:

$$\begin{aligned} \epsilon_r(\bar{T}_j) &= \text{radial thermal strain at axial node } j \text{ based on the average cladding temperature} \\ &\quad \text{(Table 8-1)} \\ \bar{r} &= \text{cladding mean radius (cold)} \end{aligned}$$

The axial thermal expansion of the cladding is:

$$(\Delta \ell_{th})_{clad} = \sum_{j=1}^{NDX} \varepsilon_z(\bar{T}_j) \Delta X_j \quad (8-39)$$

where:

$\varepsilon_z(\bar{T}_j)$  = axial thermal strain at axial node  $j$  based on average cladding temperature at node  $j$  (Table 8-1)

$\Delta X_j$  = height of axial node  $j$

### Cladding Elastic Deformation

When the pellet-cladding gap is open, elastic deformation of the cladding is driven by the difference between the fill gas and system pressures. If the gap closes, the cladding deformation is caused by the radial motion of the fuel. In both cases, the cladding is assumed sufficiently thin for the stress, strain, and temperature to be uniform throughout the cladding thickness.

In the open gap elastic deformation model, the cladding is considered as a thin cylindrical shell loaded by internal and external pressures. (Axisymmetric loading and deformation are assumed.) The radial and axial elastic deformation is the result of hoop stress and axial stress caused by pressure difference. These stresses are given by the following equations:

$$\sigma_{\theta} = \frac{r_i P_i - r_o P_o}{\tau_c} \quad (8-40)$$

$$\sigma_z = \frac{\pi r_i^2 P_i - \pi r_o^2 P_o}{\pi(r_o^2 - r_i^2)} \quad (8-41)$$

where:

$r_o$  = cladding outside radius

$r_i$  = cladding inside radius

$\tau_c$  = cladding thickness

$P_i$  = internal fill gas pressure ( $P_G$  if the gap is open, Equation 8-46;  $P_{int}$  if the gap is closed, Equation 8-49)

$P_o$  = system pressure

The radial stress component is neglected, yielding the following relationships from Hook's Law:

$$\varepsilon_{\theta} = \frac{\Delta r}{r} = \frac{1}{E} (\sigma_{\theta} - \nu \sigma_z) \quad (8-42)$$

$$\varepsilon_z = \frac{\Delta \ell}{\ell} = \frac{1}{E} (\sigma_z - \nu \sigma_{\theta}) \quad (8-43)$$

where:

$\varepsilon_{\theta}$	=	hoop strain
$\varepsilon_z$	=	axial strain
E	=	modulus of elasticity (Young's modulus)
$\nu$	=	Poisson ratio, $E/2G - 1$ where $G$ = shear modulus

The modulus of elasticity and the shear modulus are shown in Table 8-2.

The relations for the cladding radial and axial elastic deformations, then, are:

$$(\Delta r_{el})_{clad} = \varepsilon_{\theta} \bar{r} \quad (8-44)$$

$$(\Delta \ell_{el})_{clad} = \sum_{j=1}^{NDX} \varepsilon_z \Delta X_j \quad (8-45)$$

where:

$\varepsilon_{\theta}$	=	hoop strain at axial node j
$\bar{r}$	=	cladding mean radius
$\varepsilon_z$	=	axial strain at axial node j
$\Delta X_j$	=	height of axial node j

The internal fill gas pressure used to determine the cladding elastic deformation when the gap is open is calculated from the relation:

$$P_G = \frac{M \cdot R}{\frac{V_P}{T_P} + \sum_{j=1}^{NDX} \pi \Delta X_j \frac{r_{ci}^2 - r_{fo}^2}{T_G} + \sum_{j=1}^{NDX} \pi \Delta X_j \frac{r_v^2}{T_V} + \sum_{j=1}^{NDX} \pi \Delta X_j \frac{r_{fvoid}^2}{T_F}} \quad (8-46)$$

where:

M	=	gram-moles of gas in fuel rod
---	---	-------------------------------

$V_p$	=	gas plenum volume, including effects of fuel and cladding axial expansion (ft <sup>3</sup> ) (from Equations 8-37, 8-39, and 8-45)
$T_p$	=	gas plenum temperature (K) (defined as the temperature of the cladding at the top of the fuel rod + 10 K)
$\Delta X_j$	=	computational cell length at axial level j (ft)
$r_{ci}$	=	cladding inside radius including thermal and elastic expansion, and creep deformation (ft) (from Equations 8-38, 8-44, and 8-59)
$r_{fo}$	=	fuel outside radius including thermal expansion (ft) (from Equation 8-36)
$R$	=	gas constant (6.1313 ft-lbf/g-mole-K)
$r_v$	=	radius of central void (ft) (from input data)
$T_G$	=	gas gap temperature (K)
$T_v$	=	central void temperature (K)
$T_F$	=	averaged fuel pellet temperature
$r_{void}$	=	radius of additional fuel void in the fuel pellet

This is a static lumped pressure model, similar to those in FRAP or GAPCON. The pressure is assumed uniform throughout the fuel rod, with constant fission gas inventory.

In the closed gap deformation model, the cladding is considered as thin-wall tubing with a specified displacement at the inside and pressure loading at the outside surface. The radial fuel displacement at which contact occurs can be calculated as:

$$(\Delta r_{th})_{fuel} = (\Delta r_{th})_{clad} + (\Delta r_{cr})_{clad} + \tau_{g,cold} - \tau_{g|L} \quad (8-47)$$

where:

$\tau_{g L}$	=	fuel cladding gap width that defines the closed gap (i.e., $3.6(R_1+R_2)$ ) as in Equation 8-33)
$\tau_{g,cold}$	=	user-input cold fuel cladding gap width (including burnup-dependent effects)
$(\Delta r_{th})_{fuel}$	=	fuel radial thermal expansion (Equation 8-36)

$(\Delta r_{th})_{clad}$  = cladding radial thermal expansion (Equation 8-38)

$(\Delta r_{cr})_{clad}$  = cladding creep deformation (Equation 8-59)

Fuel radial displacement due to contact is assumed negligible, so the radial elastic deformation of the cladding must be equal to the applied fuel displacement on the inside surface,

$$(\Delta r'_{th})_{fuel} = (\Delta r_{th})_{fuel} - (\Delta r_{th})_{clad} - (\Delta r_{cr})_{clad} + \tau_{g|L} - \tau_{g,cold}$$

$$(\Delta r_{el})_{clad} = (\Delta r'_{th})_{fuel} \quad (8-48)$$

The pellet-cladding interfacial pressure generated by the applied displacement can be computed using the equilibrium stress (Equations 8-40 and 8-41), Hook's Law (Equations 8-42 and 8-43), and the applied displacement  $(\Delta r'_{th})_{fuel}$ . The interfacial pressure is:

$$P_{int} = \frac{(\Delta r'_{th})_{fuel} E \tau_c (r_o^2 - r_i^2)}{\bar{r} [r_i (r_o^2 - r_i^2) - r_i^2 \tau_c \nu]} + P_o \frac{r_o (r_o^2 - r_i^2) - r_o^2 \tau_c \nu}{r_i (r_o^2 - r_i^2) - r_i^2 \tau_c \nu} \quad (8-49)$$

where:

$(\Delta r'_{th})_{fuel}$  = applied fuel displacement in cladding (from Equation 8-48)  
 E = modulus of elasticity  
 $\tau_c$  = cladding thickness  
 $r_o$  = cladding outside radius  
 $r_i$  = cladding inside radius  
 $\bar{r}$  = cladding mean radius  
 $\nu$  = Poisson's ratio for the cladding  
 $P_o$  = system pressure (on the outside surface of the cladding)

The elastic deformation when the gap is closed is evaluated using the relation in Equation 8-44, but the internal pressure  $P_i$  is defined as the interfacial pressure  $P_{int}$  from Equation 8-49 instead of the fill gas pressure  $P_G$  from Equation 8-46.

### Cladding Creep Deformation

The high-temperature creep model is based on tests performed at the Berkeley Nuclear Laboratories in the United Kingdom. Three cladding material options are available. The first is used for analyses of Westinghouse manufactured Zircaloy-4 cladding, and is based on the work of Donaldson, Healey, and Horwood (1985). The second is used for analyses of Westinghouse manufactured ZIRLO<sup>®</sup> cladding, and is based on the work of Donaldson and Barnes (1989), and Donaldson, Barnes, and Hall (1989). An additional option is available for analyses of the Sandvik manufactured Zircaloy-4 cladding used in the NRU experiments, and is based on the work of Donaldson, Horwood, and Healey (1982).

The Berkeley test data indicate that high-temperature creep of the cladding materials of interest is well described by a power law stress dependence and an Arrhenius temperature dependence.

$$de/dt = A' \sigma^n \exp(-Q/RT) \quad (8-50)$$

where:

$de/dt$	=	creep rate ( $\text{sec}^{-1}$ )
$\sigma$	=	hoop stress (MPa)
$Q$	=	activation energy, cal/gm-mole
$R$	=	gas constant, 1.987 cal/gm-mole/K
$T$	=	temperature (K)
$t$	=	time

and  $A'$ ,  $n$  are material-specific functions of  $T$  and  $\sigma$ . This relationship for creep is commonly referred to as the Norton creep equation.

The time-dependent hoop stress is given by:

$$\sigma(t) = (d(t)/2\tau(t)) P(t) \quad (8-51)$$

where:

$d(t)$	=	mid-wall cladding diameter
	=	$d_0(1 + \epsilon(t))$ , where $d_0$ = initial mid-wall cladding diameter
$\tau(t)$	=	cladding thickness
	=	$\tau_0/(1 + \epsilon(t))$ , where $\tau_0$ = initial cladding thickness
$P(t)$	=	cladding pressure differential
$\epsilon(t)$	=	engineering strain

If the pressure is assumed to vary linearly over a small increment of time, such that,

$$P(t) = P_0 + (dP/dt)\Delta t,$$

where:

$P_0$	=	cladding pressure differential at the beginning of the timestep
-------	---	---

the time-dependent stress is given by:

$$\sigma(t) = \sigma_0 (1 + \epsilon(t))^2 (1 + ((dP/dt)/P_0)\Delta t), \quad (8-52)$$

where:

$$\sigma_o = \text{hoop stress at the beginning of the timestep}$$

If the temperature is assumed to vary linearly over a small increment of time, such that:

$$T(t) = T_o + (dT/dt)\Delta t,$$

where:

$$T_o = \text{temperature (K) at the beginning of the timestep}$$

Then:

$$\exp(-Q/RT(t)) = \exp(-Q/RT_o(1 + ((dT/dt)/T_o)\Delta t)) \quad (8-53)$$

A good approximation to this expression is:

$$\exp(-Q/RT(t)) = \exp(-Q/RT_o)(1 + (dT/dt)(Q/RT_o^2)\Delta t) \quad (8-54)$$

provided that  $|(dT/dt)(Q/RT_o^2)|\Delta t \leq 0.01$ .

Substituting Equations 8-52 and 8-54 into 8-50 and allowing for the possibility of negative cladding pressure differentials yields:

$$\begin{aligned} d\epsilon/dt = & (|P_o|/P_o) A' \exp(-Q/RT_o) |\sigma_o|^n (1 + \epsilon)^{2n} \\ & (1 + ((dP/dt)/P_o)\Delta t)^n (1 + (dT/dt)(Q/RT_o^2)\Delta t) \end{aligned} \quad (8-55)$$

The true strain is related to the engineering hoop strain by  $e = \ln(1 + \epsilon)$ . Therefore,  $de = d\epsilon/(1 + \epsilon)$ . If we define:

$$\begin{aligned} C_1 &= (|P_o|/P_o) A' \exp(-Q/RT_o) |\sigma_o|^n \\ C_2 &= (dT/dt)(Q/RT_o^2) \\ C_3 &= (dP/dt)/P_o \end{aligned}$$

Equation 8-55 may be rewritten as:

$$d\epsilon/(1 + \epsilon)^{2n+1} = C_1((1 + C_2\Delta t)(1 + C_3\Delta t)^n)dt$$

or

$$(1 + \epsilon)^{-(2n+1)} d\epsilon = C_1(1 + C_3\Delta t)^n dt + C_1 C_2 \Delta t (1 + C_3\Delta t)^n dt \quad (8-56)$$

Integration may be performed using standard integral tables (for example, Beyer, 1978) which yields:

$$\begin{aligned} (-1/2n)((1 + \varepsilon)^{-2n} - 1) = C_1/C_3^2((C_3 - C_2)((1 + C_3\Delta t)^{n+1} - 1)/(n + 1) \\ + C_2((1 + C_3\Delta t)^{n+2} - 1)/(n + 2)) \end{aligned} \quad (8-57)$$

The engineering hoop strain in the timestep  $\Delta t$  is therefore:

$$\varepsilon = [(1 - 2n(\text{Right Hand Side of Equation 8-57}))^{-1/2n} - 1] \quad (8-58)$$

The creep model used in WCOBRA/TRAC-TF2 calculates the incremental engineering hoop strain over a timestep  $\Delta t$  using Equation 8-58. The cladding creep deformation is then calculated as:

$$(\Delta r_{cr})_{clad} = \varepsilon(t) \bar{r} \quad (8-59)$$

where:

$$\begin{aligned} \varepsilon(t) &= \text{engineering hoop strain at end of timestep} \\ \bar{r} &= \text{cladding mean radius} \end{aligned}$$

The maximum timestep for the integration of the Norton creep equation is limited so that  $|C_2| \Delta t \leq 0.01$ , and the approximation to  $\exp(-Q/RT(t))$  remains valid. Details of the model application for the three available cladding options are summarized below.

[

]<sup>a,c</sup>

#### Westinghouse Zircaloy-4 Cladding

Donaldson, Healey, and Horwood (1985) report Westinghouse manufactured Zircaloy-4 creep data obtained under constant pressure, constant temperature test conditions. Test specimens were heated to the specified temperature and the temperature was held constant for 10 minutes prior to pressurization. The creep test results indicate the existence of two types of creep behavior (Figure 8-14). Creep in the alpha and beta phases, and part of the mixed phase region, exhibits high stress sensitivity typical of a dislocation climb mechanism. In the low stress/low temperature portion of the mixed phase region the stress sensitivity is significantly reduced. In this region, the creep mechanism is superplastic creep.

Donaldson, Healey, and Horwood (1985) report additional creep test data for [

]<sup>a,c</sup>

The creep rates shown in Figure 8-14 are programmed in WCOBRA/TRAC-TF2 in the form:

$$de/dt = A\sigma^n \tag{8-60}$$

where the coefficients A and n are functions of temperature and the creep mechanism (Table 8-3). To determine the coefficients A', Q and n for integration of Equation 8-50, the following procedure is used:

1. 
$$\left[ \frac{de/dt}{\sigma^n} \right]^{a,c} \tag{8-61}$$

where:

2. 
$$\left[ \frac{de/dt}{\sigma^n} \right]^{a,c}$$

3. Calculate n from:

$$\left[ \frac{de/dt}{\sigma^n} \right]^{a,c} \tag{8-62}$$

4. 
$$\left[ \frac{de/dt}{\sigma^n} \right]^{a,c}$$

5. Calculate Q from:

$$\left[ \frac{de/dt}{\sigma^n} \right]^{a,c} \tag{8-63}$$

6. Calculate A from:

$$\left[ \frac{de/dt}{\sigma^n} \right]^{a,c} \tag{8-64}$$

### Westinghouse ZIRLO® Cladding

Donaldson and Barnes (1989) and Donaldson, Barnes, and Hall (1989) report Westinghouse manufactured ZIRLO® cladding creep data obtained under similar test procedures as were used for the Zircaloy-4 tests, with the following notable exception. [

] <sup>a,c</sup>

The ZIRLO® cladding creep rates shown in Figure 8-15 are programmed in the form of Equation 8-60, with the coefficients A and n defined in Table 8-4. The procedure used to obtain the coefficients for the integration of the Norton creep equation is identical to that used for the Westinghouse Zircaloy-4 cladding option.

The ZIRLO® cladding creep model used in WCOBRA/TRAC-TF2 has previously been incorporated into the 1981 Evaluation Model with BASH and the NOTRUMP Evaluation Model (Davidson and Nuhfer, 1990). That reference describes a correction to the creep rate integration which is used in the alpha phase and the portion of the mixed phase region which exhibits dislocation creep, to more accurately predict the measured strain versus time. That correction is also used in WCOBRA/TRAC-TF2. Following integration of the Norton creep equation in the alpha phase and the mixed phase/dislocation creep regions, the strain accumulated during the timestep is reduced by an empirical expression which is a function of the strain accumulated in these regions, i.e.,

$$\epsilon_c = \frac{\epsilon}{(1 + x)^m} \quad (8-65)$$

where:

$\epsilon_c$	=	effective strain increment
$\epsilon$	=	strain increment calculated by Equation 8-58
x	=	summation of $\epsilon_c$ in the strain hardening regimes
m	=	[ ] <sup>a,c</sup> for the alpha phase, [ ] <sup>a,c</sup> for the mixed phase/dislocation creep region

### Sandvik (NRU) Zircaloy-4 Cladding

Donaldson, Horwood, and Healey (1982) report creep data for Sandvik Zircaloy-4 cladding specimens in the alpha phase. Testing was confined to the high alpha phase temperature range, based on the expected range of interest for the NRU Materials Test program.

The alpha phase Sandvik Zircaloy-4 cladding creep rates shown in Figure 8-16 are programmed in the form of Equation 8-60, with the coefficients A and n defined in Table 8-5. [

] <sup>a,c</sup>

[ ]<sup>a,c</sup> The procedure used to obtain the coefficients for the integration of the Norton creep equation is identical to that used for the Westinghouse Zircaloy-4 cladding option.

**Cladding Rupture**

Loss of coolant accidents result in depressurization of the reactor coolant system and heatup of the nuclear fuel rods, due to insufficient cooling. The resulting stresses on the cladding may be sufficiently high to cause rupture of the cladding. Correlations which predict the occurrence of cladding rupture and the resulting cladding strains have been incorporated into WCOBRA/TRAC-TF2 for Zircaloy-4 cladding and for ZIRLO<sup>®</sup> cladding. These correlations are described below.

Zircaloy-4 Cladding

Powers and Meyer (1980) have reviewed zircaloy cladding rupture data from a wide range of experimental facilities and have recommended the cladding rupture correlation developed by Chapman (1979). The correlation is given by:

$$T_R = 3960 - \frac{20.4\sigma_E}{1+H} - \frac{8.51 \times 10^6 \sigma_E}{100(1+H) + 2790 \sigma_E} \tag{8-66}$$

where:

- T<sub>R</sub> = rupture temperature (°C)
- σ<sub>E</sub> = engineering hoop stress (kpsi)
- H = min (1.0, HUR/28°C/sec)
- HUR = heatup rate

This correlation has been incorporated into WCOBRA/TRAC-TF2, and is used to predict the occurrence of cladding rupture for nuclear fuel rods clad with Zircaloy-4.

The cladding heatup rate in WCOBRA/TRAC-TF2 is treated in the same way as in the LOCTA-IV code (Bordelon et al., 1974). The approach can be explained by using Figure 8-17 which illustrates a number of potential scenarios. The instantaneous heatup rate is used until the cladding temperature is within [ ]<sup>a,c</sup> of the cladding burst temperature. When this condition is reached (Point A) the cladding temperature and time are recorded to be used as a reference for the calculations. As long as the cladding temperature is

[ ]<sup>a,c</sup>

$$\left[ \right]^{a,c} \tag{8-67}$$

where: [ ]

[ ]<sup>a,c</sup>

[

] <sup>a,c</sup>

[

] <sup>a,c</sup>

### ZIRLO<sup>®</sup> Cladding

Westinghouse has conducted single rod burst tests of ZIRLO<sup>®</sup> cladding over a wide range of cladding pressure differentials (100 to 2000 psi), and heatup rates (5 to 50°F/sec) (Davidson and Nuhfer, 1990). The test results have been correlated in the form of rupture temperature as a function of engineering hoop stress, consistent with the Chapman approach. However, the ZIRLO<sup>®</sup> cladding rupture temperature correlation is not dependent on the heatup rate, as the data show no systematic heatup rate dependence.

The ZIRLO<sup>®</sup> cladding rupture correlation was defined using the mean of the 10°F/sec heatup rate data. Figure 8-19 shows a comparison of the measured burst temperatures and those predicted by the correlation. The correlation predicts the data well over the entire range of heatup rates included in the test matrix.

A correlation for the ZIRLO<sup>®</sup> cladding strain following rupture has been developed using the single rod burst test data reported in Davidson and Nuhfer (1990). The resulting correlation is shown with the database in Figure 8-20. The WCOBRA/TRAC-TF2 correlation reflects the alpha phase and beta phase peaks, and [

] <sup>a,c</sup>

[

] <sup>a,c</sup>

## 8.6 [ ]<sup>a,c</sup> MODEL

[

] <sup>a,c</sup>

The FSLOCA methodology will model the hot assembly rods as [

] <sup>a,c</sup>

1. Hot Assembly (HA) Rod Component – A type of active nuclear fuel rod that describes all fuel rods in the hot assembly but the hot pin. [

] <sup>a,c</sup> A hot assembly rod is a fully functional fuel rod coupled with the thermal-hydraulic solution and core kinetics. The HA rod will consider all local uncertainty models at their nominal (as coded) value. The HA rod will deform consistently with the fuel rod deformation model discussed in Section 8.4, including creep deformation and rupture deformation. [

] <sup>a,c</sup>

2. Hot Rod (HR) Component – A type of active nuclear fuel rod that describes the single fuel pin in the hot assembly, which represents a high power fuel pin. A hot rod is a partially functional fuel rod coupled with the thermal hydraulic solution and core kinetics. All the functions of the HA rod are applied to hot rod except the creep deformation and the rupture deformation are disabled for hot rod. The hot rod considers all applicable local uncertainty models at their nominal value.

3. [

] <sup>a,c</sup>

[

]<sup>a,c</sup>

A summary of functions of rods in the hot assembly is given in Table 8-6. The local uncertainties in Table 8-6 will be explained in Section 29.

The details of [ ]<sup>a,c</sup> model are listed below.

[

]<sup>a,c</sup>

[

] <sup>a,c</sup>

[

] <sup>a,c</sup>

[

] <sup>a,c</sup>

(8-86)

[

] <sup>a,c</sup>

[

] <sup>a,c</sup>

[

] <sup>a,c</sup>

(8-86a)

[

] <sup>a,c</sup>

[

] <sup>a,c</sup>

[

] <sup>a,c</sup>

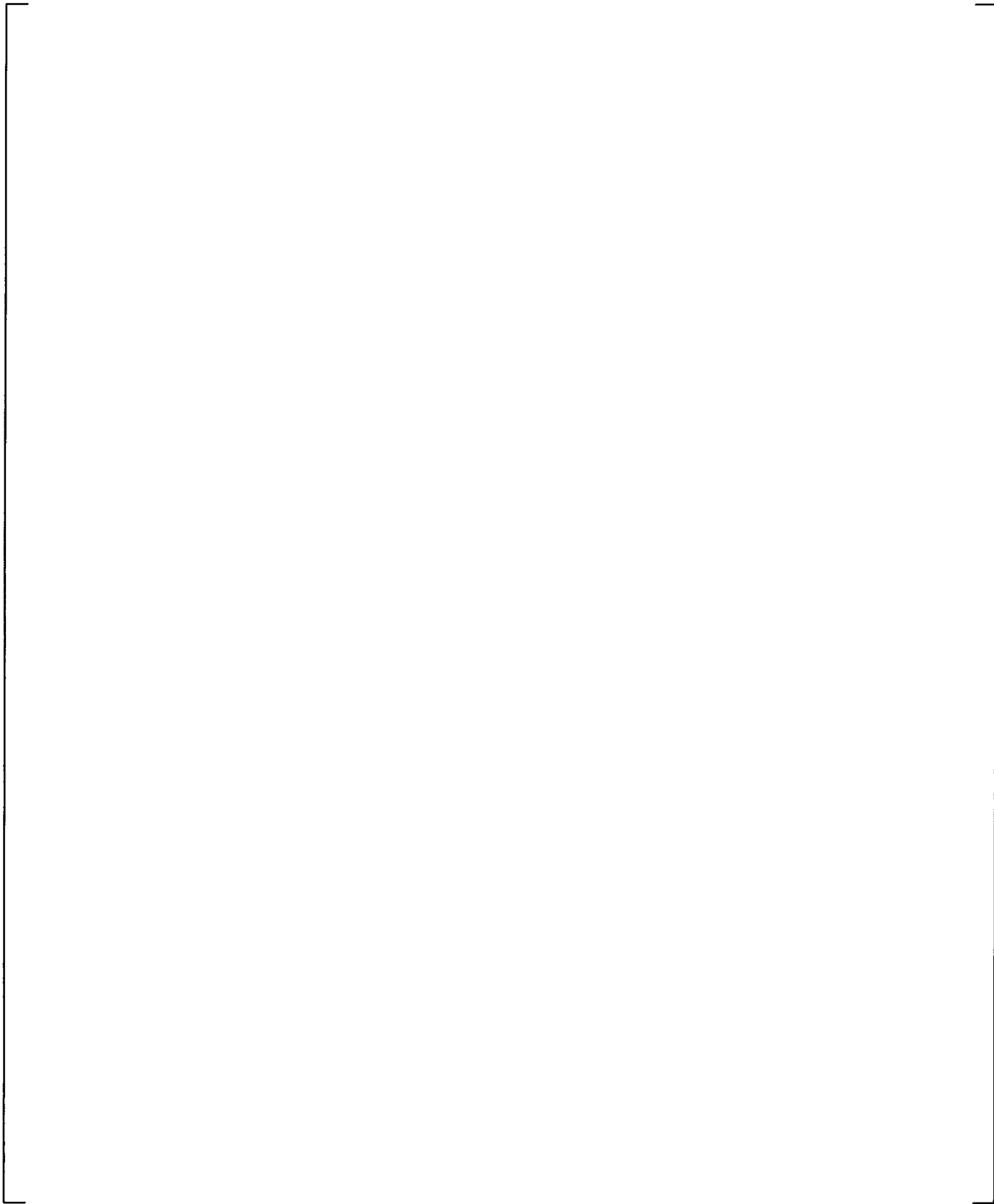
[

] <sup>a,c</sup>

Table 8-6 [ ]<sup>a,c</sup>

a,c

a,c



a,c

**Figure 8-24** [

]a,c

**Updates to Section 11.4 of WCAP-16996-NP**

**“Realistic LOCA Evaluation Methodology Applied to the**

**Full Spectrum of Break Sizes**

**(FULL SPECTRUM LOCA Methodology)”**

## 11.4 THERMAL PROPERTIES OF NUCLEAR FUEL ROD MATERIALS

A typical nuclear fuel rod is composed of uranium-dioxide fuel pellets and a zirconium based clad material. The gap between the fuel pellets and the clad is filled with the initial backfill gas and fission gas. As part of the WCOBRA/TRAC-TF2 default nuclear fuel rod model, the material properties of uranium-dioxide, Zircaloy-4, ZIRLO<sup>®</sup> alloy, and of gas mixtures are included. This section describes the calculation of the thermal properties for these fuel rod materials.

[

] <sup>a,c</sup>

### 11.4.1 Uranium Dioxide

#### Model Basis

The material properties of uranium dioxide are based on MATPRO-9 (MacDonald et al., 1976) and on MATPRO-11, Rev. 1 (Hagrman, Reymann, and Mason, 1980) calculations, with exception to the thermal conductivity model, which is the Nuclear Fuels Industries (NFI) model as modified in FRAPCON 3.3 (Lanning et al., 2005).

#### Density

The (cold) density for uranium-dioxide is assumed to be:

$$\rho_{\text{UO}_2} = 684.86f_D \quad (11-145)$$

where  $f_D$  is the fraction of theoretical density and is input by the user. The density  $\rho_{\text{UO}_2}$  has units of lbm/ft<sup>3</sup>.

#### Thermal Conductivity

The UO<sub>2</sub> thermal conductivity model accounts for the effects of burnup on thermal conductivity. The Nuclear Fuels Industries (NFI) model (Ohira and Itagaki, 1997) was selected as the starting point for a replacement of the Lucuta model (Lucuta et al., 1996) for FRAPCON 3.3 (Lanning et al., 2005). The Lucuta formula for uranium oxide pellet thermal conductivity was found to have two inaccuracies. First, it predicts values at high temperature (>2200 K) that are too large relative to credible modern data for un-irradiated fuel pellet material (Ronchi et al., 1999). Secondly, it has too little burnup degradation compared to both in-cell laser-flash diffusivity measurements on high-burnup pellet samples and in-reactor fuel temperatures measured at nominal to high burnup. For especially this second reason, the NFI model as modified in FRAPCON 3.3 is considered most appropriate. Section 2.3 in (Lanning et al., 2005) shows that the modified NFI model compares well against zero burnup (unirradiated) and irradiated test results.

The NFI model, similar to most other thermal conductivity models utilized in fuel performance codes, consists of a lead term that is inversely proportional to a temperature function  $A + BT$  (phonon term), with burnup dependence factors in its denominator, plus terms that model the electronic contribution to fuel heat transfer at high temperature. The modified NFI model implemented in WCOBRA/TRAC-TF2 is defined as follows:

$$K_{95} = \frac{1}{A + B \cdot T + f(\text{Bu}) + (1 - 0.9 \cdot \exp(-0.04 \cdot \text{Bu})) \cdot g(\text{Bu}) \cdot h(T)} + \frac{E}{T^2} \cdot \exp(-F/T) \quad (11-146)$$

where:

$K_{95}$  = Thermal Conductivity, W/m-K, for as fabricated fuel density of 95% of theoretical density (TD)

$T$  = Temperature, K

$\text{Bu}$  = Burnup, GWD/MTU

$f(\text{Bu})$  = effect of fission products in crystal matrix (solution)

$$= 0.00187 \cdot \text{Bu} \quad (11-147)$$

$g(\text{Bu})$  = effect of irradiation defects,

$$= 0.038 \cdot \text{Bu}^{0.28} \quad (11-148)$$

$h(T)$  = Temperature dependence of annealing on irradiation defects

$$= \frac{1}{1 + 396 \cdot \exp(-Q/T)} \quad (11-149)$$

$Q$  = Temperature dependence parameter = 6380 K

$A$  = 0.0452 m-K/W

$B$  = 2.46E-4 m/W

$E$  = 3.5E9 W-K/m

$F$  = 16361 K

The model is adjusted for 'as fabricated' fuel densities different from 95% TD using the Lucuta recommendation for spherical-shaped pores (Lucuta et al., 1996), as follows:

$$K_d = 1.0789 \cdot K_{95} \cdot \left\{ d / [1.0 + 0.5 \cdot (1 - d)] \right\} \quad (11-150)$$

where:

$K_d$  = Thermal Conductivity, W/m-K, for as-fabricated fuel density "d"  
 $d$  = density in fraction of TD

The range of applicability of the modified NFI correlation is provided by volume 4 of the NUREG/CR-6534 (Lanning et al., 2005) as follows:

Temperature = 300 – 3000 K  
 Rod-Average Burnup = 0 – 62 GWD/MTU  
 As-fabricated Density = 92 – 97 % TD

### Specific Heat

The specific heat in Btu/lbm-°F for uranium dioxide is given by:

$$c_{P_{UO_2}} = \left( 2.388 \times 10^{-4} \right) \left\{ \frac{K_1 \theta^2 \exp(\theta/T_K)}{T_K^2 [\exp(\theta/T_K) - 1]^2} + K_2 T_K + \frac{F_{OM}}{2} \frac{K_3 E_D}{RT_K^2} \exp(-E_D/RT_K) \right\} \quad (11-151)$$

where  $T_K$  is the temperature in degrees K and

$\theta$  = Einstein temperature (535.285 K)  
 $R$  = 8.3143 (J/mol-K)  
 $K_1$  = 296.7 (J/kg-K)  
 $K_2$  =  $2.43 \times 10^{-2}$  (J/kg-K<sup>2</sup>)  
 $K_3$  =  $8.745 \times 10^7$  (J/kg)  
 $E_D$  =  $1.577 \times 10^5$  (J/mol)  
 $F_{OM}$  = oxygen/metal ratio (2.0)

### **Model as Coded**

The equations representing the density, thermal conductivity and specific heat for uranium dioxide are coded into WCOBRA/TRAC-TF2 as described by Equations 11-145 through 11-151 without modification.

Calculations for uranium dioxide density are performed in subroutine SETUP, those for thermal conductivity in subroutines SSTEMP and TEMP, and those for specific heat in subroutines TEMP and MOVE. Values of conductivity and specific heat versus temperature are shown in Figures 11-29, 11-30 and 11-31.

### **Scaling Considerations**

Not applicable.

## Conclusions

The WCOBRA/TRAC-TF2 correlations for UO<sub>2</sub> density and specific heat are based on MATPRO-9 and MATPRO-11. The correlation for UO<sub>2</sub> thermal conductivity is the modified NFI model used in FRAPCON 3.3. The models and correlations for these properties were used in simulations of LOFT. Therefore, the uncertainty and reliability of these models is accounted for in the overall code bias and uncertainty.

### 11.4.2 Zircaloy-4

#### Model Basis

The material properties of Zircaloy-4 are based on MATPRO-9 and MATPRO-11 calculations.

#### Density

The (cold) density of Zircaloy-4 clad material is assumed to be  $\rho_{Zr} = 409.0 \text{ lbm} / \text{ft}^3$ .

#### Thermal Conductivity

The thermal conductivity in Btu/hr-ft-°F for Zircaloy-4 clad is given by:

$$k_{Zr} = 0.5779 \cdot [7.51 + 0.0209T_K - (1.45 \times 10^{-5})T_K^2 + (7.67 \times 10^{-9})T_K^3] \quad (11-152)$$

where  $T_K$  is temperature in degrees Kelvin.

#### Specific Heat

WCOBRA/TRAC-TF2 calculates the specific heat for Zircaloy-4 by linearly interpolating between values from a built-in table. Table 11-14 lists the values used to determine the specific heat of Zircaloy-4.

#### Model as Coded

The equations for the density, thermal conductivity and specific heat of Zircaloy-4 are coded into WCOBRA/TRAC-TF2 as described above without modification. Density is calculated in subroutine SETUP and HEAT, conductivity in subroutines STEMP, TEMP, and HEAT and specific heat in subroutines TEMP, HEAT, and MOVE. Curves of conductivity and specific heat versus temperature are shown in Figures 11-32 and 11-33.

#### Scaling Considerations

Not applicable.

## Conclusions

The WCOBRA/TRAC-TF2 correlations for the density, thermal conductivity, and specific heat of Zircaloy-4 are based on MATPRO-9 and MATPRO-11. These property relations were used in simulations of LOFT.

### 11.4.3 ZIRLO<sup>®</sup> Alloy

#### Model Basis

The ZIRLO<sup>®</sup> alloy developed by Westinghouse represents a modification to Zircaloy-4 which was achieved by reducing the tin and iron content, eliminating the chromium, and adding a nominal one percent niobium. Table 11-15 shows a comparison of the two alloys.

Since tin is an alpha phase stabilizer and niobium is a beta phase stabilizer, the reduction in tin and the addition of niobium result in reductions in the temperatures at which the ZIRLO<sup>®</sup> alloy undergoes the alpha to beta phase change, relative to Zircaloy-4. Measurements performed by Westinghouse show that the ZIRLO<sup>®</sup> alloy starts the transformation at 1023 K and ends at 1213 K.

Since the ZIRLO<sup>®</sup> and Zircaloy-4 alloys are both about 98 percent zirconium, it should not be expected that the material properties are significantly different, except to the extent that they are affected by the differences in the phase change temperatures. Density, thermal expansion, thermal conductivity, and specific heat of both alloys have been measured by the Properties Research Laboratory using samples cut from Westinghouse production tubing (Taylor, Groot, and Larimore, 1989). Evaluation of the test results indicated that the materials are sufficiently similar that the Zircaloy-4 material properties can be used for the ZIRLO<sup>®</sup> alloy, with the exception of the specific heat (Davidson and Nuhfer, 1990). The specific heat of the ZIRLO<sup>®</sup> alloy is based on an adjustment to Table 11-14, which considers the difference in phase change temperatures.

#### Density

The (cold) density of the ZIRLO<sup>®</sup> cladding material is taken to be identical to that of Zircaloy-4 (409.0 lbm/ft<sup>3</sup>).

#### Thermal Conductivity

The thermal conductivity of the ZIRLO<sup>®</sup> cladding material is taken to be identical to that of Zircaloy-4, given by Equation 11-152.

#### Specific Heat

The specific heat shown in Table 11-14 for Zircaloy-4 includes both the true specific heat and the alpha to beta phase heat of transformation. The specific heat for the ZIRLO<sup>®</sup> cladding material was obtained by adjusting Table 11-14 to account for the difference in phase change temperatures, assuming both the true specific heat and the heat of transformation are the same for the two alloys. The true specific heat is taken

to be equal to the total specific heat in Table 11-14 for  $T \leq 1090$  K,  $0.085$  Btu/lbm-°F for  $T \geq 1213$  K,  
and:

$$\left[ \dots \right]^{a,c} \quad (11-153)$$

$$\left[ \dots \right]^{a,c} \quad (11-154)$$

where:

$$\left[ \dots \right]^{a,c} \quad (11-155)$$

WCOBRA/TRAC-TF2 calculates the specific heat for the ZIRLO<sup>®</sup> cladding material using the resulting total specific heat values, shown in Table 11-16.

### Model as Coded

The density, thermal conductivity, and specific heat of the ZIRLO<sup>®</sup> cladding material are coded into WCOBRA/TRAC-TF2 as described above, without modification. Figure 11-34 shows a comparison of specific heat for ZIRLO<sup>®</sup> cladding material with that of Zircaloy-4.

### Scaling Considerations

Not applicable.

### Conclusions

Comparisons of the material properties for the ZIRLO<sup>®</sup> and Zircaloy-4 cladding materials have shown that the Zircaloy-4 relations for density and thermal conductivity can also be applied to the ZIRLO<sup>®</sup> alloy. The difference in the phase change temperatures of the two alloys requires that different specific heat correlations be used. The specific heat correlation for the ZIRLO<sup>®</sup> alloy is based on an adjustment to the Zircaloy-4 correlation, which accounts for the different phase change temperature range. This correlation will be used for analyses of nuclear reactors which utilize the ZIRLO<sup>®</sup> cladding material.

$$\left[ \dots \right]^{a,c}$$

### 11.4.4 Fuel Rod Gas Mixtures

#### Model Basis

For the gas mixture in the fuel-clad gap, only the thermal conductivity is calculated. The fill gas in the WCOBRA/TRAC-TF2 fuel rod model assumes that the gas is a mixture composed of helium, xenon, argon, krypton, hydrogen, and nitrogen. The thermal conductivity of the gas mixture as a function of temperature is determined, as described in MATPRO-11 Rev. 1 (Hagrman, Reymann, and Mason, 1980), from the relation:

$$k_{\text{gas}} = \sum_{i=1}^N \frac{k_i}{1 + \sum_{\substack{j=1 \\ j \neq i}}^N \psi_{ij} \frac{n_j}{n_i}} \quad (11-156)$$

where  $N$  = number of component gases, and where:

$$\psi_{ij} = \Phi_{ij} \left[ 1 + 2.41 \frac{(M_i - M_j)(M_i - 0.142M_j)}{(M_i + M_j)^2} \right] \quad (11-157)$$

and

$$\Phi_{ij} = \frac{\left[ 1 + \left( \frac{k_i}{k_j} \right)^{1/2} \left( \frac{M_i}{M_j} \right)^{1/4} \right]^2}{2^{3/2} \left( 1 + \frac{M_i}{M_j} \right)^{1/2}} \quad (11-158)$$

where:

- $M_i$  = molecular weight of gas species  $i$
- $n_i$  = mole fraction of gas species  $i$
- $k_i$  = thermal conductivity of gas species  $i$

The thermal conductivities of the six component gases are evaluated in Btu/hr-ft-°F as a function of temperature from the following relations:

<u>Gas</u>	<u><math>k</math>(Btu/hr-ft-°F)</u>	
Helium	$(1.314 \times 10^{-3}) \Gamma_{\text{gas}}^{0.668}$	(11-159)
Argon	$(1.31 \times 10^{-3}) \Gamma_{\text{gas}}^{0.701}$	(11-160)

$$\text{Krypton} \quad (1.588 \times 10^{-5}) T_{\text{gas}}^{-0.92331} \quad (11-161)$$

$$\text{Xenon} \quad (1.395 \times 10^{-5}) T_{\text{gas}}^{0.872} \quad (11-162)$$

$$\text{Hydrogen} \quad (5.834 \times 10^{-4}) T_{\text{gas}}^{0.8213} \quad (11-163)$$

$$\text{Nitrogen} \quad (7.35 \times 10^{-5}) T_{\text{gas}}^{0.846} \quad (11-164)$$

where:

$$T_{\text{gas}} = \text{gas temperature } (^{\circ}\text{R})$$

### Model as Coded

Equations 11-156 through 11-164 for gap gas thermal conductivity are coded in WCOBRA/TRAC-TF2 as described without modification in subroutine GTHCON.

### Scaling Consideration

Not applicable.

### Conclusions

Thermal conductivity for the gas mixture in the fuel-clad gap is calculated using the equations in MATPRO-11 Rev. 1 (Hagrman, Reymann, and Mason, 1980).

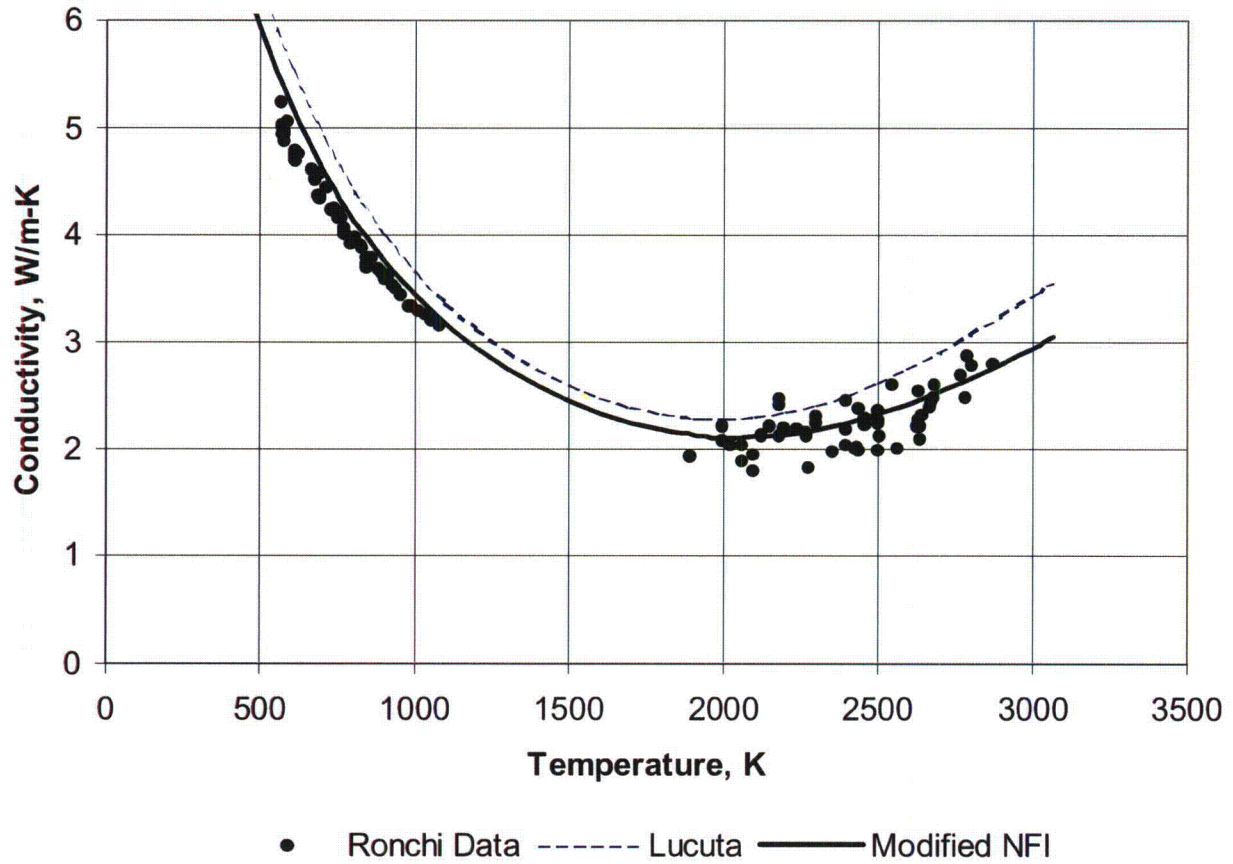


**Figure 11-29** Modified NFI and Lucuta Model Predictions Compared to Measured Conductivity on Unirradiated Pellet Material (Ronchi et al., 1999), from Figure 2.4 of (Lanning et al., 2005)

**Updates to Sections 25.1, 25.2 and 25.8 of WCAP-16996-NP**

**“Realistic LOCA Evaluation Methodology Applied to the Full**

**Spectrum of Break Sizes**

**(FULL SPECTRUM LOCA Methodology)”**

## 25 PLANT SOURCES OF UNCERTAINTY

We have, to this point, assessed the ability of WCOBRA/TRAC-TF2 to simulate the key phenomena identified in the PIRT. In addition, it has been demonstrated that compensating errors or bias, due to the increase in scale from the experiments to the **pressurized water reactor (PWR)**, result in a more conservative estimate of the LOCA analysis results relative to several key phenomena. However, there may be differences in PWR response to the LOCA, which may result in some models being more important for the PWR than for the experiment. In addition, variability in plant initial and boundary conditions introduce additional uncertainty. In this section, these additional aspects are discussed. The objective of this section is to develop a plan for performing various sensitivity or scoping studies with the PWR models described in Section 26, in order to identify those parameters which have an important influence on the calculation of the **peak cladding temperature (PCT)** in the PWR, and to make decisions about which variables should be considered for uncertainty propagation.

For some parameters, the uncertainty will be explicitly treated within the uncertainty analysis. For other parameters, a bounding approach may be employed (such as for the containment back-pressure).

### 25.1 PLANT PHYSICAL CONFIGURATION

The plant physical configuration consists of those parameters which define the geometrical and hydraulic configuration of the reactor at the time the LOCA occurs. These parameters are listed and defined below:

1. Dimensions
2. Flow resistances
3. Pressurizer location, relative to broken loop
4. Accumulator Tank Elevation
5. Hot assembly location, relative to vessel upper internals
6. Hot assembly type
7. Steam generator tube plugging level

#### Dimensions

Reactor dimensions, volumes, and surface areas are obtained directly from component drawings. Some variability exists in these dimensions due to tolerances and approximations which may have been made in geometrical calculations. Dimensions also vary from nominal due to thermal expansion. Thermal expansion is estimated to increase volumes by about [

] <sup>a,c</sup>

Fuel assembly grids, control rod guide tubes, and steam generator tubes may be affected, in some cases, by high stresses resulting from the combination of seismic and LOCA loads, an assumption required by 10 CFR 50, Appendix A, General Design Criterion 4. A dynamic analysis of the Reactor Coolant System (RCS) under combined seismic and LOCA loads is performed to demonstrate that key RCS components will continue to perform their safety function. Structural analyses performed as part of the original plant design basis have confirmed that Emergency Core Cooling System (ECCS) safety function and core

shutdown capability are maintained. These analyses have also indicated that for some plants, the pressure differentials and structural movements which are predicted may result in minor deformation of fuel assembly grids, control rod guide tubes, and/or steam generator tubes. In the case of the fuel assembly, some crushing of the grids in assemblies at the periphery of the core may be calculated. This may push fuel rods closer together, reducing the available flow area. Steam generator tubes may be slightly deformed at support plate locations, reducing the flow area through the tube bundle and increasing the flow resistance during reflood. For larger breaks, control rod guide tubes may be displaced from their nominal positions, preventing control rod insertion and causing the core to shutdown on voids early in the LOCA, and to remain shut down due to boron alone. These deformations, while not compromising safety functions, were found to affect the LOCA analysis results.

The combined effects of LOCA and seismic loads may potentially lead to some degree of grid crushing in the core, due to the baffle plates impacting the peripheral assemblies. If the impact on the peripheral assemblies is large enough, these assemblies may subsequently impact in-board assemblies, and so on. If the loads are large enough for grid damage to occur, test data and analyses show that the damage is typically limited to no more than two rows or rods per assembly, with elevations towards the mid-plane of the core.

[

] <sup>a,c</sup>

---

[

] <sup>a,c</sup>

[

] <sup>a,c</sup>

### Modeling Approach

[

] <sup>a,c</sup>

### **Flow Resistance**

The flow resistance in the vessel and loops during a LOCA is as much a function of the models used to calculate the friction factor, as it is the plant configuration. However, flow resistance is included in this category because some changes in plant configuration affect this parameter. The steady-state hydraulic resistance of virtually all the major components in a PWR was determined from scaled testing. The accuracy of the loss coefficients obtained from these tests has, over the years, been confirmed by the accurate prediction of steady-state flow and temperature conditions of operating reactors during numerous plant startup cycles. The accuracy of these predictions, using loss coefficients for subcomponents which are typically subject to large uncertainties may also be a result of the fact that the pressure distribution in a reactor circuit consists of many components. [

] <sup>a,c</sup> The uncertainty in  
the pressure drop under LOCA transient conditions is discussed in Section 29.1.2.

When the LOCA occurs, reverse flow through some components and two-phase flow may significantly increase the uncertainty of the predicted flow resistance. One area in particular where reverse flow introduces additional resistance not present during normal operation is the broken cold leg inlet nozzle. Another area where additional resistance is introduced is the broken loop pump.

During several large scale ECCS tests conducted in the past years, it was observed that there was a significant pressure drop across the inlet nozzle of the broken cold leg. In the Cylindrical Core Test Facility (CCTF) reflood tests, this pressure drop was observed to result in a significant pressurization of the downcomer during reflood, resulting in increased reflood rates (Akimoto et al., 1984). Part of this loss was attributed to the increased dynamic head resulting from the reverse flow from a large reservoir, the reactor vessel, to the cold leg nozzle. Other contributors were losses associated with two-phase flow. A review of recent Upper Plenum Test Facility (UPTF) data has confirmed this finding as described in Section 29.1.2.

During a cold leg break, the flow rate through the broken loop pump increases substantially, to the point where the pump acts as a resistance. The effect of this additional flow resistance must also be taken into account, and is a source of additional uncertainty. The flow in the intact loop typically continues in the same direction at lower flow rates, therefore the predicted pressure drop is less subject to uncertainty.

#### Modeling Approach

[

] <sup>a,c</sup>

#### **Pressurizer Location**

The pressurizer may be on the broken loop or one of the unbroken loops. Its location arises as a source of uncertainty because it may introduce some asymmetry into the reactor configuration at the time of the LOCA.

#### Modeling Approach

[

] <sup>a,c</sup>

#### **Accumulator Tank Elevation**

The accumulator tanks may sit below, at, or above the cold leg elevation. The elevation of the accumulator relative to the cold leg will impact the maximum flow during accumulator injection, the duration of accumulator injection, and the amount of liquid which remains in the accumulator after accumulator injection into the cold leg terminates.

### Modeling Approach

[

] <sup>a,c</sup>

### **Hot Assembly Location**

Approximately 40 percent of the fuel assemblies in the core of a PWR lie beneath control rod guide tubes which extend into the upper head. These guide tubes, arranged in an approximate checkerboard pattern, house reactor control rods used for reactor control and shutdown, and extend into the reactor vessel upper head. The remaining fuel assemblies lie below open holes in the core plate, flow mixers attached to the core plate, or support columns of several possible designs (Section 26). As a result, for larger breaks (during the blowdown phase) the fuel assemblies will receive varying amounts of flow from the upper head and upper plenum depending on their position. [

] <sup>a,c</sup>

### Modeling Approach

The configuration of the guide tubes is such that specific modeling of these flowpaths is considered necessary, particularly in view of the connection to the upper head, which contains a large volume of water. Consequently, the core and upper plenum geometry in the WCOBRA/TRAC-TF2 model is designed to specifically include separate channels for guide tubes and core plate open hole locations. As described in Section 26, each reactor internal layout is examined, and the hot assembly is located where reduced direct flow is expected to occur.

### **Hot Assembly Type**

The basic design of a PWR fuel assembly has remained essentially unchanged through the years; the standard Westinghouse fuel assembly, for example, consists of an array of fuel rods in a 14x14, 15x15, 16x16 or 17x17 square matrix. Approximately 90 percent of the matrix is occupied by fuel rods; the remainder is occupied by thimble tubes. Five or more spacer grids hold the array together; some or all of the grids contain mixing vanes which serve to enhance flow turbulence, improving heat transfer during normal operation.

Variations in this standard design may occur to achieve improved fuel utilization. Typical changes made to a fuel assembly design are the following:

1. Changes in Fuel Rod Diameter – The fuel rod may be “optimized” by reducing its diameter, thus reducing the overall amount of fuel required. These changes are marginal in nature. For example, the standard Westinghouse 14x14 fuel rod diameter is 0.422 inches. For the optimized designs the diameter is 0.400 inches. Since smaller rods are designed to the same linear powers as standard rods, their surface heat fluxes and adiabatic heating rates are slightly higher. On the other hand, the amount of coolant in the core is also higher, because of the larger flow area.

2. Changes in Grid Design – The grid may be made of stainless steel, Inconel, or zirconium alloys. Typically, if the fuel rod diameter has been changed, the grids are modified slightly such that the overall hydraulic loss is the same as the standard design.

An additional design improvement is to incorporate additional mixing vane grids along portions of the rod, which further improve heat transfer characteristics, and offset reductions in departure from nucleate boiling (DNB) margin brought about by a smaller rod.

3. Changes in Fuel Enrichment – Axial and radial “blankets” are sometimes provided to reduce neutron leakage from the core. These blankets consist of regions of low reactivity fuel, or annular fuel. These blankets affect the axial and radial power distribution in the core, and are explicitly considered when these distributions are calculated.
4. Burnable Absorbers – Burnable absorbers are often used to reduce soluble boron requirements and improve power distributions. Burnable poisons may be discrete (i.e., loaded in thimbles) or integral (i.e., coatings or dopings of the fuel). Burnable absorbers affect axial and radial power distributions in the core, and are explicitly accounted for in core design calculations. Integral absorbers may also cause the internal pressure of the fuel rod, which generally increases with burnup, to increase at a different rate. Rod internal pressure causes swelling and possible burst during the LOCA.
5. Changes in Cladding Material – New alloys more resistant to corrosion are being developed. Their plastic strain characteristics may be different, and may therefore affect the LOCA results.
6. Other Changes – Minor modifications in upper and lower fuel assembly tie plates, mixing vane grid design, and removal of thimble plugging devices, are other changes which may occur from reload to reload, but which are not expected to change the LOCA results significantly.

### Modeling Approach

[

] <sup>a,c</sup>

### **Steam Generator Tube Plugging Level**

Steam generator tubes may require plugging for various reasons. Typically, tube plugging takes place during a normal outage. Plugs are inserted into each end of the degraded tube. This removes the tube completely from the RCS volume, and reduces the total flow area through the steam generator. The increased resistance and reduced volume may affect the blowdown transient and reflood behavior for larger breaks or the loop seal clearing in small breaks, and is a variation which must be considered in the LOCA analysis.

## Modeling Approach

[

] <sup>a,c</sup>

### 25.2 PLANT INITIAL OPERATING CONDITIONS

Reactor operating conditions and their variations are described by two groups of parameters:

1. Core power parameters. These parameters define the core power distribution and fuel stored energy at the time of the LOCA.
  - a. Total core power
  - b. Peak linear heat rate (PLHR)
  - c. Hot assembly peak linear heat rate
  - d. Hot rod average power
  - e. Hot assembly average power
  - f. Axial power distribution
  - g. Low power region relative power
  - h. Time-in-Cycle
  - i. Reactor operating power history
  - j. Moderator temperature coefficient (MTC)
  - k. Hot full power (HFP) boron concentration
  
2. Reactor primary fluid conditions. These parameters describe the primary fluid thermodynamic state at the time of the LOCA.
  - a. Core average fluid temperature
  - b. Pressurizer pressure
  - c. Loop flow rate
  - d. Upper head fluid temperature
  - e. Pressurizer level
  - f. Accumulator water temperature
  - g. Accumulator pressure
  - h. Accumulator water volume
  - i. Accumulator line resistance
  - j. Accumulator boron concentration

The basis for the choice of these parameters is discussed in the following sections.

#### 25.2.1 Core Power Parameters

A summary of the core modeling is given below. There are four core channels and [

] <sup>a,c</sup>

[

] <sup>a,c</sup> simulation the following fuel rods are modeled:

Rod 1: The rod with the highest linear heat rate [ <sup>a,c</sup> assumed to also have the highest average power and to reside in the assembly with the highest average power.

Rod 2: All the other (average) rods in the highest power assembly [ <sup>a,c</sup>

Rod 3: All the average rods in the assemblies residing under non-guide tube structures (e.g. support columns, free standing mixers, orifice plates, and open holes).

Rod 4: All the average rods in the assemblies residing under guide tubes.

Rod 5: All the average rods in the assemblies residing on the periphery of the core.

[

] <sup>a,c</sup>

There are three distinct regions (the hot assembly, the two average channels, and the low power channel) which serve to resolve the radial power distribution in the core.

Each fuel rod group has parameters describing the peak linear heat rate, the average linear heat rate, the axial distribution of power, and the number of physical rods modeled by the rod group. [

] <sup>a,c</sup>

The axial and radial core power distributions are of basic importance to the uncertainty analysis. The parameters which affect these distributions, and their variations, are described in the following section.

#### 25.2.1.1 Core Power Distributions

The nuclear design of the reactor core meets constraints on the local power distribution in the fuel. Power distributions are typically characterized in terms of hot channel factors. These factors relate peak pellet power and hot rod power to core average quantities. These factors and other terms which will be used are defined below:

Core average heat flux (AFLUX) is the average thermal power produced per unit length of active fuel, kW/ft.

Peak linear heat rate (PLHR) is the maximum linear heat rate produced in the reactor, kW/ft.

Hot assembly peak heat rate (HAPHR) is the peak linear heat rate of an average rod in the hot assembly, kW/ft.

Hot assembly average power (HAFLUX) is the average power per unit length in the hot assembly, kW/ft.

Hot rod average power (HRFLUX) is the average power per unit length in the hot rod, kW/ft.

Total peaking factor ( $F_Q$ ) is the ratio of the peak linear heat rate to the core average linear heat rate (PLHR/AFLUX).

Enthalpy rise peaking factor ( $F_{\Delta H}$ ) is the ratio of hot rod average power to core average linear heat rate (HRFLUX/AFLUX).

PWR power distributions are often separated into their respective radial and axial components. The radial component is sensitive to the fuel and absorber loading pattern and the presence of control rods. Radial distributions change slowly with time and fuel depletion and are relatively insensitive to power level, xenon concentration/distribution, axial burnup distribution, and axial fuel design feature. By contrast, PWR axial distributions are relatively insensitive to the loading pattern but are quite sensitive to control bank position, xenon concentration/distribution, coolant density distribution, and reactor power.

The existence of this radial/axial power distribution separability has historically been utilized by the nuclear designer. As noted above, PWR radial power distributions are slowly varying in time, provided that the presence of control rods is accounted for accurately. Axial power distributions are dependent on cycle time as well as plant operating parameters such as current power level, recent changes in power level/distribution, prior operating history, control bank position (or operating strategy), and the time during a transient power maneuver (or the xenon distribution). These characteristics allow the analysis of transient three-dimensional power distributions to be performed by superposition of transient axial power distributions on steady-state, appropriately rodded, radial power distributions rather than the rigorous direct solution for the three-dimensional power distribution. While the methods and calculations used to design reload cores are extremely reliable, and have been confirmed by measurements taken in many operating reactors, it is a normal practice to design cores with some margin, such that measured power distributions will always fall below the core power limits, even when measurement uncertainties are added. These core power limits are determined from the body of safety analyses which support the FSAR and Technical Specifications, and ensure that regulatory limits will not be exceeded for any postulated transient.

Assembly power distributions in a typical Westinghouse designed PWR reload core are shown in Figures 25.2-1 and 25.2-2. The radial power distribution can typically be divided into three core regions: a low power peripheral region, high power assemblies distributed throughout the core (feed or non-feed), and average power regions also distributed throughout the core. These figures show the predicted power of assemblies in a reload core. This is a typical low leakage core loading pattern, in which low power assemblies are situated around the periphery of the core, while high power assemblies are in the interior of the core.

[

] <sup>a,c</sup>

Within the fuel assembly, individual fuel rods vary in power due to the presence of burnable absorbers and water holes near the thimble tubes. Figure 25.2-3 is a histogram showing the distribution of rod powers within the high power assembly of several different Westinghouse fuel designs. The powers are expressed as a fraction of the maximum power allowed by the Technical Specifications. The maximum calculated rod power is therefore more than [ ]<sup>a,c</sup> lower than the maximum allowed value, to accommodate measurement uncertainties during surveillance and up to additional [ ]<sup>a,c</sup> for “good measure” or operational allowance. It can be seen that most of the fuel rods are at powers near the middle of the distribution, and that the hot assembly power distribution can be modeled with a single average rod and a single hot rod. The cumulative distribution is shown in Figure 25.2-4, and the average hot assembly power calculated from these distributions summarized in Table 25.2-1, and is seen to lie approximately [ ]<sup>a,c</sup> below the maximum calculated (hot rod) value.

The steady-state axial power distribution also varies as a function of time. Figure 25.2-5 shows the core average axial power distribution near the beginning of cycle, near the middle of cycle and near the end of cycle for a typical reload core. During the cycle, the steady-state axial peak moves away from the center of the core as the core is depleted. The depletion of the center of the core also affects any transient axial power distributions.

While a PWR is designed to easily follow load demand, the most likely state of the reactor is full power and equilibrium conditions. Under these conditions, the axial peaking is relatively low. Measurements taken of the maximum peaking factor at hot full power (HFP), nominal conditions are usually well below the Technical Specification limits. The margin to peaking factor limits is intended to allow for the less frequent occurrence of transient reactor operation, usually consisting of power reductions and increases to follow load. [ ]<sup>a,c</sup>

In summary, it is seen that the design of a core (its geometry, fuel enrichment, and loading pattern) establishes the maximum radial peaking in the core. The radial distribution is determined almost entirely by the core loading, and cannot be easily changed by external controls in normal operation. Hence, to assure that the measured hot rod power will always lie below the limit, core designs are set allowing for additional margin beyond the four percent required by Technical Specifications.

### 25.2.1.2 Transient Power Distributions

Short term changes in reactor power distributions are typically attributable to changes in reactor power level. Changes in power level may require control rod motion, and result in changes in coolant density profiles and xenon distribution. Changes in xenon distribution are a strong function of the magnitude and duration of the power change maneuver as well as the operating strategy used during the maneuver.

Westinghouse and Combustion Engineering (CE) core design methodologies used to generate axial power distributions have been previously reviewed by the USNRC. Distinct methods are employed in design based on the axial flux difference (AFD) Technical Specifications employed. (AFD is a measure of the axial power distribution, and is the axial flux difference between the top and bottom halves of the core.)

Westinghouse plants use the Constant Axial Offset Control (CAOC) or Relaxed Axial Offset Control (RAOC) core design method. The CAOC methodology (Morita et al., 1974) requires the core designer to

simulate various types of load follow maneuvers throughout the cycle to establish the limiting axial power distributions. The approach taken is conservative in that daily load follow swings to various power levels are assumed throughout the cycle. This method is used with plants whose AFD Technical Specification is defined as an allowable band (typically  $\pm 5$  percent) about a target AFD.

Another approach is used for plants with a fixed AFD Technical Specification. The RAOC methodology (Miller et al., 1983) considers the core parameters (power level, xenon distribution, and control rod position) that can affect power distributions and establishes the maximum variability possible in these parameters throughout a given cycle. These parameters are then treated as independent variables and all possible combinations are checked. Any axial shapes that are found to be within the AFD operating space defined by the Technical Specifications are taken to be possible.

CE plants do not control via AFD. Instead their monitoring and protective systems use the concept of axial shape index (ASI) (Combustion Engineering, 1986; Combustion Engineering, 1998; Combustion Engineering, 1975). ASI is similar to AFD, in that ASI is also a measure of the axial power distribution, and is the negative of percent axial offset divided by 100.

Typical transient distributions generated by the CAOC methodology are shown in Figures 25.2-6 through 25.2-8 for different times throughout the cycle. [

] <sup>a,c</sup>

An additional characteristic of these transient power shapes is that fission products do not have sufficient time to build up in the high power region of the fuel rod. Consequently, if the reactor was shut down for any reason at the time the maximum transient linear shapes occurred, the decay heat generated is substantially lower at the peak power location than if the core had been operating indefinitely at these PLHR's. This phenomenon is not credited in the FULL SPECTRUM LOCA methodology.

The reactor heat source is made up of three major constituents. Fission energy is by far the largest component of the heat, comprising from roughly 93 to 100 percent of the total heat source for full power operation. The stored energy contribution to the LOCA transient is, therefore, directly related to the fission rate distribution at the time of the LOCA. The magnitudes of the decay and actinide heat sources make them a small contribution to the stored energy component. The decay and actinide components are, however, the principal contributors to core heat generation later in the LOCA transient since the fission rate during this portion of the transient is negligible. The decay and actinide heat sources are independent of the instantaneous fission rate at any given point in time but dependent upon the fission rate time history. Their concentrations determine the decay power available since the decay power for radionuclide decay is determined by the product of the energy release per decay, the decay constant, and the concentration. The concentration of a non-absorbing fission product is dependent upon the fission rate

time history, the fission product yield per fission, and the decay constant. Since the yield and time constant for a given fission product are constant for a specified isotope, the time dependent fission product concentration depends only upon the fission rate time history.

Decay heat is the result of a multitude of radionuclide decays (approximately 350 isotopes). These decay processes have been simplified in the ANSI/ANS 5.1-1979 decay heat standard to a summation of 23 exponentials for each fissile isotope. In the absence of significant absorption or isotope decay chain cross-coupling, the ANSI/ANS 5.1-1979 decay heat standard is a 23 group “pseudo-nuclide” representation of the fission product decay process. The magnitude of the decay heat source at any given point in the reactor, therefore, depends on the time history of the fission rate. The decay heat source for a given point in the reactor will be in effective equilibrium (production rate = decay rate) only if the fission rate has been maintained for the period of time corresponding to ten to twenty time constants for that nuclide. Figure 25.2-10 illustrates a point evaluation of decay equilibrium fraction versus sinusoidal fission rate period. [

] <sup>a,c</sup>

### 25.2.1.3 Power Distribution Uncertainties

After a core has been designed and loaded, it is monitored to confirm that the core operates as designed, and to ensure that the reactor is operating within specified limits. The detailed reactor power distribution is monitored by means of in-core detectors. (There are several other core monitoring systems as well.) The readings from these detectors (which are fission chambers and convert the local neutron flux to a current signal) are transformed to fission rate distributions using analytical factors, based on the specific core design (Spier et al., 1988).

The core power distribution is measured during steady-state operation at regular intervals. The following quantities are typically obtained as the result of measurement and data processing:

- $F_{\Delta H}$  The enthalpy rise hot channel factor is the ratio of the integral of local power along the rod (pin) with the highest integrated power in the core to the average rod power.
- $F_{xy}(z)$  The elevation dependent radial peaking factor is the maximum local power density in the plane at elevation  $z$  divided by the average power density of the plane.
- $F_Q(z)$  The elevation dependent heat flux hot channel factor is the maximum local linear power density at elevation  $z$  divided by core average linear power density.

Because the above peaking factors are derived from a combination of instrument measurements and analytical model calculation, the uncertainty associated with these factors is a combination of the two factors.

The peaking factors defined above are typically measured on a monthly basis. In addition to the peaking factors defined above, the core axial flux difference is measured on a continual basis by the ex-core

nuclear detectors. This measurement is equivalent to the axial flux difference discussed previously, and provisions are incorporated in the plant computer to provide alarms if limits are exceeded.

The calculational uncertainty on radial power distribution ( $F_{\Delta H}$ ) has been shown (Spier et al., 1988) to be bounded by a factor of [ ]<sup>a,c</sup> through benchmarks to critical experiments and other data. There is also an additional uncertainty associated with measuring the radial power distribution, which is bounded by a factor of four percent. It is desirable to assure that the plant will not routinely experience flux map measurements which exceed the ( $F_{\Delta H}$ ) limit after a four percent uncertainty is applied due to combined effects of calculational and measurement uncertainties. To accomplish this, Westinghouse standard practice is to design the core such that it is predicted to be at least [ ]<sup>a,c</sup> below the ( $F_{\Delta H}$ ) limit on a best-estimate basis. With this approach, the most probable condition is for the core to be measured at least [ ]<sup>a,c</sup> below the Technical Specification limit after measurement uncertainty is applied. Typical measurements shown in Figure 25.2-11 show this is indeed the case.

The margin inherent in the design as it relates to the total peaking factor  $F_Q(z)$  is also reflected in typical measurements. Design calculations are performed to conservatively calculate the possible effects of adverse xenon distributions on the maximum total peaking factor. These penalty factors are generated assuming xenon transients are initiated in the core and shift the axial distribution to the full range allowed by the AFD Technical Specifications. The most probable condition for the core is at an equilibrium xenon condition which will produce  $F_Q$  values well below the limits. The total peaking factor measurement for a typical core during a cycle is shown in Figure 25.2-12. The maximum measured values include an uncertainty of 8.15 percent when compared to the Technical Specification.

Nuclear design calculations are performed assuming nominal pellet diameter, density, etc. These calculations form the basis of the analytic factors used to convert in-core measurements to rod power. Manufacturing uncertainties such as pellet diameter and the effects of rod bow introduce an additional uncertainty to point measurements. These uncertainties are accounted for in the FSLOCA methodology.

Rod bow and manufacturing uncertainties are both applied to the hot rod peaking factor measurement as described in the following paragraphs. These factors are not applied to measurements of the hot assembly and hot rod power. Local linear heat rate depends on the local mass of  $UO_2$  per unit length, or more specifically, per pellet and also on the local channel geometry. The local mass varies as a result of manufacturing variations in pellet dimensions and fuel enrichment. [

] <sup>a,c</sup>

A similar statement can be made for rod bow. [

] <sup>a,c</sup>

A detailed study of the in-core flux mapping system and its accuracy was performed by Westinghouse (Spier et al., 1988). Because the “measured” values of  $F_{\Delta H}$  and  $F_Q$  are actually inferred values obtained from the raw measurement using core model group constants, error contributions from both measurement

and modeling sources were considered. Two uncertainties are defined: a measurement uncertainty, to be applied to the inferred peaking factor during normal core surveillance such that the true values are bounded at a high confidence level, and a calculational uncertainty, to be applied to the calculated peaking factors during the core design such that the true values are bounded at a high confidence level. The two uncertainties contain several common components, and so are similar in magnitude. In the best-estimate LOCA methodology, we are concerned with the calculational uncertainty of the predicted peaking factors.

The calculational uncertainty is composed of several independent subcomponents which are summarized in Table 25.2-2. Some of these components are related to uncertainties which should be applied only to the hot rod. In subsequent application of these uncertainties (Section 29.4), these components will be applied separately when considering the calculational uncertainties associated with groups of fuel rods such as the hot assembly. [

] <sup>a,c</sup>

A final uncertainty related to the power distribution is that associated with the total core power. Core power is inferred from an energy balance using feedwater flow and temperature, and steam flow and pressure. The maximum error from this measurement is typically  $\pm 2$  percent, [ <sup>a,c</sup>. Some plants have employed improved uncertainty measurement systems which reduce this uncertainty below 2 percent.

#### 25.2.1.4 Power Distribution Modeling Approach

Summarizing the preceding sections, the core power distribution is seen to exhibit the following characteristics:

1. The radial power distribution is primarily controlled by core geometry, fuel enrichment, burnable absorber loading, and core loading patterns. It is relatively insensitive to operational procedures such as load follow.
2. The axial power distribution is sensitive to operational procedures (such as load follow), which produce non-equilibrium xenon distributions in the core, and core burnup. Large axial power distribution variations have a small effect on the radial power distribution. Axial power distributions which produce the limiting  $F_Q$  occur during transient operation. [ <sup>a,c</sup>
3. The power distribution in the core is well described by the following parameters: the average linear heat rate, the hot assembly linear heat rate, the low power assembly linear heat rate, and the peak linear heat rate.

<sup>2</sup> Clarification on the determination of the rod bow uncertainty component was provided as part of RAID-6.4 in (Bajorek, et al., 1998) for prior Westinghouse best-estimate LOCA evaluation models.

4. The average power of the rods in the assembly which contains the hot rod is typically [ ]<sup>a,c</sup> or more lower than the hot rod.
5. The axial peak power may occur at any location within approximately two feet from the ends of the core, during both transient and steady-state conditions.

As described in Section 26, the PWR core is modeled with sufficient detail to resolve both the radial and axial power distributions present in the core. The radial power distribution is resolved using [ ]<sup>a,c</sup>

There are several parameters which play a role in the calculation of rod power in WCOBRA/TRAC-TF2. Each parameter, in turn, contributes some uncertainty. Based on the general discussion of power distributions, the parameters as used in WCOBRA/TRAC-TF2 are described in more detail below. A final summary of uncertainty contributors is presented later in this section, after the discussion of the fuel rod model.

As described previously, there are four core channels and [ ]<sup>a,c</sup> are defined as:

Rod 1: The rod with the highest linear heat rate [ ]<sup>a,c</sup> assumed to also have the highest average power and to reside in the assembly with the highest average power.

Rod 2: All the other (average) rods in the highest power assembly [ ]<sup>a,c</sup>

Rod 3: All the average rods in the assemblies residing under non-guide tube structures (e.g. support columns, free standing mixers, orifice plates, and open holes).

Rod 4: All the average rods in the assemblies residing under guide tubes.

Rod 5: All the average rods in the assemblies residing on the periphery of the core.

[ ]<sup>a,c</sup>

Each fuel rod has input parameters describing the average linear heat rate, and the axial distribution of power relative to the core average linear heat rate. The important parameters used in WCOBRA/TRAC-TF2 for these fuel rods are described below. The "0" designates initial, or steady-state values of parameters which will change during the LOCA transient.

The reactor power parameters described below are directly related to several quantities which are also measured in the plant during normal operation. These are the total peaking factor ( $F_Q$ ), the hot channel

factor ( $F_{\Delta H}$ ), and the AFD. Other quantities of lesser importance are the moderator temperature coefficient (MTC) and the coolant boron concentration. The Technical Specifications call for specific uncertainties and margins to be applied to the measured values of some of these quantities before they are compared to the Technical Specification limit. In the discussion below, these quantities will normally be described in terms of calculated or expected values, without local uncertainties, and will be designated with subscript BE (Best-Estimate).

**Initial Core Average Linear Heat Rate**

The parameter defining core power in WCOBRA/TRAC-TF2 is the core average linear heat rate, calculated by:

$$AFLUX(0) = P(0)/(NFR*L) \tag{25-1}$$

where:

- L = nominal active fuel length
- P(0) = initial core power
- NFR = total number of fuel rods

There is a tendency for the fuel pellet stack (L) to shrink during the cycle, which would increase AFLUX based on Equation 25-1. However, [

] <sup>a,c</sup> The only uncertainty affecting AFLUX is the core power measurement uncertainty, which results from calorimetric errors in measuring feedwater flow and temperature. As noted in Section 25.2.1.3, the range of this error is estimated as [ ] <sup>a,c</sup>

The axial power distributions of the core average rods (Rods 3, 4, and 5) are [

] <sup>a,c</sup> These distributions will be illustrated later in the section, when the power distribution modeling is described.

**Peak Linear Heat Rate (PLHR)**

The peak linear heat rate (PLHR) for the hot rod (Rod 1) [ ] <sup>a,c</sup> defined by:

$$\left[ \right]_{a,c} \tag{25-2}$$

[

] <sup>a,c</sup>

[

] <sup>a,c</sup>

For the hot rod, the PLHR can also be expressed as,

[

] <sup>a,c</sup>

(25-3)

[

] <sup>a,c</sup>

The variation due to transient operation is the result of assumed load follow operations and other operational transients, which introduce relatively short lived skewed power shapes with relatively high peaking factors compared to equilibrium conditions, when the plant returns to full power. Limiting transient power distributions are generated during the core design analysis to confirm that maximum values remain below limits established in the Technical Specifications. The calculated maximum peaking factor is obtained from the [core design analysis using approved core design methods](#).

[

] <sup>a,c</sup>

**Hot Assembly Rod Peak Linear Heat Rate**

The hot assembly rod peak linear heat rate is defined as:

$$\left[ \right]^{a,c} \quad (25-4)$$

[

] <sup>a,c</sup>

Therefore HAPHR(0) can be written as:

$$\left[ \right]^{a,c} \quad (25-5)$$

Typically, the relationship in power of the hottest rod in an assembly to the assembly average will depend upon details in the design of that assembly, such as the location of the hot rod in the assembly. In this

analysis, it is conservatively assumed that the [ ]<sup>a,c</sup> and the peak power is offset by a constant factor equal to the difference in average power. Further discussion of the validity of this assumption is provided in the next subsection.

There are two items to consider when developing the relationship between the hot rod, which is a single rod, and the hot assembly rod, which represents the average of all the rods in the hot assembly minus the hot rod. The first item is the actual difference between the hot rod and the hot assembly rod powers. The second is the difference in the uncertainty associated with various quantities for the hot rod and the hot assembly rod.

Examination of rod census data indicates that the minimum difference between the hot rod and the hot assembly average rod is [ ]<sup>a,c</sup>. Absent all uncertainties, this is a conservative estimate of the relationship which will exist between the hot rod and the hot assembly average rod during normal operation for the entire fuel cycle. As a general approach, the hot assembly average rod power will be calculated using the [ ]<sup>a,c</sup> difference. However, if additional information is available in the form of a core design limit, an alternative and less conservative approach may be taken to bound the hot assembly average power. In Equations 25-4 and 25-5 and the discussion that follows, it is assumed that the general approach (where the difference is [ ]<sup>a,c</sup>) is taken.

A second consideration is the uncertainty associated with the hot rod and with the hot assembly average rod. For a single rod at a single axial location, the following uncertainties exist:

1. Uncertainty in the actual linear heat rate, relative to what is predicted.
2. Uncertainty in the actual fuel pellet geometry. The pellet at a particular location may be slightly larger or be slightly more enriched than the value intended during manufacture.
3. Uncertainty in the hot rod subchannel geometry. The subchannel may be slightly distorted due to rod bow.

The overall uncertainty for the hot assembly average rod peaking factor should be less than that for the hot rod, since we are concerned with the average value over a number of rods, [ ]<sup>a,c</sup>. This is indicated in Table 25.2-2.

For a single axial location on a single rod, all of these uncertainties must be considered. Since the local axial linear heat rate as specified by  $F_Q$  is defined at a single location, all of these uncertainties must be considered for the hot rod, hence the full column of numbers in Table 25.2-2 for the hot rod  $F_Q$ . For integral quantities such as the rod total power as specified by  $F_{\Delta H}$ , local uncertainties such as pellet dimensions should not contribute significantly to the integral uncertainty. [ ]<sup>a,c</sup>

] <sup>a,c</sup>

[ a,c ]

(25-6)

[

] a,c

[ a,c ]

(25-7)

[

] a,c

[ a,c ]

(25-8)

[

] a,c

$$[ \quad ]^{a,c}$$

The result of the application of these different uncertainties is that the uncertainty associated with the power on the hot rod is typically larger than the uncertainty associated with the power in the hot assembly average rod. These uncertainties are discussed in Sections 29.4.1.2 and 29.4.2.1.

**Hot Rod Average Linear Heat Rate**

Since the hot rod has a very small effect on the hot assembly fluid conditions (it is only one rod among about 150), its total power is not as important as the power in the hot assembly rod. However, total power will affect hot rod gap pressure and cladding burst times.

$$[ \quad ]^{a,c} \quad [ \quad ]^{a,c} \quad (25-9)$$

where:

$$[ \quad ]^{a,c}$$

Therefore:

$$[ \quad ]^{a,c} \quad (25-10)$$

$F_{\Delta H, BE}$  is defined as the maximum expected average linear heat rate of the highest power rod [  $\quad ]^{a,c}$  relative to the core average linear heat rate. Typically, the calculated  $F_{\Delta H, BE}$  for a core design is augmented by four percent to account for calculational and measurement uncertainties and up to an additional [  $\quad ]^{a,c}$  for “good measure” or operational allowance. The reason for the application of additional margin in  $F_{\Delta H}$  is that, unlike total peaking factor, there are few alternatives short of reducing power if the measured value exceeds the Technical Specification.

**Hot Assembly Average Linear Heat Rate**

The hot assembly rod (Rod 2) average linear heat rate during steady-state is defined as:

$$[ \quad ]^{a,c} \quad (25-11)$$

[

$$\left[ \frac{P_{\text{hot rod}}}{P_{\text{hot assembly average rod}}} \right]^{a,c} \quad (25-12)$$

The actual thermal power produced in the hot assembly rod relative to its nuclear power may be slightly different from the hot rod, due to different levels of redistribution. [

]^{a,c}

| As discussed in Section 25.2.1.1, a review of a large number of core designs indicates that the minimum difference between the hot rod and the hot assembly average rod is [ ]^{a,c} lower (Figure 25.2-4). This is a conservative estimate of the relationship which will exist between the hot rod and the hot assembly average rod during normal operation, during the entire fuel cycle. The relative nuclear power generated in the hot assembly average rod is therefore assumed to be [ ]^{a,c} lower than the best-estimate value of the hot rod relative nuclear power,  $F_{\Delta H, BE}$ . As previously discussed, however, if additional information is available in the form of a core design limit, an alternative and less conservative approach may be taken to bound the hot assembly average power.

**Axial Power Distribution**

Axial power distributions vary widely due to burnup and transient operation. The distributions have been considered in prior evaluation models using [

]^{a,c}

[

]<sup>a,c</sup>

**Low Power Region (PLOW)**

The power in the rod (Rod 5) representing the low power peripheral region of assemblies is determined from the core design and usually varies from [

]<sup>a,c</sup> If this region has a low average power, the interior channels (Rods 3 and 4) have a higher power. A relative power [ ]<sup>a,c</sup> of the core average is typical of current and future low leakage loading patterns. An average value expected for future cycles is assumed as discussed in Section 29.3.1.

### Time-in-Cycle

The time-in-cycle impacts a number of different parameters significant to the LOCA transient behavior. The fuel peaking factors, initial stored energy, rod internal pressure, corrosion, axial power distribution and decay heat are several examples of burnup dependent parameters. The impact of the time-in-cycle is considered in the uncertainty analysis as discussed in Section 29.4.1.1, Volume 3 of this topical.

### Prior Operating History

As discussed previously, the power distributions which generate high peaking factors are relatively short lived. A detailed accounting of the buildup of fission products would show that after shutdown, the axial power distribution would revert back to the original, steady-state distribution. This effect will be [

] <sup>a,c</sup>

### Transient Power Maneuver

[

] <sup>a,c</sup>

#### 25.2.1.5 Moderator Temperature Coefficient (MTC)

The moderator temperature coefficient (MTC) affects reactor shutdown during the first few seconds of blowdown. The larger (more positive) this value, the less responsive the reactor is to the increased fluid temperature which occurs in the first second or two of the LOCA. [

] <sup>a,c</sup>

#### 25.2.1.6 Hot Full Power (HFP) Boron Concentration

The initial primary fluid boron concentration coupled with the moderator temperature coefficient discussed previously dictate the core power response during the blowdown phase of a LOCA transient. The initial HFP boron concentration is modeled [

] <sup>a,c</sup>

### 25.2.1.7 Summary of Core Power Parameters

The consideration of the various core power distribution parameters described above is summarized as follows. [

] <sup>a,c</sup> (More details on this uncertainty treatment are provided in Section 29.4.) In Figure 25.2-14, a possible axial power distribution as input into the WCOBRA/TRAC-TF2 PWR model is shown. The hot rod peak power is offset by [ <sup>a,c</sup> from the hot assembly average rod power (assuming the general approach), and is offset from the average rod power by the total axial peaking ( $F_{\Delta H}$ ). The low power rod is offset from the average rod power, in turn, by the factor PLOW.

### 25.2.2 Plant Fluid Conditions

The plant fluid conditions listed at the beginning of this section are those which are sufficient to define an overall thermodynamic state of the fluid. Since WCOBRA/TRAC-TF2 calculates a steady-state condition prior to the LOCA, the thermodynamic state cannot be over-specified. Thus, four basic quantities are defined for the primary fluid; its average temperature, pressure, volume, and flow rate. Then, the states of significant fluid regions which are isolated from the RCS during steady-state, but which subsequently become part of the RCS during the LOCA, such as the upper head and the accumulator, are defined. The section below is a brief description of how fluid conditions typically are controlled in a PWR.

#### 25.2.2.1 Overview of Plant Fluid Conditions

A nuclear power plant is equipped with a variety of control systems. For example, the reactor control system in conjunction with the electric load demand program controls the neutron generation rate within the core such that core heat generation rates are proportional to the demanded electric power output. Other control systems are available for control of plant response to rapid disturbances arising from abnormal conditions and for the control of processes which maintain the plant in an economically desirable operating condition.

The static and dynamic behavior of the power production process can only be determined by reliable and accurate measurements of process variables. The application of these measurements by the control and protection systems is then accomplished in a manner which assures proper corrective action and provides protection for the plant and public against extreme accidents. This is normally accomplished by the feedback process where process variables are controlled to a predetermined value, commonly referred to as a setpoint. When measurements deviate from the setpoint, the deviation is noted as an error by the controller(s) and action is taken to restore the process to its correct state point or condition.

Setpoints generally represent either a desired, or "target," value for a process control variable, or a limit or bounding value, that a process control variable may have. In the case of a "target" or control setpoint, variation from the desired value will result in some corrective action to return the plant to the control

setpoint. For example, the pressurizer water level control setpoint is approximately 35 percent of the full-scale reading of the measurement span, with either heaters or spray being actuated with a  $\pm 5$  percent variation of full span from the 35 percent span. Violation of limiting or bounding setpoints results in a more radical plant response.

From the preceding example of the pressurizer, it is readily seen that relatively small variations from control setpoints will result in plant control systems initiating corrective action. These small spans are called control bands. Thus, for a plant maintained at equilibrium conditions, the process control parameters may be taken to vary from their respective setpoints by no more than the bounds of their respective control bands. In particular, for process parameters which are subject to automatic control, such as the pressurizer level, the likelihood of the process parameter being significantly different from the target value is extremely small. For those process parameters subject to less frequent surveillance, the potential variation may be larger.

Trip setpoints define the limits within which the plant may operate. Again referring to the example of the pressurizer, the plant will continue to operate temporarily with a pressurizer water level between 17 and 92 percent of full-scale of the measured span, with the plant control systems acting to achieve a level of between 30 to 40 percent of full-scale reading. Owing to operator and/or automatic actions however, prolonged operation outside the control bands is extremely unlikely. The trip setpoints are established to allow the plant flexibility in responding to changes in operating conditions while providing for the health and safety of the public.

Plant operation parameter variations that are significant for LOCA analyses are listed in Table 25.2-4 for a typical PWR. All but primary side loop flow may be considered process control parameters for a nuclear power plant; direct controlling of primary coolant flow rate is not provided for. For a typical plant, the variability of these parameters about their nominal or setpoint values is seen to be small, with a control band of about [ ]<sup>a,c</sup> on primary loop pressure and fluid temperature, [ ]<sup>a,c</sup> on core power, and about [ ]<sup>a,c</sup> on water volumes.

### 25.2.2.2 Fluid Conditions Modeling Approach

In addition to the process parameters identified in Table 25.2-4, additional RCS fluid conditions have been found to be important in past LOCA analyses. The reactor vessel upper head is supplied by a small bypass flow from the upper downcomer. While the incoming fluid is at the temperature of the cold leg ( $T_{\text{cold}}$ ), the upper head fluid may be at a different average temperature because of the low bypass flow rate which results in some flow from the upper plenum, which is at a higher temperature ( $T_{\text{hot}}$ ). The initial temperature of the fluid in the upper head ( $T_{\text{UH}}$ ) has been found to strongly affect the blowdown PCT in other evaluation models (for Large Break LOCA). Typically, plants can be separated into two categories: those with sufficient bypass flow to maintain ( $T_{\text{UH}}$ ) near ( $T_{\text{cold}}$ ), and those with low bypass flow, in which ( $T_{\text{UH}}$ ) remains close to  $T_{\text{hot}}$ .

The bypass flow mentioned above is one component of several bypass flows, which reduce the core flow rate relative to the loop flow rate by about four to eight percent. This bypass flow has an indirect effect on the LOCA transient by affecting the fluid temperature rise through the core, but is not expected to affect the LOCA transient directly by virtue of the different steady-state fluid conditions.

Not all the process parameters described in Section 25.2.2.1 are independent. Typically, if core power, primary flow, and secondary temperature and pressure are specified, the primary fluid temperature and pressure will seek appropriate levels consistent with these boundary conditions. In the modeling of these parameters, the secondary side conditions are adjusted as required to obtain primary side conditions consistent with the Technical Specifications and planned operation. Since the secondary-side model is rather detailed, the secondary-side conditions required to achieve the appropriate primary-side conditions are generally consistent with expected operational values.

Although the accumulator is isolated from the RCS by a check valve during normal operation, it is considered part of the RCS in this methodology. The performance of the accumulator during the LOCA depends on several factors including the water and cover gas initial pressure, temperature, and volume. These are all subject to some variation. Typically, pressure and volume are controlled to within plus or minus 10 percent or less. Since the accumulators reside within containment, the long term temperature of the containment atmosphere will affect the accumulator water temperature. The variation in containment temperature is likely to be seasonal to some degree, and is limited in most plants to a maximum value to avoid problems with equipment degradation. In general, therefore, the accumulator temperature range is plant specific. The accumulator line is subject to the same uncertainties as identified earlier for flow resistance; however, plant startup tests reduce this uncertainty to some extent as discussed in Section 29.3.2, Volume 3.

While accumulator boron concentration is not likely to have a significant effect on the LOCA PCT, it is modeled to ensure that recriticality does not occur in the short-term following a LOCA.

The parameters chosen to represent the reactor initial fluid conditions are:

1. Average fluid temperature ( $T_{avg}$ ), degrees F
2. Pressurizer pressure ( $P_{RCS}$ ), psia
3. Loop flow rate ( $W_{loop}$ ), gpm per loop
4. Upper head fluid temperature ( $T_{UH}$ ), degrees F
5. Pressurizer level ( $L_p$ ), percent of full span
6. Accumulator temperature ( $T_{ACC}$ ), degrees F
7. Accumulator pressure, ( $P_{ACC}$ ) psia
8. Accumulator water volume, ( $V_{ACC}$ ) cubic feet
9. Accumulator line fl/D ( $K_{ACC}$ )
10. Accumulator boron concentration, ( $C_{ACC}$ ) ppm

The effects that the above parameters have on the LOCA transient are considered as part of the uncertainty analysis. The treatment of the fluid condition uncertainties is discussed in Section 29.3.2, Volume 3.

**Table 25.2-1 Hot Assembly Rod Power Census Summary for Westinghouse Fuel**


a,c

**Table 25.2-2 Peaking Factor Uncertainties**


a,c

**Notes:**

1. Spier et al. (1988)
2. [ ]<sup>a,c</sup>
3. Uncertainties are given in terms of one standard deviation divided by average value (coefficient of variation), percent. The total uncertainty is the square root sum of squares of the components.

**Table 25.2-3 Rod Bow F<sub>Q</sub> Uncertainties**


a,c

**Notes:**

1. Uncertainties are given in terms of one standard deviation divided by average value (coefficient of variation).
2. Argall et al. (1979)
3. [ ]<sup>a,c</sup>

<b>Table 25.2-4 Typical Westinghouse Plant Operation Parameters</b>	

a,c

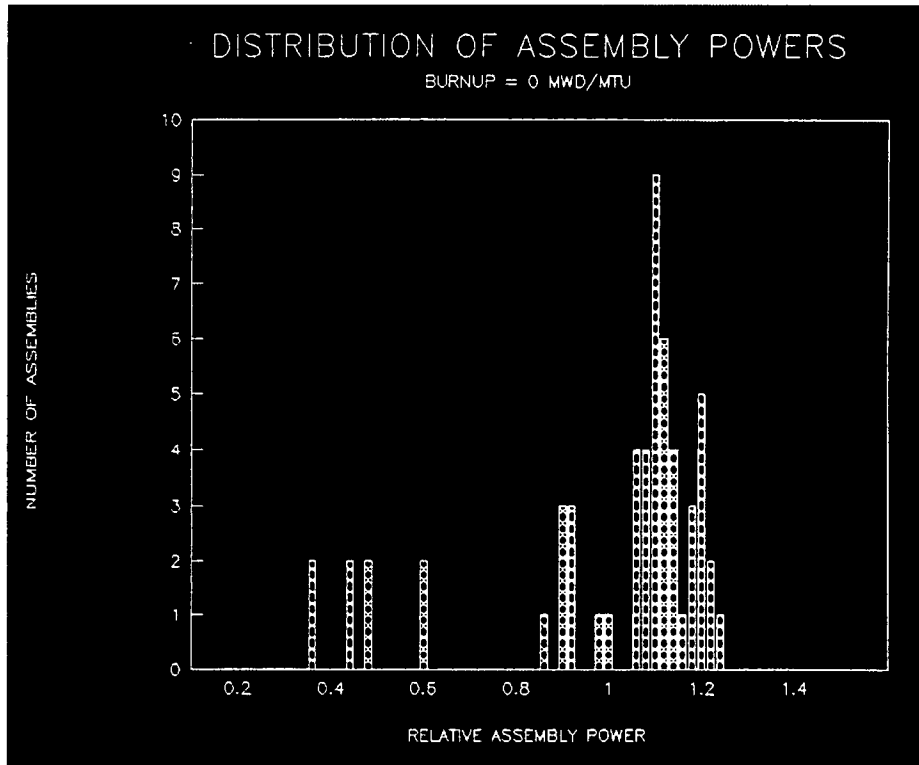
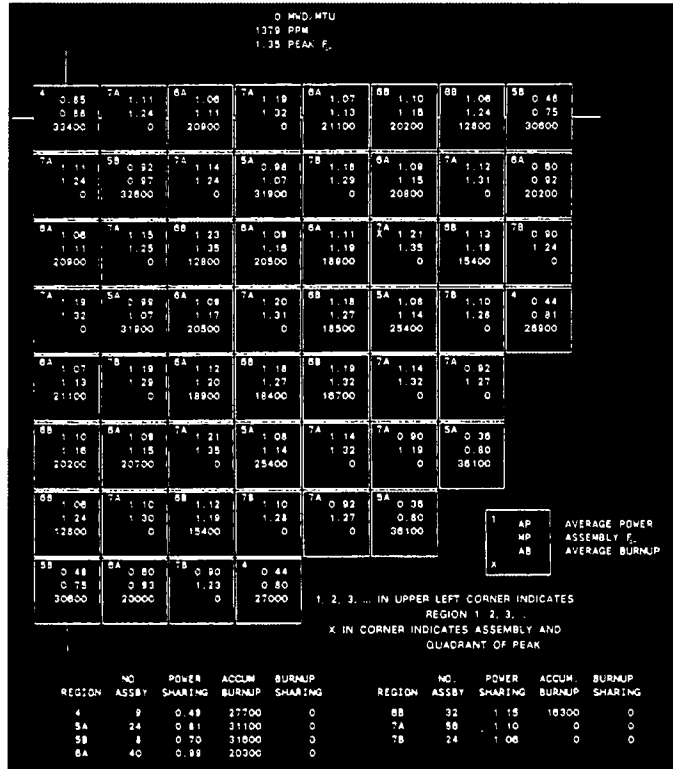


Figure 25.2-1 Typical Assembly Power Map and Assembly Power Distribution, Beginning of Cycle

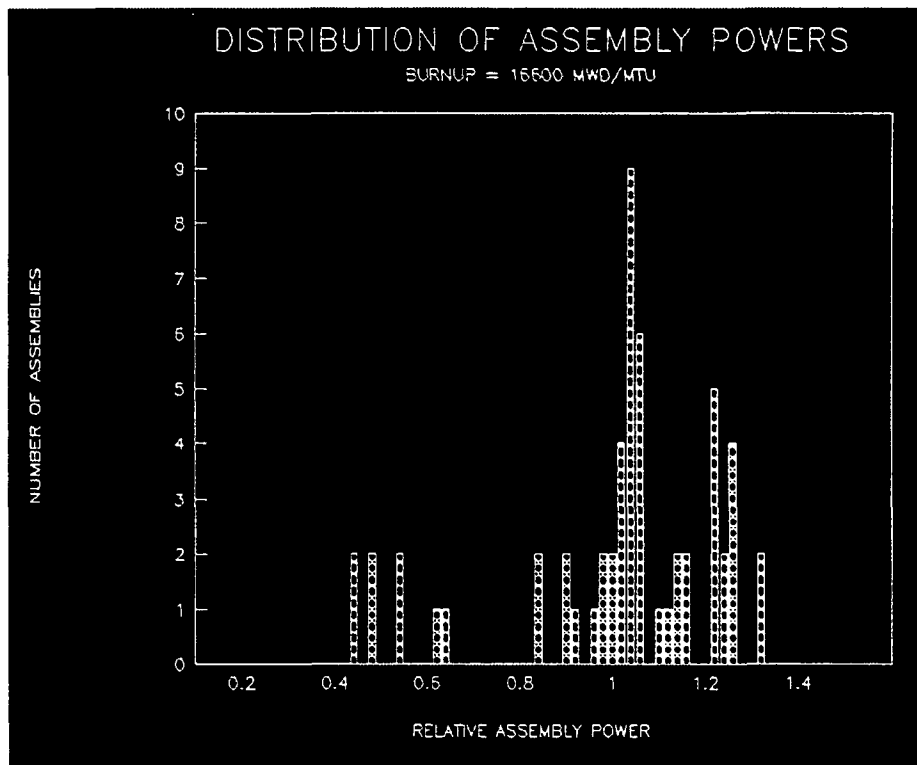
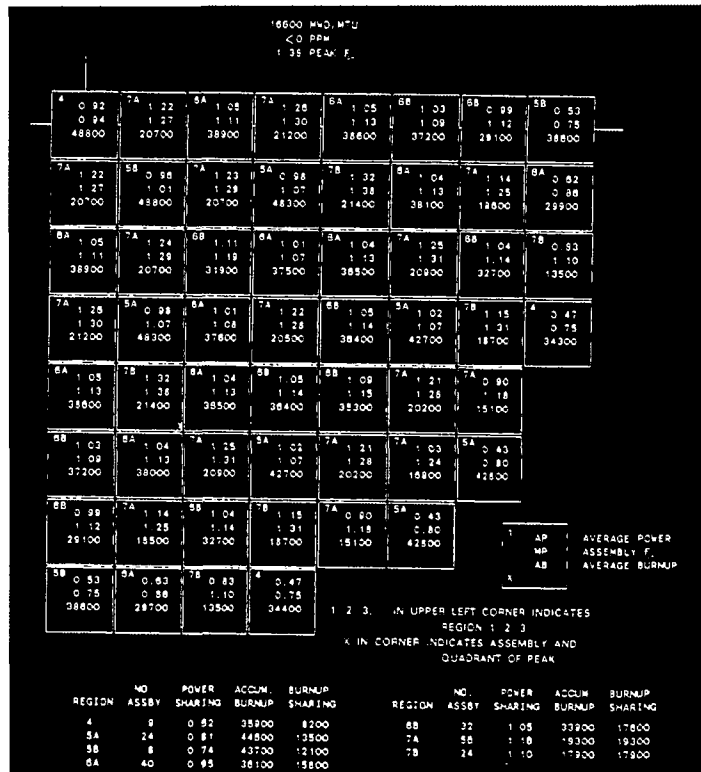
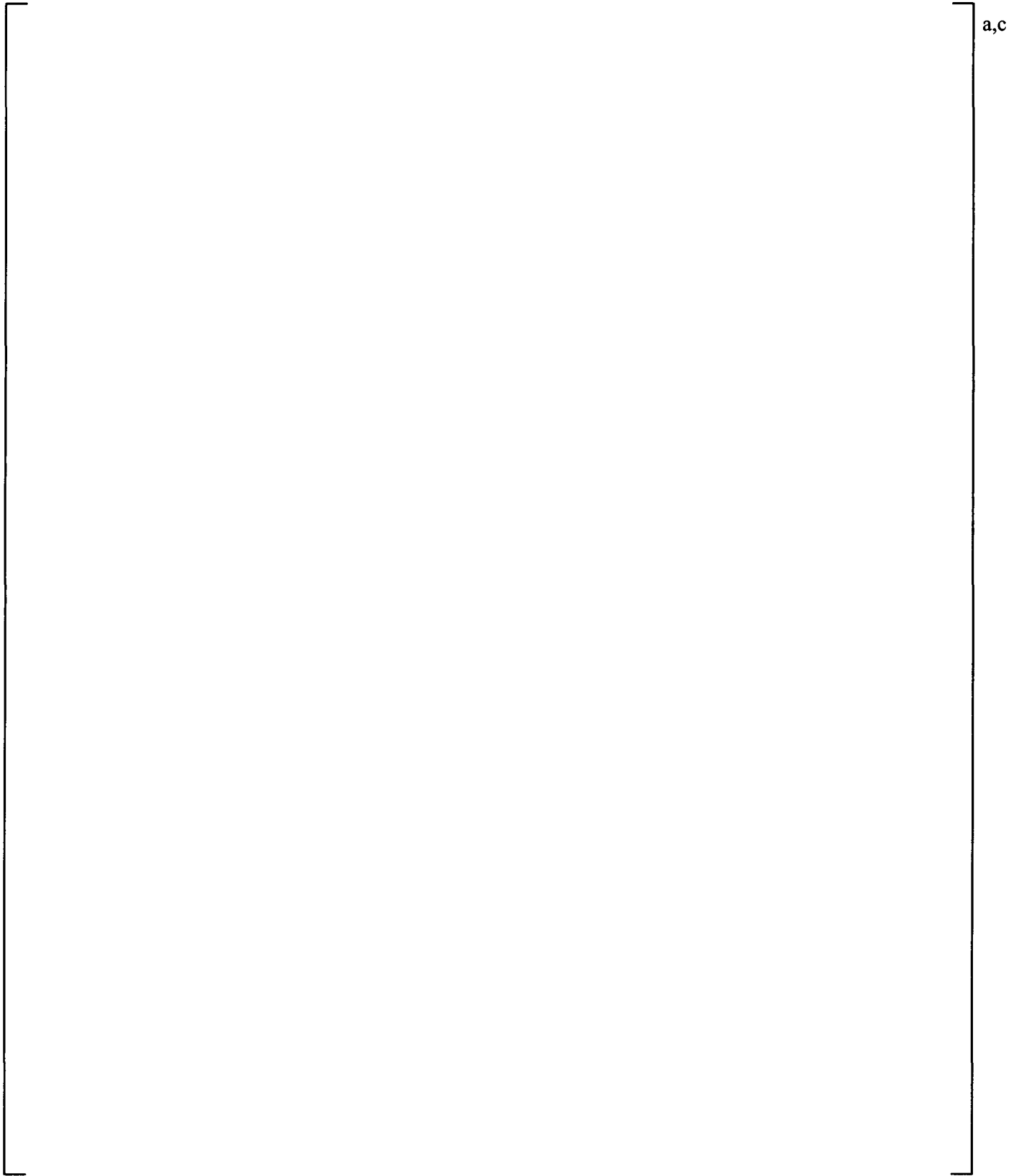
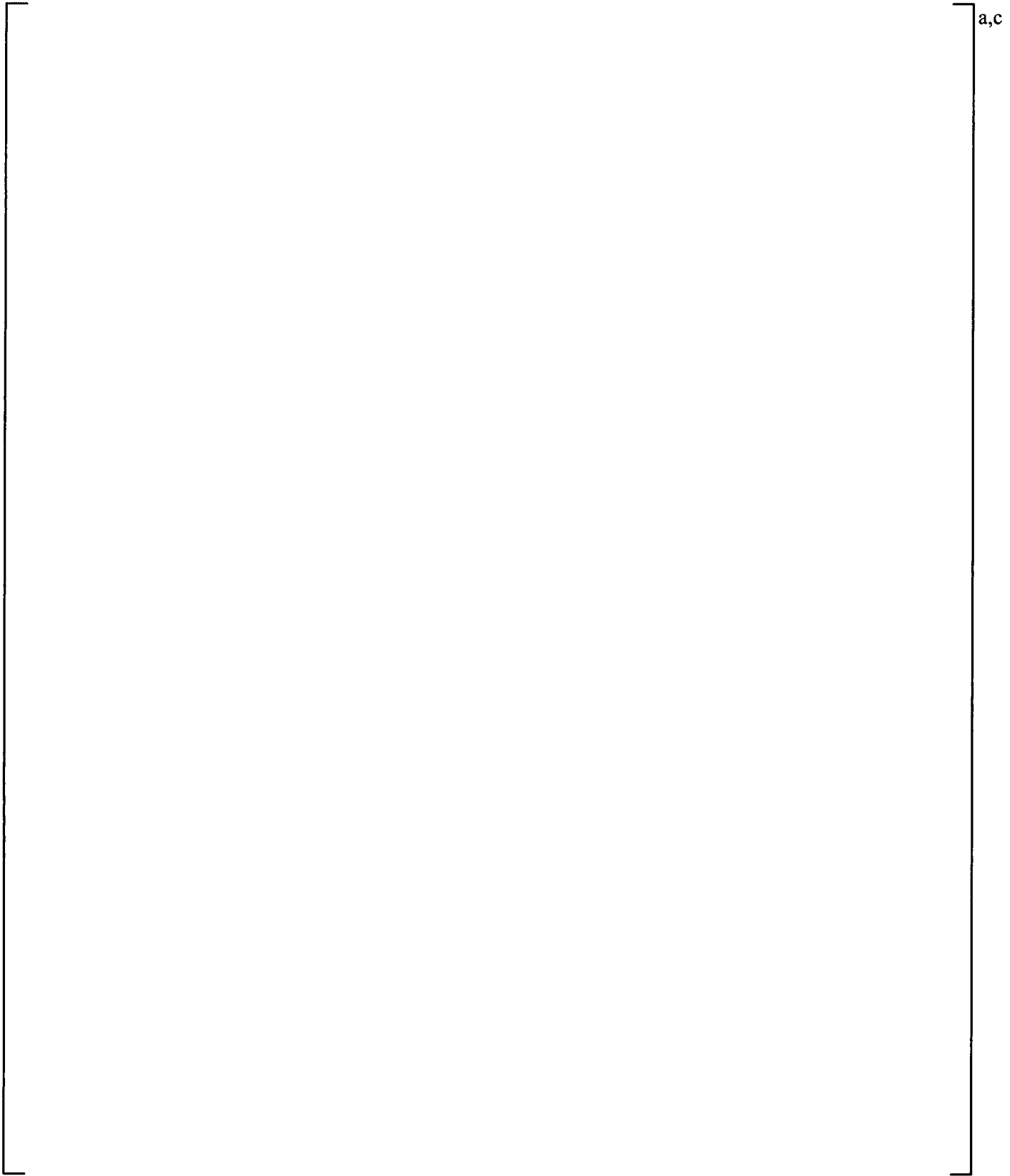


Figure 25.2-2 Typical Assembly Power Map and Assembly Power Distribution, End of Cycle



**Figure 25.2-3 Typical Hot Assembly Fuel Rod Power Distribution**



**Figure 25.2-4 Hot Assembly Rod Power Census for Typical Westinghouse Fuel Designs**

a,c

**Figure 25.2-5** **Relative Axial Power Distribution near Beginning of Cycle, Middle of Cycle and End of Cycle During Full Power Steady-State Conditions**

a,c

**Figure 25.2-6 Typical Transient Axial Power Distributions near Beginning of Cycle**

a,c

**Figure 25.2-7 Typical Transient Axial Power Distributions near Middle of Cycle**

a,c

**Figure 25.2-8 Typical Transient Axial Power Distributions near End of Cycle**

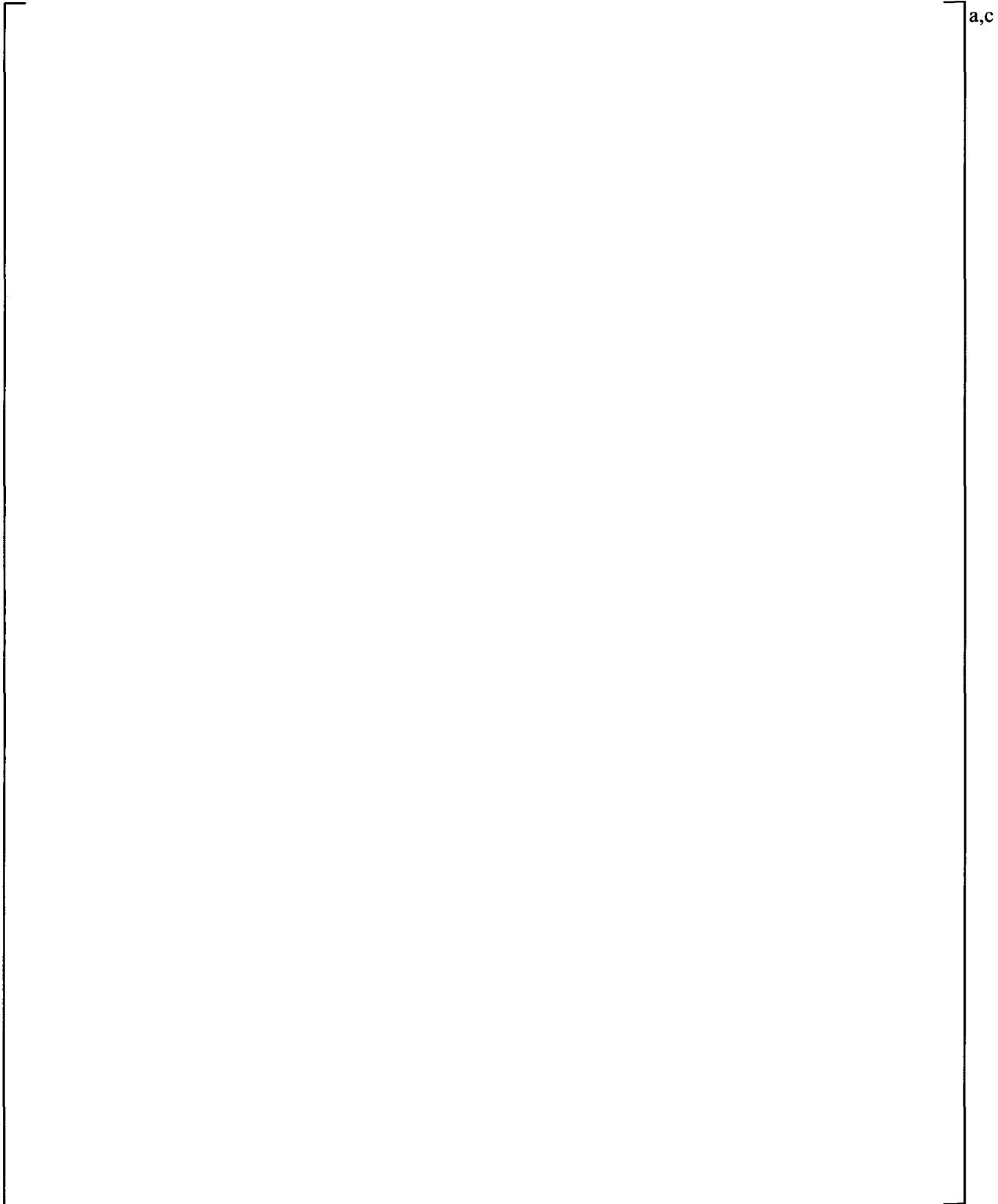


**Figure 25.2-9 [**

**]<sup>a,c</sup>**

a,c

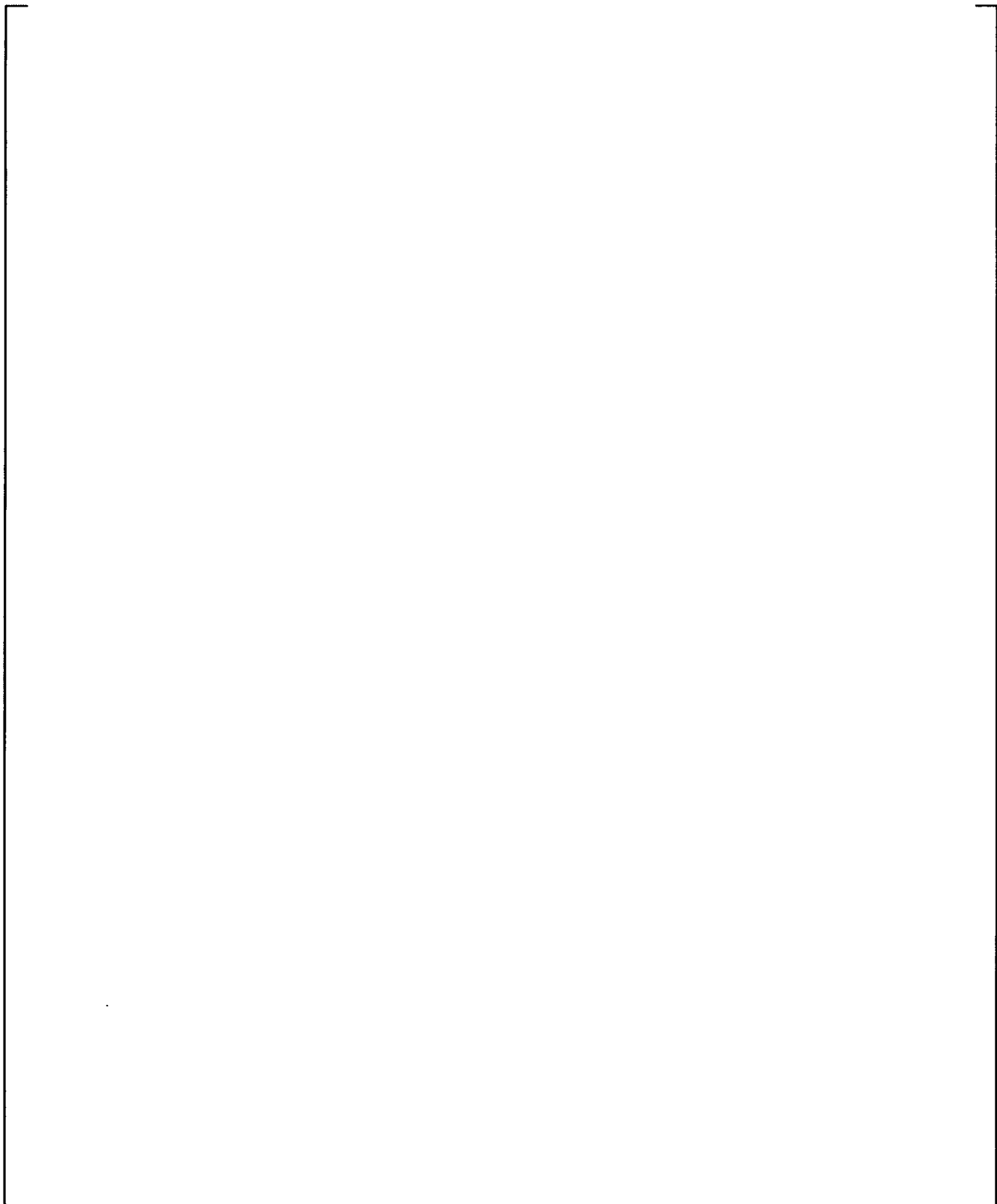


**Figure 25.2-10 Effect of Load Follow Maneuver Period on Decay Heat Equilibrium Fraction for Various Times After Trip**

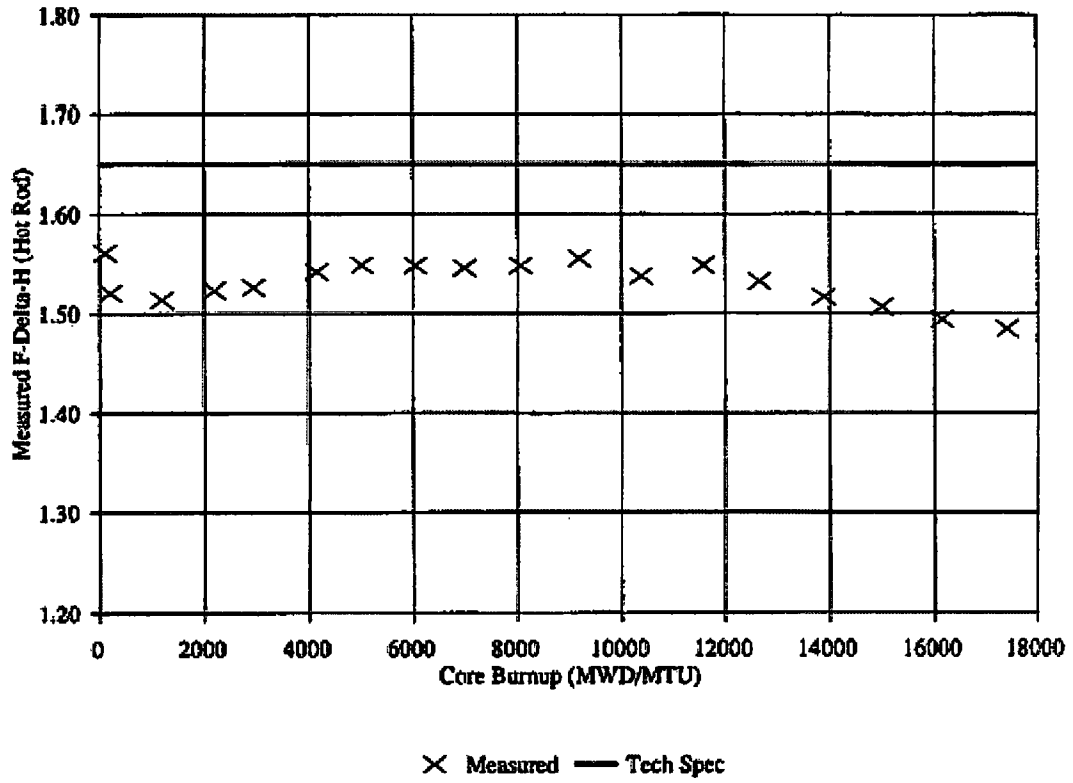


Figure 25.2-11 Typical Measurement of Enthalpy Rise Hot Channel Factor  $F_{\Delta H}$

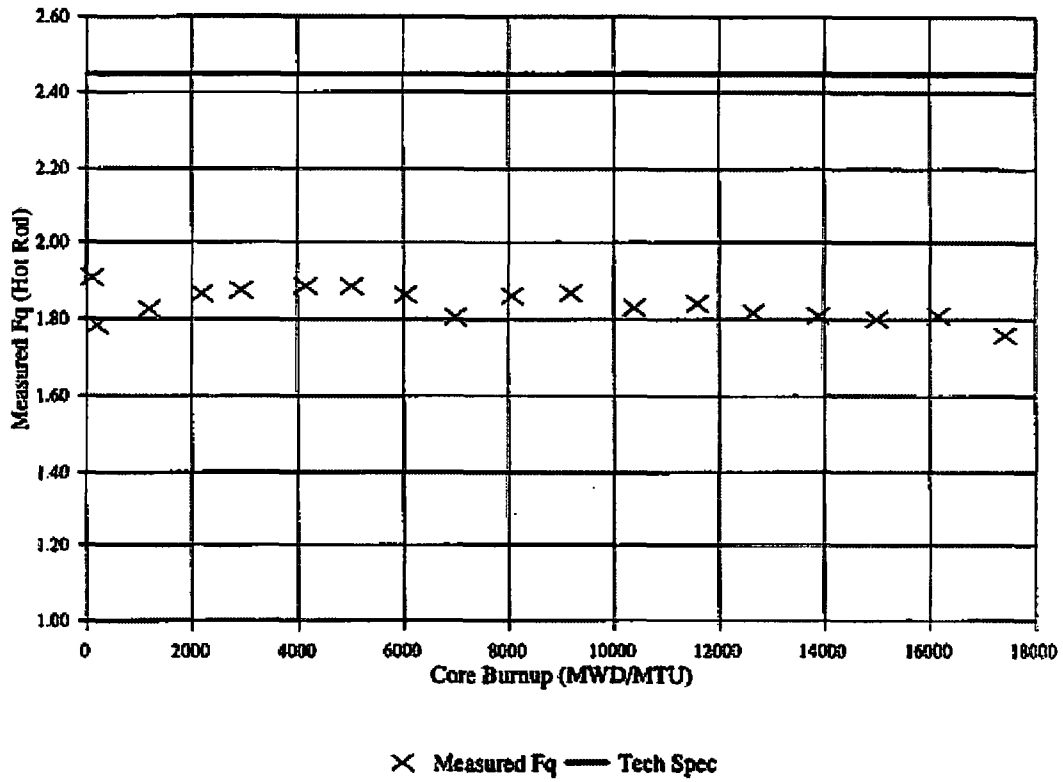
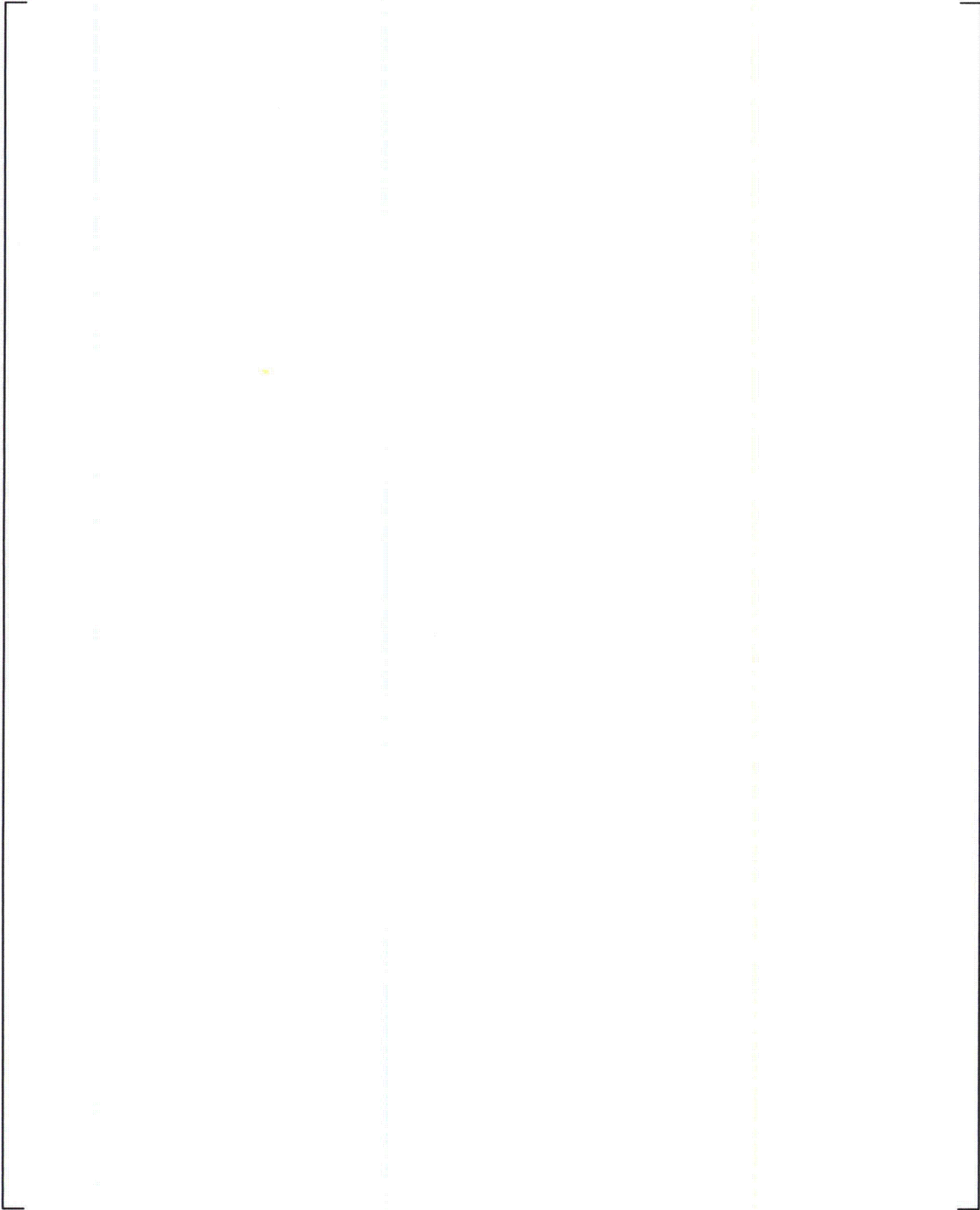


Figure 25.2-12 Typical Measurement of Total Peaking Factor  $F_Q$



a,c

Figure 25.2-13 [

]a,c

a,c

**Figure 25.2-14 Typical WCOBRA/TRAC-TF2 Axial Power Distribution**

## 25.8 REFERENCES

1. American Nuclear Society, 1979, "American National Standard for Decay Heat Power in Light Water Reactors," ANSI/ANS-5.1-1979.
2. Akimoto, H., et al., 1984, "Pressure Drop through Broken Cold Leg During Reflood Phase of Loss-of-Coolant Accident of PWR," Journal of Nuclear Science and Technology, 21 [16].
3. Argall, B. M., et al., 1979, "Fuel Rod Bow Evaluation," WCAP-8691, Revision 1.
4. Bajorek, S. M., et al., March 1998, "Code Qualification Document for Best Estimate LOCA Analysis," Volume 1 Revision 2, and Volumes 2 through 5, Revision 1, WCAP-12945-P-A (Proprietary).
5. Bordelon, F. M. and Murphy, E. T., 1974, "Containment Pressure Analysis Code (COCO)," WCAP-8327 (Proprietary), WCAP-8306 (Non-Proprietary).
6. Bordelon, F. M., et al., 1974, "Westinghouse Emergency Core Cooling System Evaluation Model – Summary," WCAP-8339.
7. Bordelon, F. M., et al., 1975, "The Westinghouse ECCS Evaluation Model: Supplementary Information," WCAP-8471-P-A (Proprietary).
8. Combustion Engineering, 1975, "Assessment of the Accuracy of PWR Safety System Actuation as Performed by the Core Protection Calculators (CPC)," CENPD-170-P.
9. Combustion Engineering, 1986, "C-E Setpoint Methodology, C-E Local Power Density and DNB LSSS and LCO Setpoint Methodology for Analog Protection Systems," CENPD-199-P, Rev.1-P-A.
10. Combustion Engineering, 1998, "C-E Setpoint Methodology." CENPD-199-P, Rev.1-P-A, Supplement 2-P-A.
11. Letter from Johnson, W. J. to Richardson, J. E., December 1990, "Steam Generator Tube Deformation," NS-NRC-90-3557.
12. Mendler, O. J., 1975, "Method of Analysis and Evaluation of Jet Impingement Loads from Postulated Pipe Breaks," WCAP-8957.
13. Miller, R. W., et al., 1983, "Relaxation of Constant Axial Offset Control/ $F_q$  Surveillance Technical Specification," WCAP-10216-P-A.
14. Morita, T., et al., 1974, "Power Distribution Control and Load Following Procedures," WCAP-8385-P-A.

15. Nissley, M. E., et al., 2005, "Realistic Large-Break LOCA Evaluation Methodology Using the Automated Statistical Treatment Of Uncertainty Method (ASTRUM)," WCAP-16009-P-A and WCAP-16009-NP-A.
16. Salvatori, R., 1973, "Topical Report, Reactor Coolant Pump Integrity in LOCA," WCAP-8163.
17. Spier, E. M., et al., 1988, "Evaluation of Nuclear Hot Channel Factor Uncertainty," WCAP-7308-L-P-A.
18. U.S. Nuclear Regulatory Commission, 1989, "Best-Estimate Calculations of Emergency Core Cooling System Performance," Regulatory Guide 1.157.

**Updates to Sections 26.4 and 26.5 of WCAP-16996-NP**

**“Realistic LOCA Evaluation Methodology Applied to the Full**

**Spectrum of Break Sizes**

**(FULL SPECTRUM LOCA Methodology)”**

## 26.4 STEADY STATE CALCULATION/CALIBRATION

Steady-state acceptance criteria are necessary because the above-mentioned fluid and core conditions are likely to differ somewhat from plant-to-plant and the degree to which these parameters are matched in the WCOBRA/TRAC-TF2 simulation must be consistent. Table 26.4-1 shows the acceptance criteria used in WCOBRA/TRAC-TF2 for acceptable simulation of plant conditions. A checklist for a number of significant parameters is given below, which utilizes this table to verify whether these variables have reached their acceptable steady-state values.

[

] <sup>a,c</sup>

[

] <sup>a,c</sup>



## 26.5 REFERENCES

1. Bajorek, S. M., et al., March 1998, "Code Qualification Document for Best Estimate LOCA Analysis," Volume 1 Revision 2, and Volumes 2 through 5, Revision 1, WCAP-12945-P-A (Proprietary).
2. Bordelon, F. M. and Murphy, E. T., 1974, "Containment Pressure Analysis Code (COCO)," WCAP-8327 (Proprietary), WCAP-8306 (Non-Proprietary).
3. Bordelon, F. M., et al., 1974, "Westinghouse Emergency Core Cooling System Evaluation Model – Summary," WCAP-8339.
4. Bordelon, F. M., et al., 1975, "The Westinghouse ECCS Evaluation Model: Supplementary Information," WCAP-8471-P-A (Proprietary).
5. Crede, T. M., et al., 2013, "Westinghouse Performance Analysis and Design Model (PAD5)," WCAP-17642-P (Proprietary), WCAP-17642-NP (Non-Proprietary).
6. Shimeck, D. J., March 1988, "COSI SI/Steam Condensation Experiment Analysis," WCAP-11767 (Proprietary).

**Updates to Sections 29.4.1, 29.4.2, 29.5.1 and 29.7**

**of WCAP-16996-NP**

**“Realistic LOCA Evaluation Methodology Applied to the**

**Full Spectrum of Break Sizes**

**(FULL SPECTRUM LOCA Methodology)”**

## 29 ASSESSMENT OF UNCERTAINTY ELEMENTS

The list of dominant phenomena was identified by the PIRT discussed in Section 2. The PIRT included all processes covering the scenarios that span the full spectrum of break sizes. A summary of the important phenomena was provided in Section 2.3.3. The code models associated with such phenomena were then assessed against an independent dataset comprised of separate effect tests (SETs) and integral effect tests (IETs). This was the subject of Sections 12 through 23. Section 24 provides a synthesis of the assessment as well as an analysis of potential compensating errors.

The code assessment exercise leads to the determination and quantification of model biases and uncertainties (EMDAP Step 20). Consistent with the CSAU roadmap, the uncertainty has to be ultimately propagated or convoluted statistically during the plant analysis. The statistical procedure used to propagate the uncertainties is the subject of Section 30. The approach is based on a Monte Carlo convolution of the uncertainty contributors. The procedure is designed to generate a sample of the LOCA 'population' and then develop probabilistic statements that show compliance with the 10 CFR 50.46 criteria.

In general, the uncertainty parameters fall into three categories:

1. **Nominal without Uncertainty** – The nominal (expected or midpoint) value of the parameter is used without consideration of uncertainty when the variation in the parameter is tightly controlled, such as pressurizer level, or when the sensitivity of the transient to the value of the parameter is negligible, such as the initial reactor coolant system (RCS) boron concentration. An example of a model treated as nominal without uncertainty is the offtake model (Section 29.1.1.1).
2. **Bounded** – A conservative value of the parameter is used when the parameter varies gradually as a function of operating history, when the sensitivity of the transient to variations in the parameter is small, or when the effort to develop and justify a detailed uncertainty treatment is judged to exceed the benefits of doing so. Bounded plant parameters are discussed in Section 29.3.1. An example of a phenomenon treated in a bounding manner is steam binding.
3. **Nominal with Uncertainty** – The Westinghouse methodology includes three categories of uncertainty contributors to the overall uncertainty assessment. These are the thermal-hydraulic model uncertainties, the power-related parameter uncertainties, and the initial and boundary condition uncertainties.

Tables 29-1 through Table 29-5 provide the list of the uncertainty contributors or parameters that are explicitly considered in the FSLOCA methodology. The uncertainty contributors [

] <sup>a,c</sup>

[ ]<sup>a,c</sup> For most models, ranging capabilities on key parameters has been included in the code such that the solution can be randomly biased during the Monte Carlo convolution of the uncertainties. The objective of Section 29.1 is to develop and justify the probability density function (PDFs) associated with such key parameters.

While a PDF was developed and justified for most of the models, in some instances a bounding approach was judged to be adequate for the purpose of the uncertainty analysis. This was the case when a complete characterization of the individual model biases and uncertainty could not be pursued, because of the complexity of the process, and/or because limitations in experimental data caused the effort of developing a detailed uncertainty treatment for each individual component to exceed the benefit of doing so. In those circumstances the objective of the exercise was to demonstrate that the biases associated with that specific complex phenomenon, albeit not quantified, are conservative with respect to engineering figures of merit in the context of a realistic but still conservative LOCA simulation. In those cases the validity of the approach was also supported by compensating error analyses (Section 24). [ ]

[ ]<sup>a,c</sup>

The analysis of the uncertainty on the break flow is [ ]

[ ]<sup>a,c</sup> The discussion of the break model methodology deserves a section itself and Section 29.2 is dedicated to this topic.

Core power related parameters are listed in Table 29-4. The time in cycle is the first parameter selected since many fuel related parameters are a function of burnup. The methodology is presented in Section 29.4.1.

Uncertainties associated with the fuel rod models are listed in Tables 29-3 and 29-4. Some of these parameters are characterized as local uncertainties since the effect is postulated to mainly affect the local peak cladding temperature (PCT) or maximum local oxidation (MLO) and the effect on the global T/H response is expected to be minimal. [ ]

[ ]<sup>a,c</sup>

All the other uncertainty parameters are associated with the plant parameters listed in Table 29-5. Section 29.3 is dedicated to the topic.

Section 29.5 provides a review of the PIRT and summarizes the conclusions from the perspective of model biases and uncertainty of all phenomena ranked high (H). This corresponds to EMDAP Step 20. Finally, Section 29.6 addresses experimental accuracy in the context of Step 9 of the EMDAP roadmap.









**Table 29-5 Initial and Boundary Conditions Considered in Uncertainty Methodology Defined in Section 29.3.2**


a,c

## 29.4 CORE AND FUEL ROD MODEL UNCERTAINTIES

### 29.4.1 Initial Reactor State Uncertainties

#### 29.4.1.1 Time in Cycle

[

] <sup>a,c</sup>

| Hot Rod Burnup

[

] <sup>a,c</sup>

[

] <sup>a.c</sup>

[

] <sup>a,c</sup>

| Hot Assembly Rod Burnup

[

] <sup>a,c</sup>

| Core Balance Rods

[

] <sup>a,c</sup>

### 29.4.1.2 Reactor Core Power Distributions and Global Uncertainties

Reactor core power distributions are characterized by radial and axial power distributions, as discussed in Section 25.2.1. The steady-state radial distribution is established by core loading pattern, fuel enrichment, fixed burnable poisons, etc., and is not subject to wide variation during normal operation (Section 25.2.1.1). The maximum of the radial distribution is defined by  $F_{\Delta H}$  (hot rod average power divided by the core average rod average power). Predictions of  $F_{\Delta H}$  are accurate to within [ ]<sup>a,c</sup> at > 95 percent probability (Section 25.2.1.3). [ ]<sup>a,c</sup>

Steady-state axial distributions are established by core loading pattern and burnup. The axial distribution tends to vary widely as a result of changes in reactor power, xenon transients, boron or control rods. The maximum of the radial distribution times maximum of the axial distribution is  $F_Q$  (maximum linear heat rate divided by the core average linear heat rate). Transients are simulated in the core design process, yielding a wide range of possible power distributions and  $F_Q$  values. As described in Section 25, [ ]<sup>a,c</sup>

Plants operate in “baseload” (i.e., full power, control rods out) nearly all the time. In baseload operation,  $F_Q$  varies slowly with time. However, the Technical Specifications allow for transient operation. Figure 29.4.1-4 shows the effect of a typical load follow maneuver on peaking factor ( $F_Q \times$  power), for a plant with a Technical Specification (Tech Spec)  $F_Q$  limit of [ ]<sup>a,c</sup>. In the Westinghouse FSLOCA methodology, [ ]<sup>a,c</sup>

[

] <sup>a,c</sup>

[

] <sup>a,c</sup>

[

] <sup>a,c</sup>

Other sources of uncertainty in the power related parameters involve: 1) the accuracy with which the power distribution in the hot assembly and remainder of the core can be defined; 2) the accuracy with which the power at the hot spot (most limiting elevation of the hot rod) can be defined, including local uncertainties. The latter is addressed in Section 29.4.2.

The following contributors are considered, [

] <sup>a,c</sup>.

- Radial power distribution
- Total peaking factor and axial power distribution
- Initial core power level
- Decay heat
- Gamma redistribution

### Radial Power Distribution

The hot assembly and core radial power distribution is modeled by defining the following variables:

- Hot rod average relative power,  $F_{\Delta H}$ . The hot rod average relative power,  $F_{\Delta H}$  will be ranged according to its calculational uncertainty. This global uncertainty, as shown in Table 25.2-2, has a standard deviation equal to [ ] <sup>a,c</sup> of the nominal value.
- Hot assembly average power is [ ] <sup>a,c</sup> lower than  $F_{\Delta H}$ , minimum (Section 25), [

] <sup>a,c</sup>

- Power in the assemblies in the core periphery (PLOW), as a percent of average assembly power ( [ ]<sup>a,c</sup> are typical lower and upper bounds). Variations in this parameter will have a small effect on the power of the core average rods surrounding the hot assembly. [ ]<sup>a,c</sup>

### Total Peaking Factor and Axial Power Distribution

As previously discussed, the axial power distribution is [ ]<sup>a,c</sup>

The initial power generation rate, as a function of elevation, is specified for the hot rod by the initial axial and radial power distributions (peaking factors  $F_Q$  and  $F_{\Delta H}$ ) on the hot rod. The uncertainty associated with the total peaking factor  $F_Q$  (Tables 25.2-2 and 25.2-3) can be divided into two components; one closely coupled to the uncertainty in the hot assembly power, and one associated only with local uncertainties and therefore independent of the hot assembly. Since there is a fixed radial power distribution in the assembly, a fluctuation in the hot assembly power results in a similar fluctuation in the hot rod. This situation is illustrated in Figure 29.4.1-12. Fluctuations in the hot assembly rod are assumed to also affect the thermal-hydraulics (i.e., they affect the heat transfer coefficient boundary condition), and so the uncertainties are considered in the global thermal-hydraulic solution accordingly. [ ]<sup>a,c</sup>

[ ]<sup>a,c</sup>

### Initial Core Power, Decay Heat, Gamma Redistribution

The remaining variables, core average power, gamma redistribution, and decay heat, contribute additional uncertainty to the peak linear heat rate. The uncertainty in core power ( $AFLUX_0$ , [ ]<sup>a,c</sup>) was quantified in Section 25.2.1.3. Increases (decreases) in  $AFLUX$  result in proportional increases (decreases) in rod powers for all rods as described in Section 25.2.1.4.

Uncertainty in decay heat is considered through the application of ANSI/ANS 5.1-1979 Standard (DH, normal distribution). See also Section 9.7.

[ ]<sup>a,c</sup>

[ ]<sup>a,c</sup>

[

] <sup>a,c</sup>

Table 29.4.1-1 [ ]<sup>a,c</sup>


a,c

a,c

**Figure 29.4.1-1 Maximum Rod Average Power at a Given Rod Burnup at Various Times During a Typical Cycle**



a,c

| **Figure 29.4.1-2** [

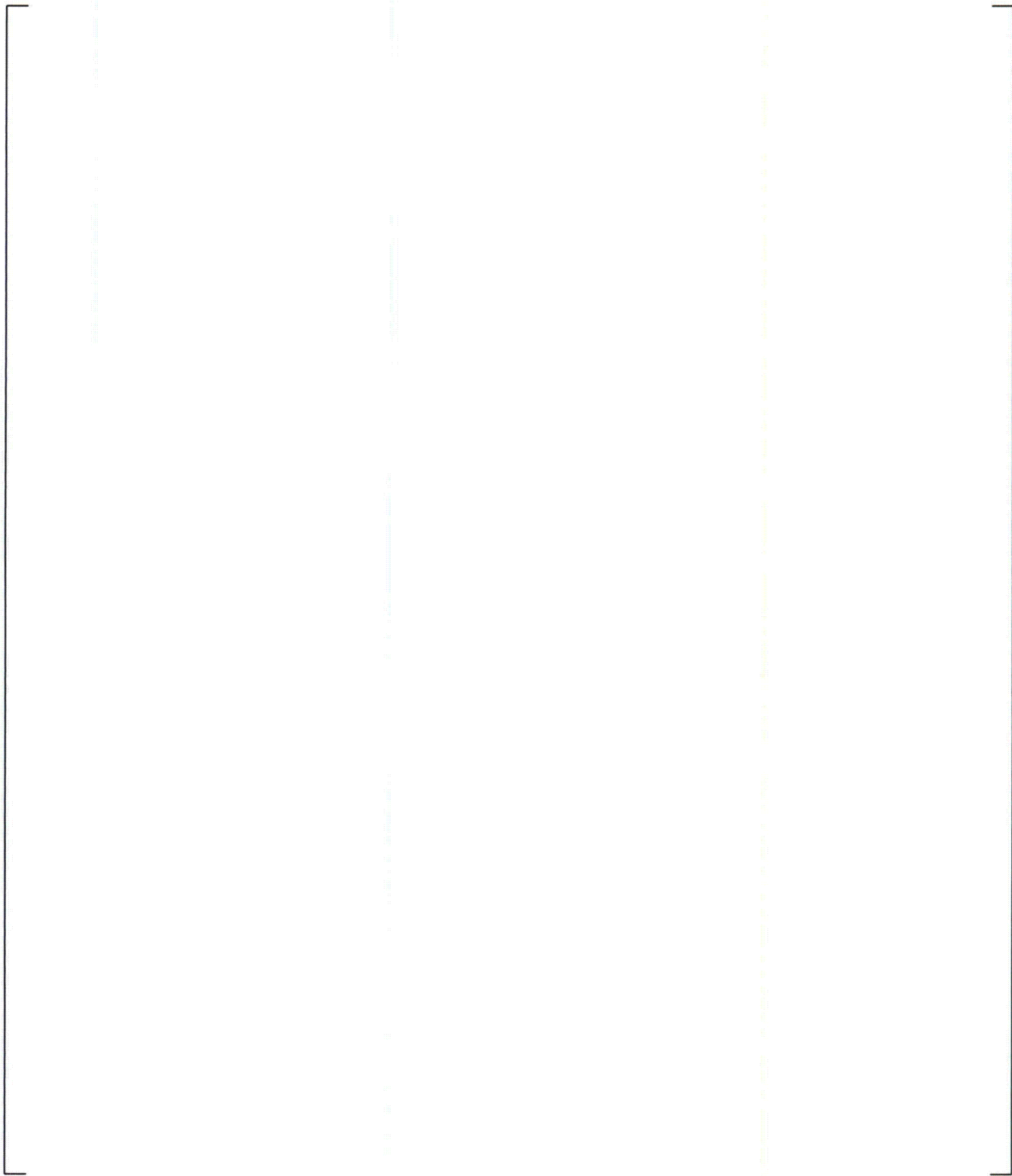
] <sup>a,c</sup>

a,c

**Figure 29.4.1-3 Fuel Pellet Average Temperatures as a Function of Rod Average Burnup  
for 0.422-inch Outer Diameter Fuel**

a,c

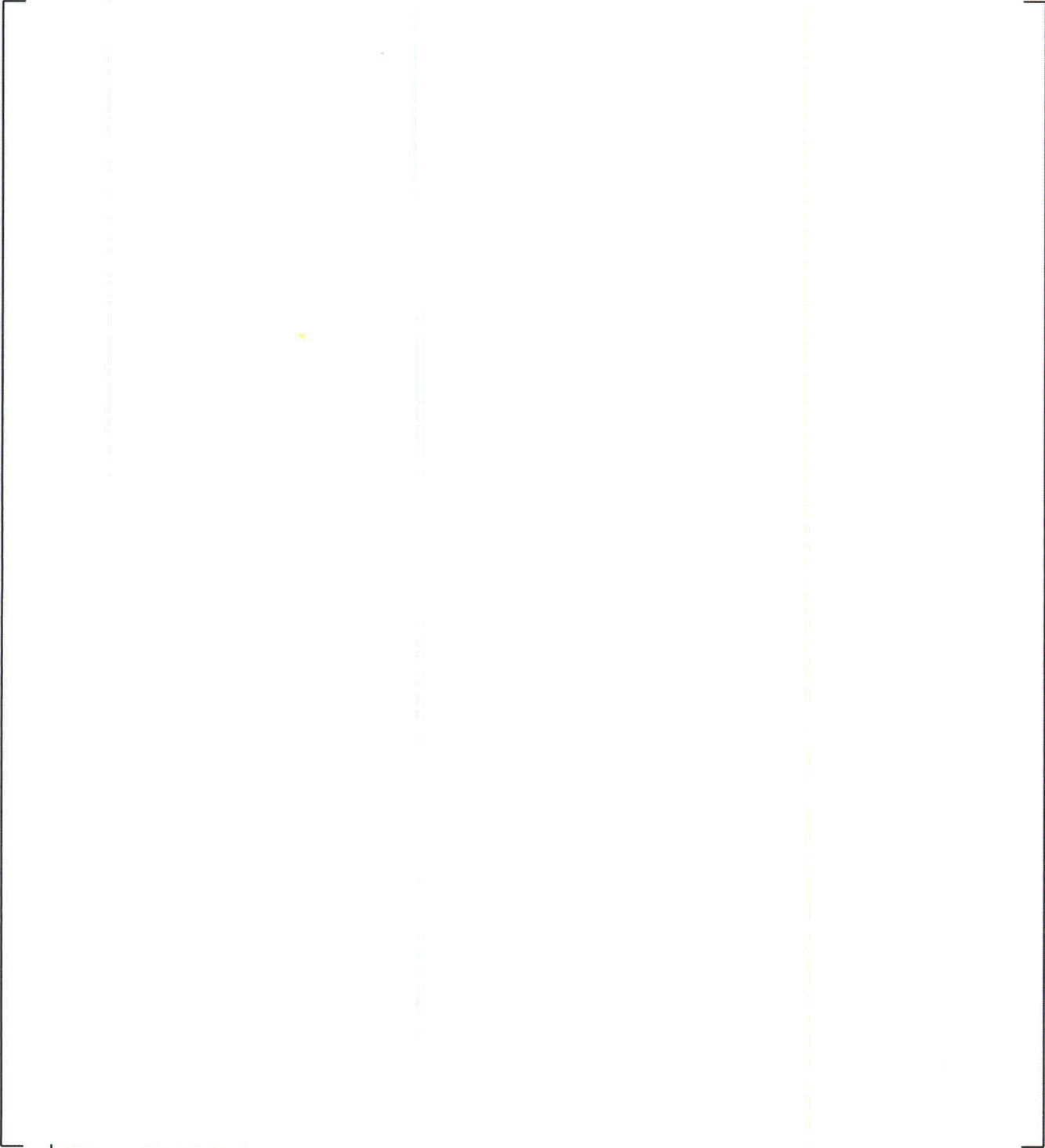
**Figure 29.4.1-4 Effect of Load Follow on  $F_Q$**



a,c

| **Figure 29.4.1-5** [

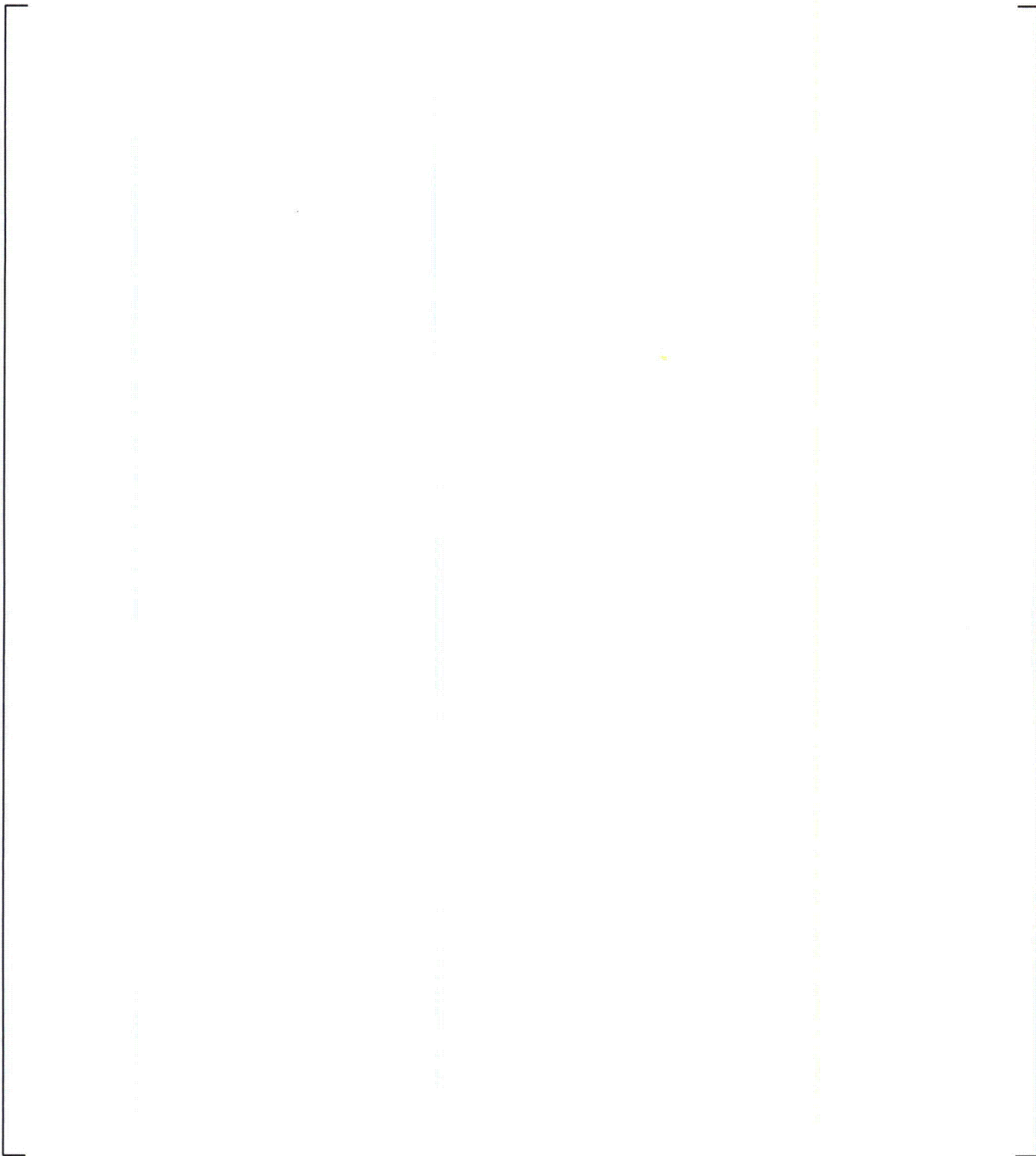
] <sup>a,c</sup>



a,c

Figure 29.4.1-6 [

] a,c



a,c

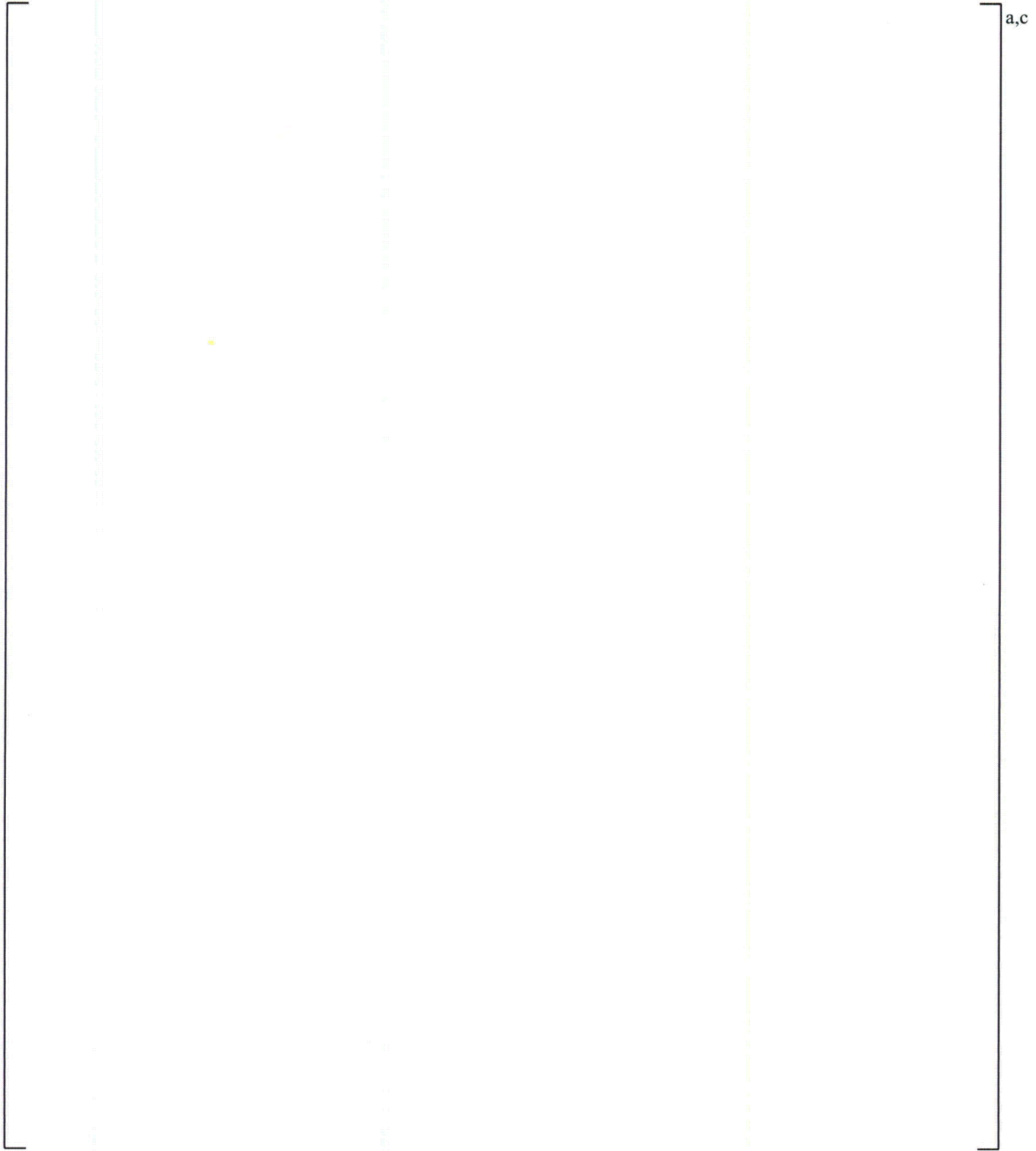
| **Figure 29.4.1-7** [

] <sup>a,c</sup>

a,c

Figure 29.4.1-8 [

]a,c



a,c

| **Figure 29.4.1-9 Example Bottom Skewed Axial Power Distribution [ ]<sup>a,c</sup>**

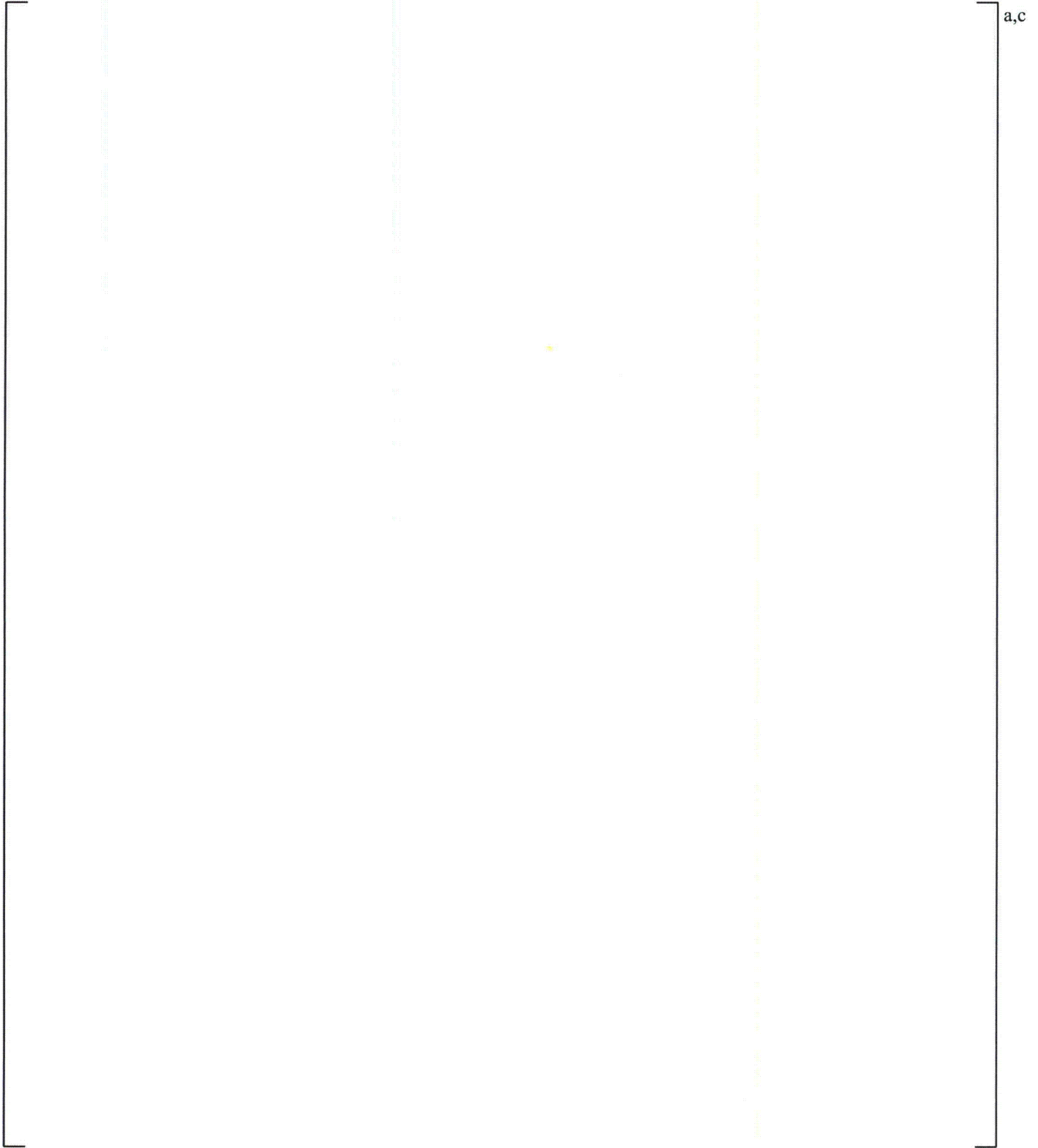
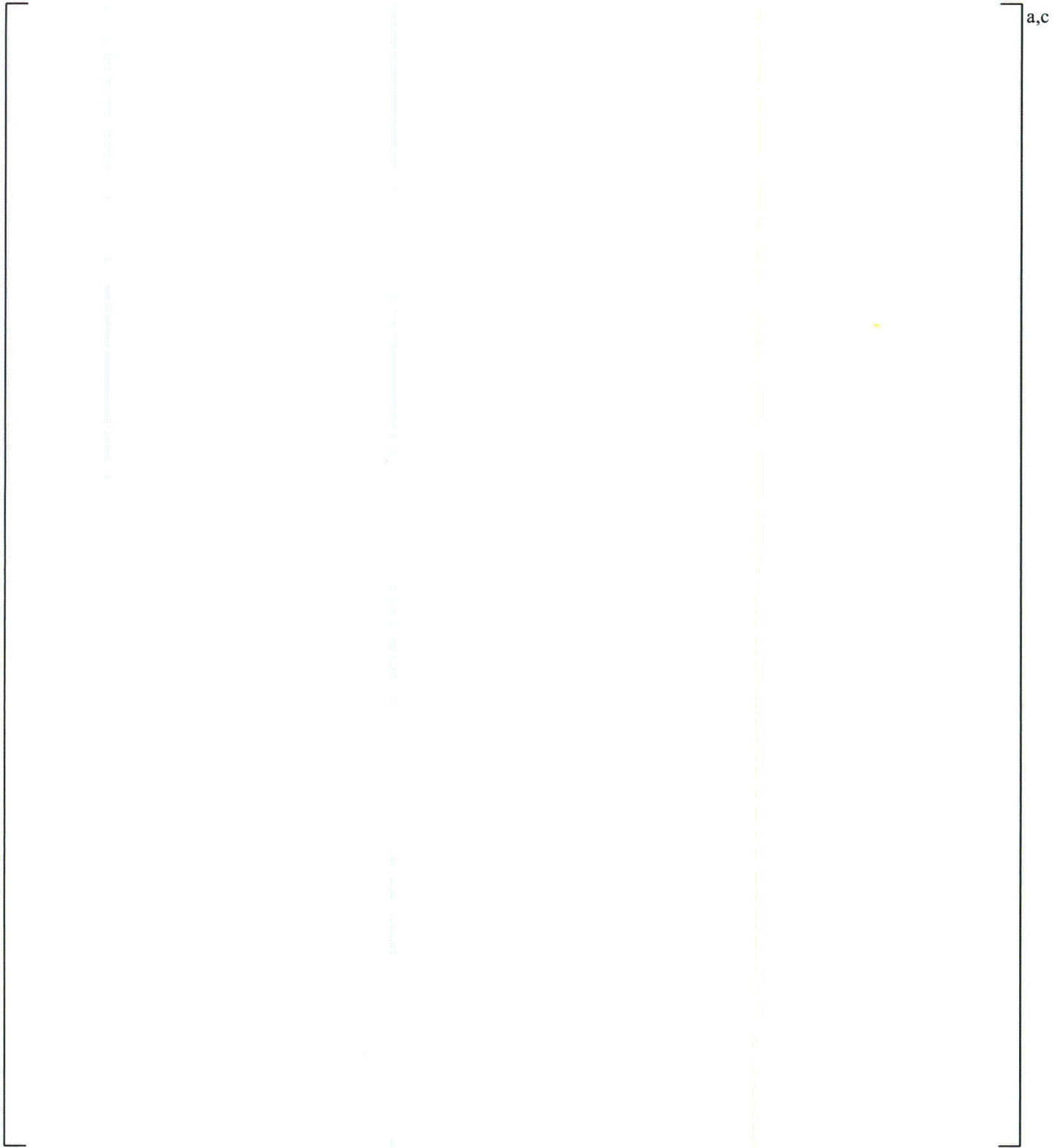


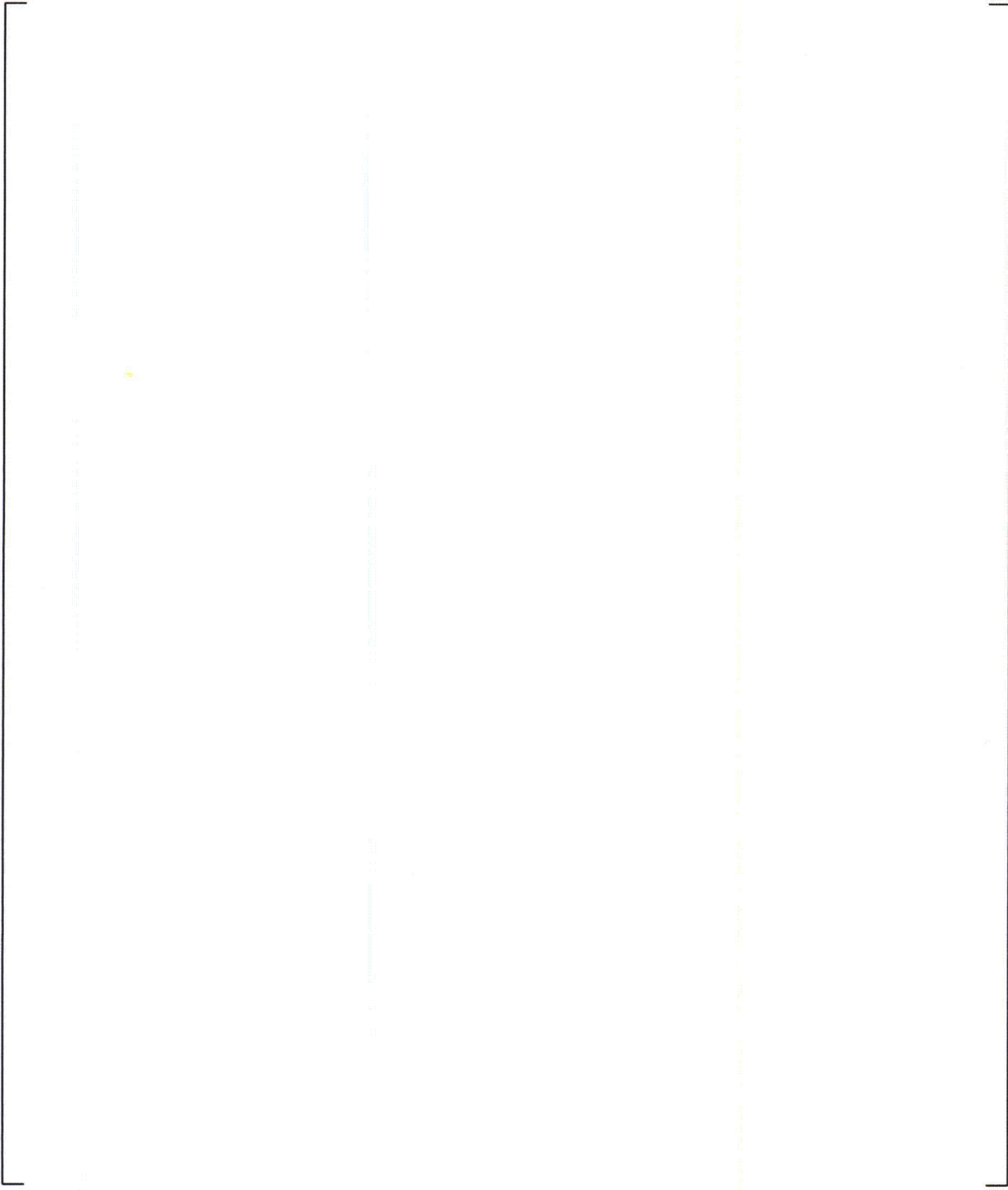
Figure 29.4.1-10 Example Top Skewed Axial Power Distribution [ ]<sup>a,c</sup>



a,c

| **Figure 29.4.1-11** |

]a,c



a,c

| **Figure 29.4.1-12** [

] <sup>a,c</sup>

## 29.4.2 Hot Rod Local Models Uncertainty

Beside the uncertainty in hot rod local power discussed in the previous section, several other uncertainty contributors in the fuel rod models and heat transfer from the rod to the fluid contribute to the local hot spot uncertainty.

The fuel rod modeling was presented in Sections 8.3 through 8.6 (Volume 1). These included the fuel conduction model, the pellet-cladding gap conductance model, the fuel rod deformation model, the cladding reaction with water or steam models, and [ ]<sup>a,c</sup>. The heat transfer from the fuel rod to the fluid was discussed in Section 7 and its assessment is provided in Sections 14 and 15. The discussion in Sections 7 and 8 focuses on the models as coded, while here the discussion is expanded to describe the treatment of the uncertainty associated with those models.

In particular, the following contributors are considered:

- Hot rod peaking factor
- Hot rod radial peaking, [manufacturing tolerances](#), and rod bow uncertainties
- [ ]<sup>a,c</sup>
- Cladding burst temperature
- Cladding burst strain
- [ ]<sup>a,c</sup>
- Zirconium-water reaction
- Fuel relocation
- Convective heat transfer coefficient from the rod to the fluid

Models are considered ‘local’ when the effect of the uncertainty in those models has an effect limited to local processes, such as the local cladding temperature or local cladding oxidation, while the impact of such uncertainties on the ‘global’ thermal-hydraulic process is negligible. The hot rod peaking factor uncertainty reflects the power difference between the hot rod and the hot assembly rod. The additional uncertainty related to hot rod radial peaking, [manufacturing tolerances](#), and rod bow is captured by the local linear heat rate uncertainty. [ ]

[ ]<sup>a,c</sup> The uncertainties in the cladding burst temperature, the cladding burst strain, [ ]<sup>a,c</sup>, Zirconium-water reaction, fuel relocation, and convective heat transfer coefficient are incorporated into [ ]<sup>a,c</sup>.

In the previous ASTRUM methodology (Nissley, M. E., et al., 2005) the WCOBRA/TRAC solution was followed by the execution of a one-dimensional conduction code (HOTSPOT) [ ]

[ ]<sup>a,c</sup>

HOTSPOT is essentially a one-dimensional conduction code used to resolve the heat conduction [ ]<sup>a,c</sup>. Driven by boundary conditions on the fluid side calculated with WCOBRA/TRAC, HOTSPOT was used to simulate the transient conduction [ ]<sup>a,c</sup>. The models in HOTSPOT were consistent with the corresponding models in WCOBRA/TRAC.

[

] <sup>a,c</sup>

The uncertainty methodology for the heat transfer coefficients will be discussed in more detail in Section 29.4.3. The FSLOCA methodology for modeling the hot assembly rods was discussed in Section 8 and is briefly summarized here:

[

] <sup>a,c</sup>

29.4.2.1 [

] <sup>a,c</sup>

[

] <sup>a,c</sup>

### **Fuel Internal Heat Generation – Local Uncertainty**

As discussed in Section 29.4.1.2, the uncertainty in total peaking factor  $F_Q$  is comprised of components that are global in nature, and hence are closely coupled with hot assembly power, and components that are local in nature. The local uncertainties, which do not affect the global thermal-hydraulic solution, are accounted for [ <sup>a,c</sup>. From Tables 25.2-2 and 25.2-3, the local uncertainties in the

local heat generation arise from the combination of [

] <sup>a,c</sup>. The total standard deviation ( $\sigma$ ) can be expressed as:

$$\left[ \left( \left[ \right] \right)^2 + \left( \left[ \right] \right)^2 \right]^{a,c} \tag{29.4.2-1}$$

] <sup>a,c</sup> The local uncertainty amounts to:

$$\left[ \left( \left[ \right] \right)^2 + \left( \left[ \right] \right)^2 \right]^{a,c} \tag{29.4.2-2}$$

where [

] <sup>a,c</sup>

### Cladding Burst Temperature

The rupture criteria for Zircaloy-4 cladding and ZIRLO<sup>®</sup> cladding introduced in Section 8.4.1 are applicable for both the hot assembly rod and [

] <sup>a,c</sup>.

Cladding burst is calculated by monitoring the stress on the cladding and using the cladding rupture correlations to predict the rod burst as described in Section 8.4. The cladding burst temperature can be correlated fairly well as a function of hoop stress for ZIRLO<sup>®</sup> cladding as shown in Figure 8-19 in Section 8.4. Figure 29.4.2-1 is replication of Figure 8-19 with a band of [ ] <sup>a,c</sup> of the calculated burst temperature shown. The [

] <sup>a,c</sup>.

The [ ] <sup>a,c</sup> uncertainty range on cladding burst temperature is used for both Zircaloy-4 and ZIRLO<sup>®</sup> cladding. The ZIRLO<sup>®</sup> data shown in Figure 29.4.2-1 actually indicates a smaller uncertainty than the assumed [ ] <sup>a,c</sup>. These data were obtained by Westinghouse using a consistent testing method. The zircaloy data from Powers and Meyer (1980), which were used to develop the zircaloy burst temperature and burst strain models in Section 8.4.1 (Volume 1), show scatter more consistent with the [ ] <sup>a,c</sup> range (Figure 1 of Powers and Meyer, 1980). This is believed to be at least partly attributable to the variety of testing methods used to obtain the Zircaloy-4 data. Although it is believed that the ZIRLO<sup>®</sup> cladding testing methods are as valid as those in Powers and Meyer, there may be some uncertainty due to the testing method, and the larger uncertainty for both cladding materials is used.

[

] <sup>a,c</sup>

[

]a.c

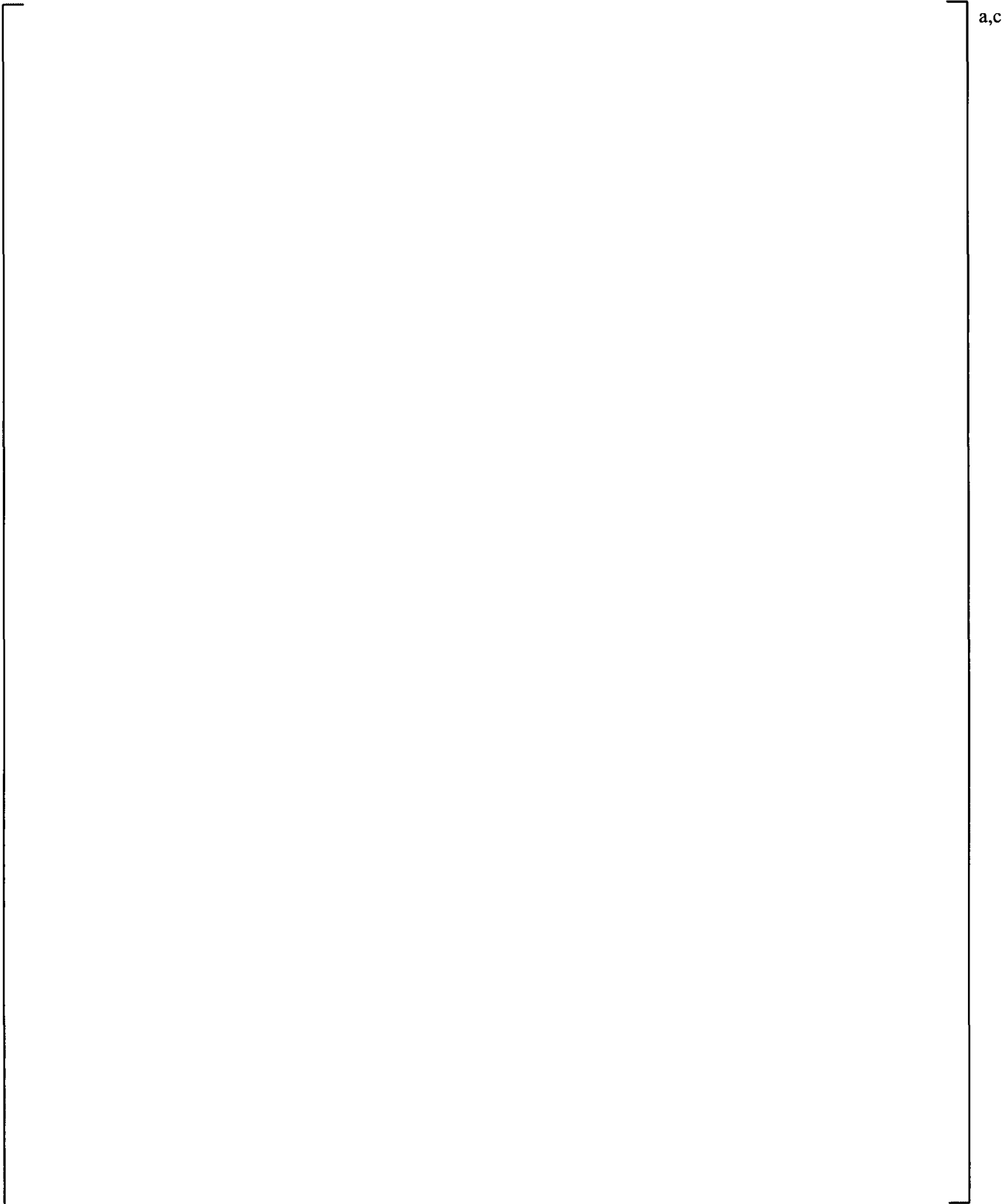


**Figure 29.4.2-1 ZIRLO® Cladding Burst Temperature Data and Correlation**

## Cladding Burst Strain

The burst strain discussed in Section 8.4, as shown in Figures 8-18 and 8-20 for the respective Zircaloy-4 and ZIRLO<sup>®</sup> cladding, is applied to hot assembly rod. However, the data in Figures 8-18 and 8-20 show wide scatter. Burman (1980) discussed how burst occurs randomly at “hot spots” which are the results of a wide range of azimuthal temperature gradients around the cladding. Burman also argued that in fuel rods these gradients can be larger due to random contact of the pellet against the cladding, which then causes smaller burst strains to occur.

For the cladding burst strain of the [ ]<sup>a,c</sup>, Figures 29.4.2-2 and 29.4.2-3 revisit the data of maximum burst strain as a function of burst temperature for the Zircaloy-4 and ZIRLO<sup>®</sup> cladding at different heatup rates to identify the influence of heat up rate. In both cases the scatter is very large for both alpha phase and beta phase, and low uncertainty for the alpha/beta transition region is observed. Thus, three burst temperature ranges are identified: [ ]

[ ]<sup>a,c</sup> Figures 29.4.2-4 to 29.4.2-6 show the Zircaloy-4 burst data in the form of histograms for burst temperature ranges [ ]<sup>a,c</sup>, indicating the frequency of occurrence of a particular burst strain within a range of burst temperatures. [ ]

[ ]<sup>a,c</sup> except for the difference in the transition temperature. The effect of heatup rate on cladding strain is evident [ ]

[ ]<sup>a,c</sup>

[

] <sup>a,c</sup>

[ ] <sup>a,c</sup>

(29.4.2-3)

[

] <sup>a,c</sup>

[ ] <sup>a,c</sup>

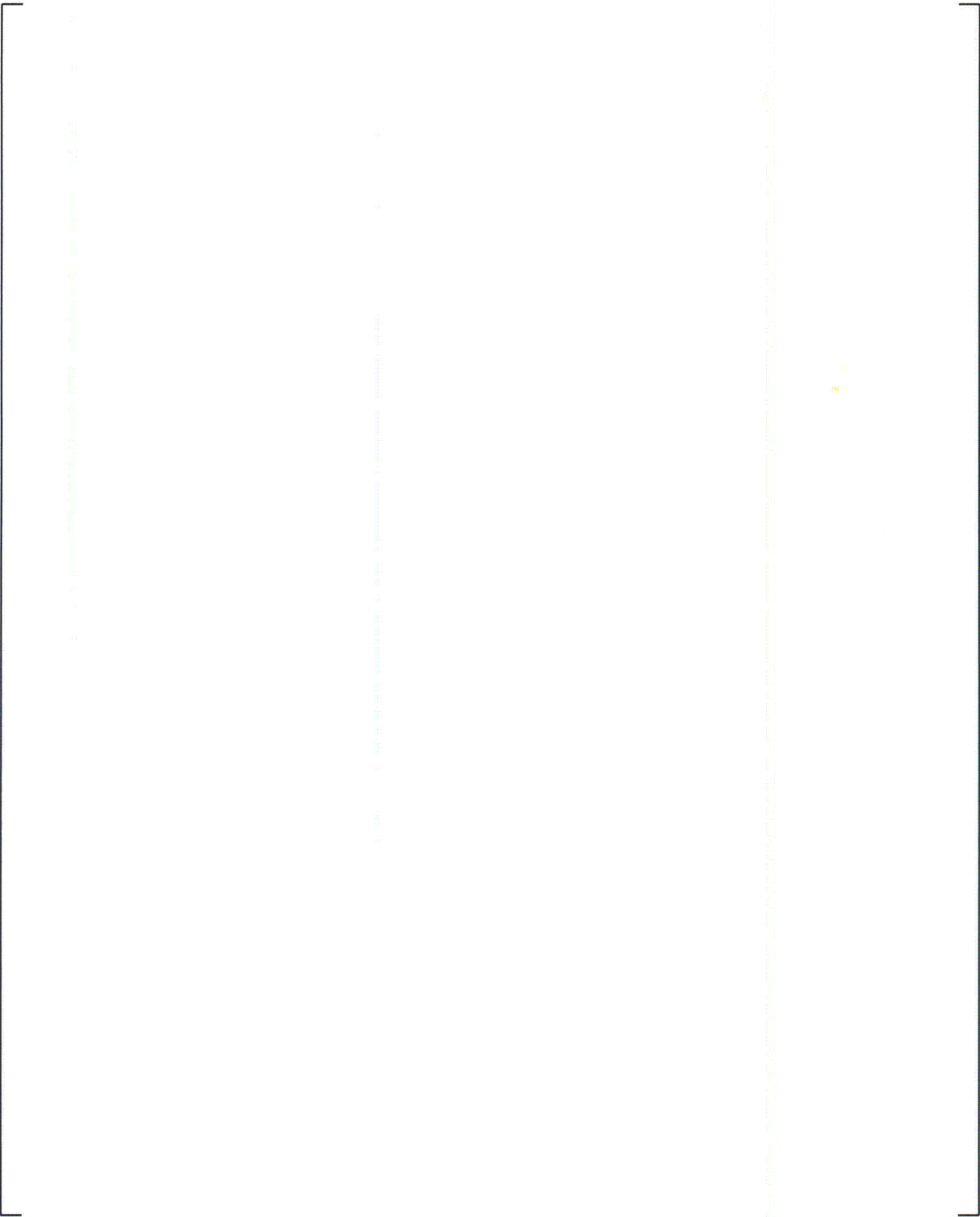
(29.4.2-4)

[ ] <sup>a,c</sup>

(29.4.2-5)

[

] <sup>a,c</sup>



a,c

Figure 29.4.2-2 [

]a,c

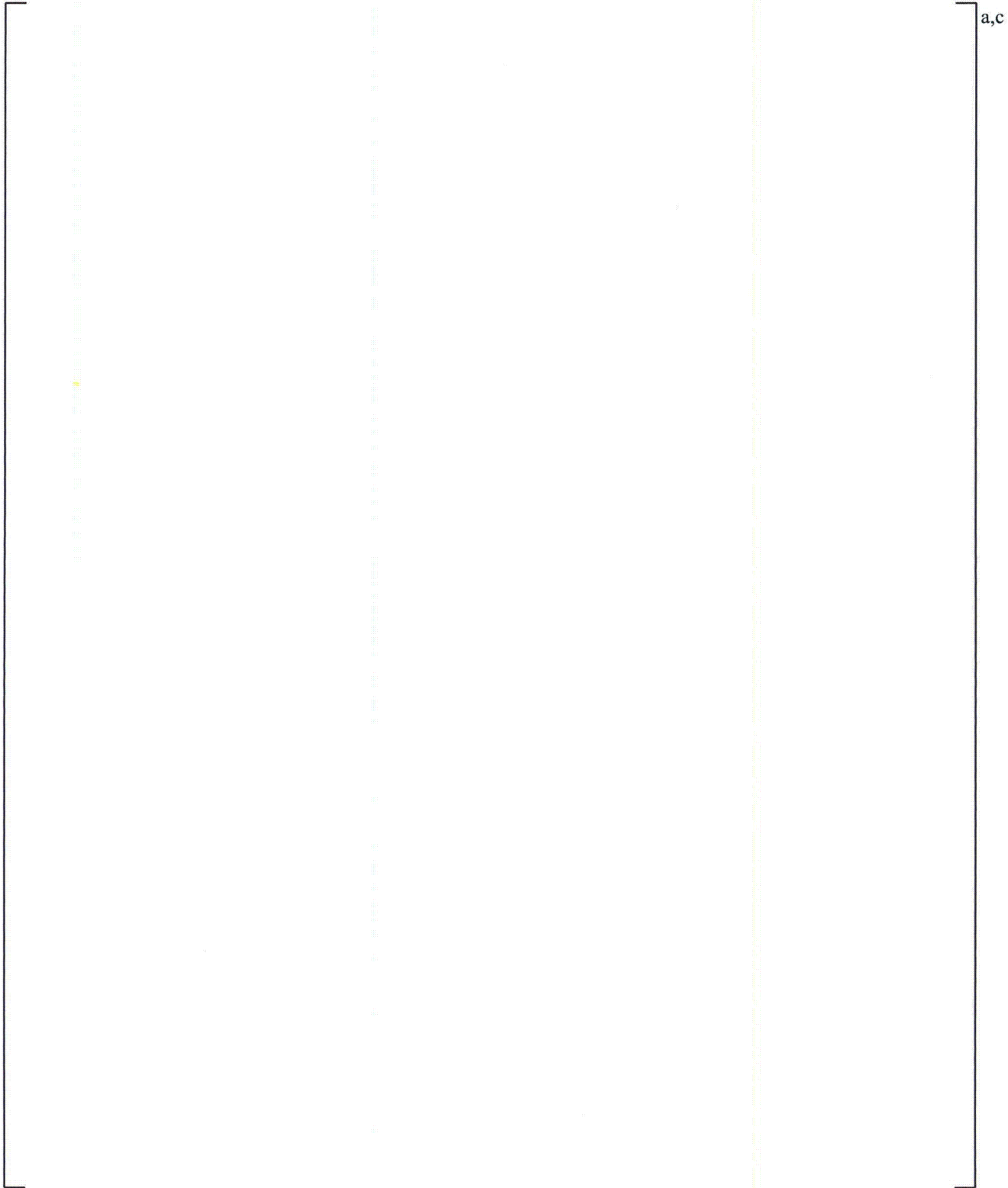


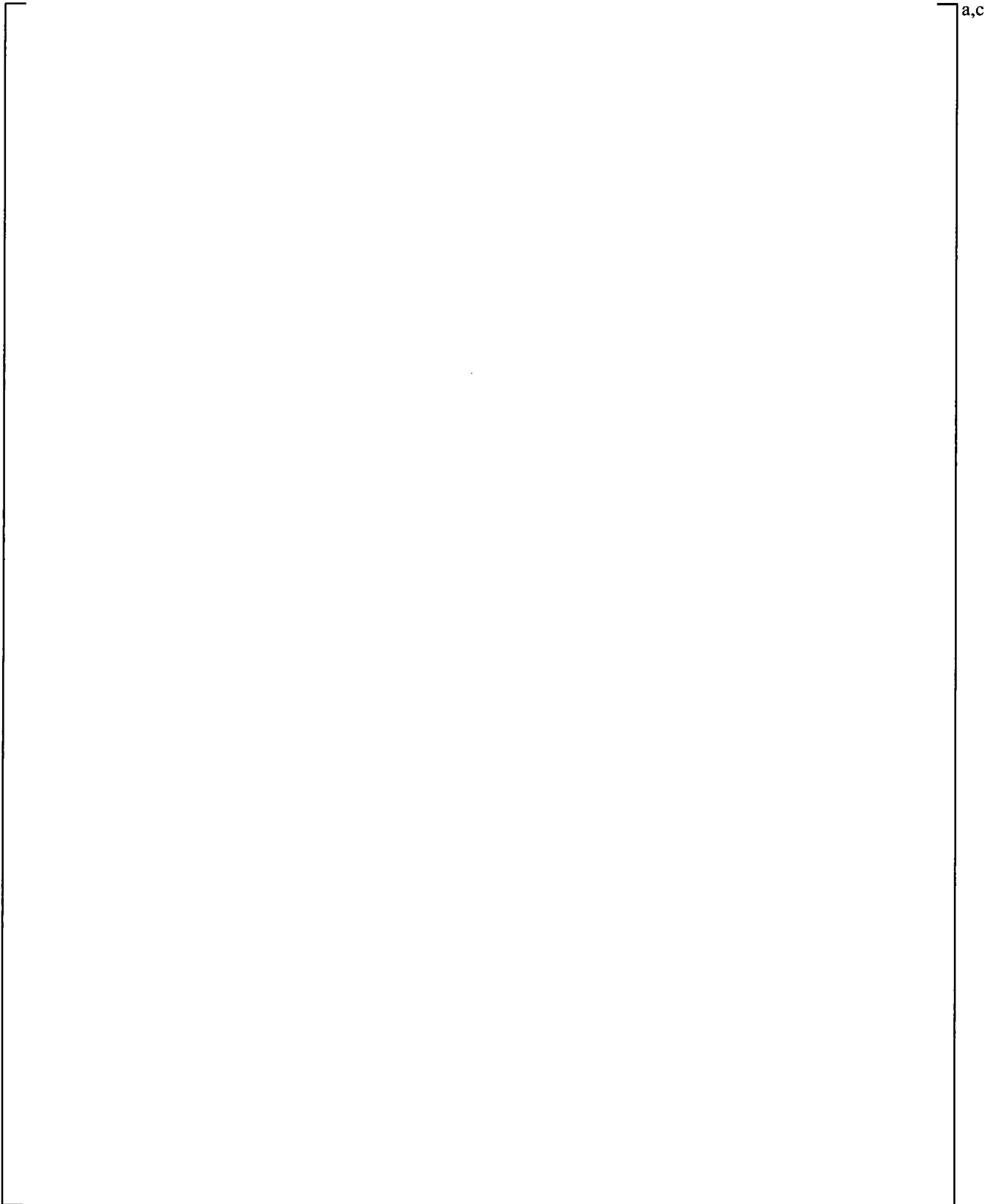
**Figure 29.4.2-3** [

]<sup>a,c</sup>

a,c

**Figure 29.4.2-4** [

] <sup>a,c</sup>



a,c

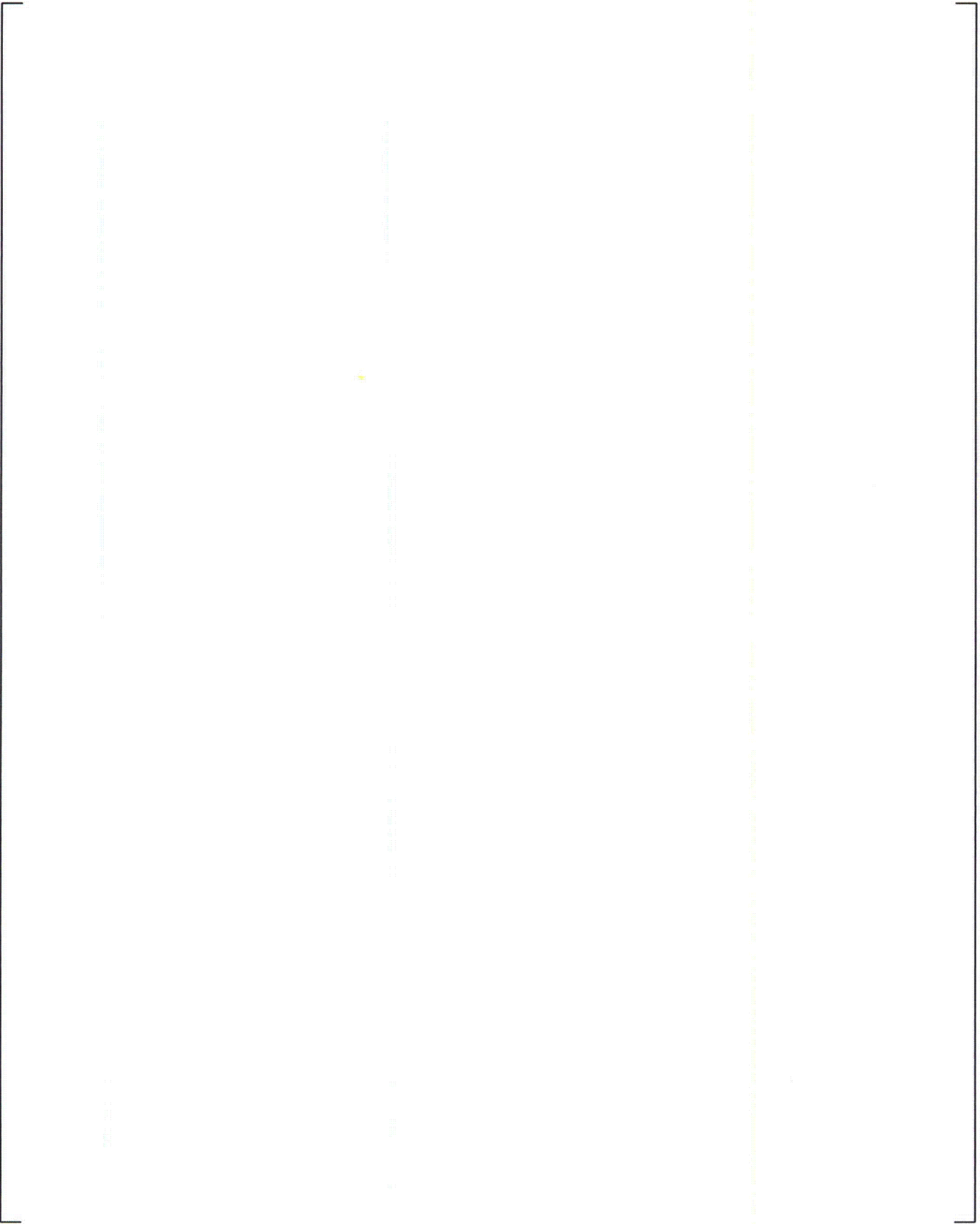
| **Figure 29.4.2-5** |

]<sup>a,c</sup>

a,c

**Figure 29.4.2-6**

a,c



a,c

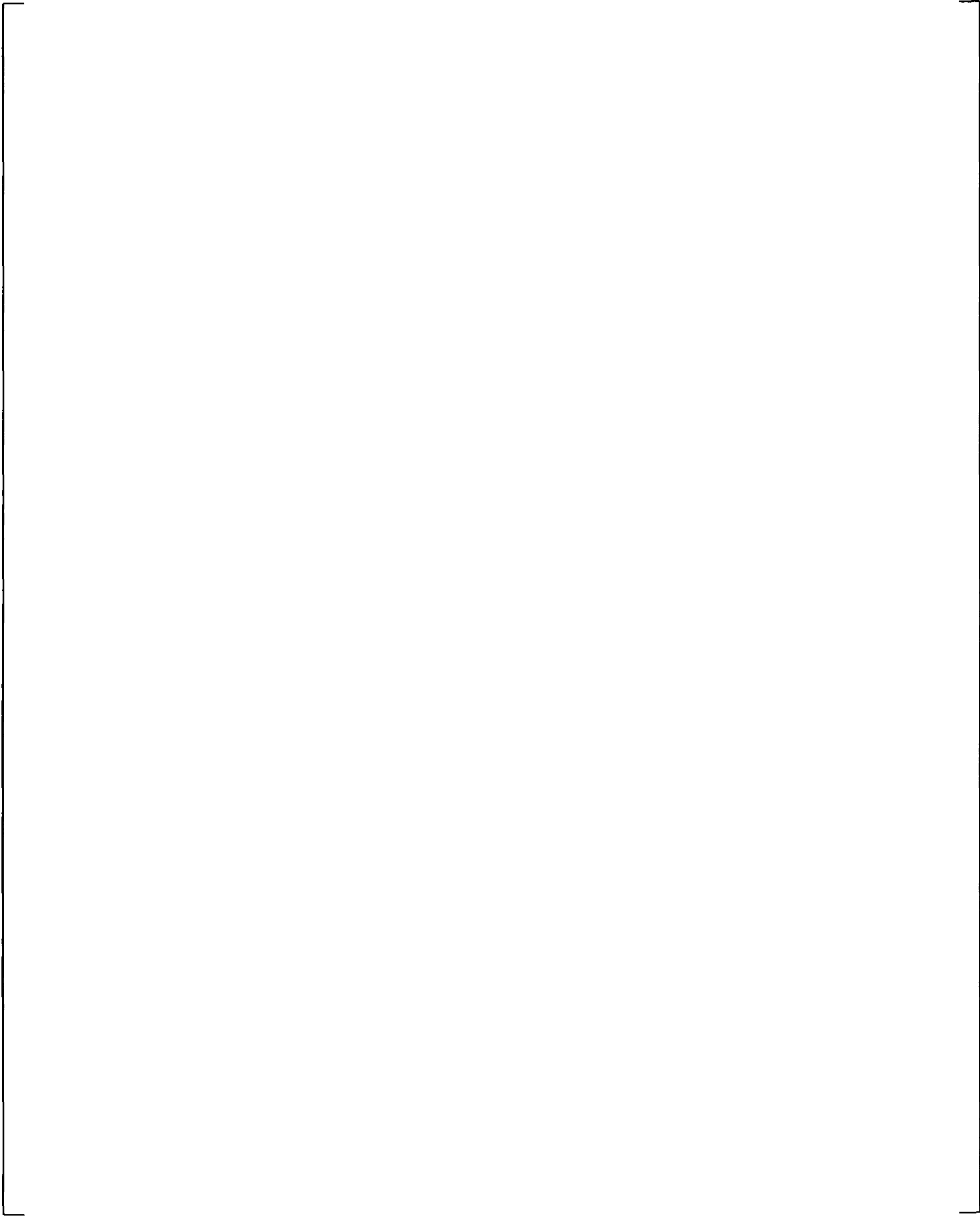
**Figure 29.4.2-7** [

]a,c

a,c

Figure 29.4.2-8 [

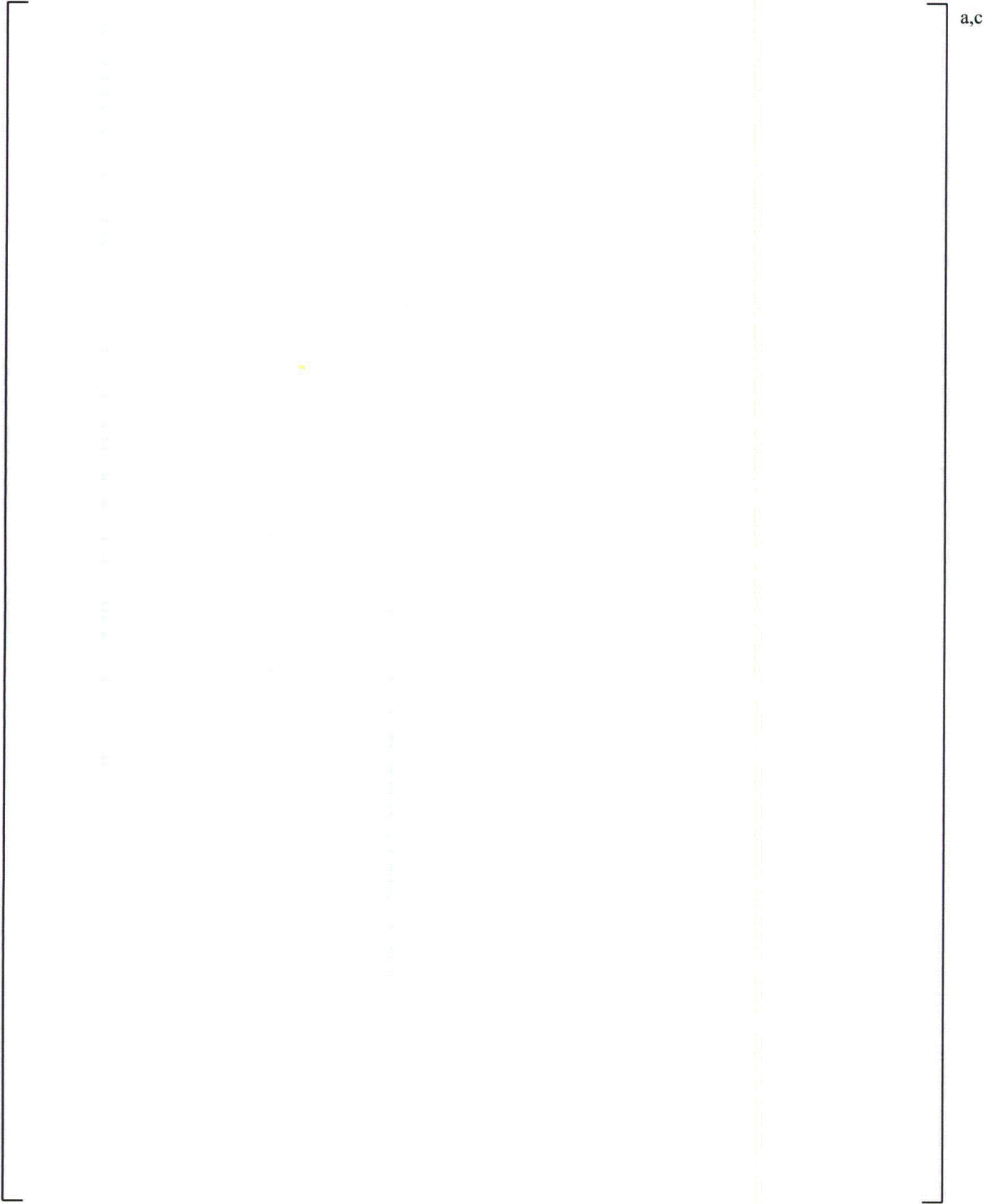
]a,c



a,c

| **Figure 29.4.2-9** |

]a,c



a,c

Figure 29.4.2-10 [

]a,c

### Fuel Relocation Following Burst

The phenomenon of fuel relocation following cladding burst was discussed in Section 8.6.1. The fuel density at the burst region of [ ]<sup>a,c</sup> is measured by packing fraction. The packing fraction is the ratio of the volume of fuel within the burst region to the total volume within the burst region. The INEL (Broughton, 1981) studied data from several sources and used several measurement methods. In addition, NNC performed additional analyses using photographs of the fuel cross sections. These data are summarized in Table 29.4.2-1. A plot of this data versus burst strain (Figure 29.4.2-11) appears to confirm [ ]<sup>a,c</sup>. From these different measurement methods, the uncertainty on packing fraction was estimated.

The numbers of occurrences as a function of packing fractions are plotted in Figure 29.4.2-12. The range was calculated by taking the difference between the maximum and minimum value, and dividing by the average value. A histogram of the data is shown in Figure 29.4.2-12. [ ]<sup>a,c</sup>

<b>Burst Strain Percent</b>	<b>Packing Fractions Percent (Various Measurement Methods)</b>			
29	79	70	66	65
35	63	70	42	63
42	71	67	59	58
47	71	-	62	-
48	62	70	61	74
74	66	-	52	-



Figure 29.4.2-11 [

] <sup>a,c</sup>



Figure 29.4.2-12 Distribution of Packing Fraction Data

### Zirconium-Water Reaction and its Uncertainty

The zirconium-water reaction rate calculations are performed using methods described in Volume 1, Section 8.5. When [

] <sup>a,c</sup> are from Cathcart and Pawel (1977). The prediction interval at 95 percent probability for these equations was calculated from the data using the following equation (Draper and Smith, 1981):

$$Y + t(95\%, n-2) \left[ 1 + \frac{1}{n} + \frac{(X - \bar{X})^2}{\sum (X_i - \bar{X})^2} \right]^{1/2} s \quad (29.4.2-6)$$

Where  $t(95\%, n-2)$  is the 95 percentage point of a t-distribution with  $n-2$  degrees of freedom, to account for sample size,  $\bar{X}$  is the average of the  $X$  values, and  $s^2$  is the residual mean square of the data around the reaction equation line. The equation above is the prediction interval for the next "point estimate" of the reaction rate; the uncertainty interval for the prediction of the mean of the data is smaller (the equation is similar to that above except that the 1 is missing).

The "uncertainty" cited in [

] <sup>a,c</sup> A model is assumed of the form:

$$\ln(\delta^2 / 2) = A + B(1/T(K)) \quad (29.4.2-7)$$

The regression output is shown in Table 29.4.2-2b. The output shows that the constants A and B are:

[  
] <sup>a,c</sup>

These numbers compare to those in Table A2 of Cathcart and Pawel:

A = -1.70986  
B = -20100

[

] <sup>a,c</sup>

**Pre-Accident Corrosion**

NRC Information Notice 98-29 (Roe, 1998) provides clarification that the 10 CFR 50.46(b)(2) maximum local oxidation (MLO) criterion of 17% “includes both pre-accident oxidation and oxidation occurring during a LOCA.” In the FSLOCA uncertainty methodology, therefore, ‘MLO’ results are the sum of the two. At high rod average burnup, the uncertainty in pre-accident corrosion can become important when comparing the total calculated MLO against the 17% limit.

The approved corrosion models for ZIRLO<sup>®</sup> and Optimized ZIRLO<sup>™</sup> cladding (Garde et al., 2013) are incorporated into the PAD5 code as described in Section 3.3.1 of (Crede et al., 2013). The corrosion models were developed based on rod oxide measurements collected from cladding material in post-irradiation exams (PIEs), including data from operating plants. A calibration database was used to develop the model forms and for the determination of the final model coefficients, and a separate validation database was used to independently validate the models.

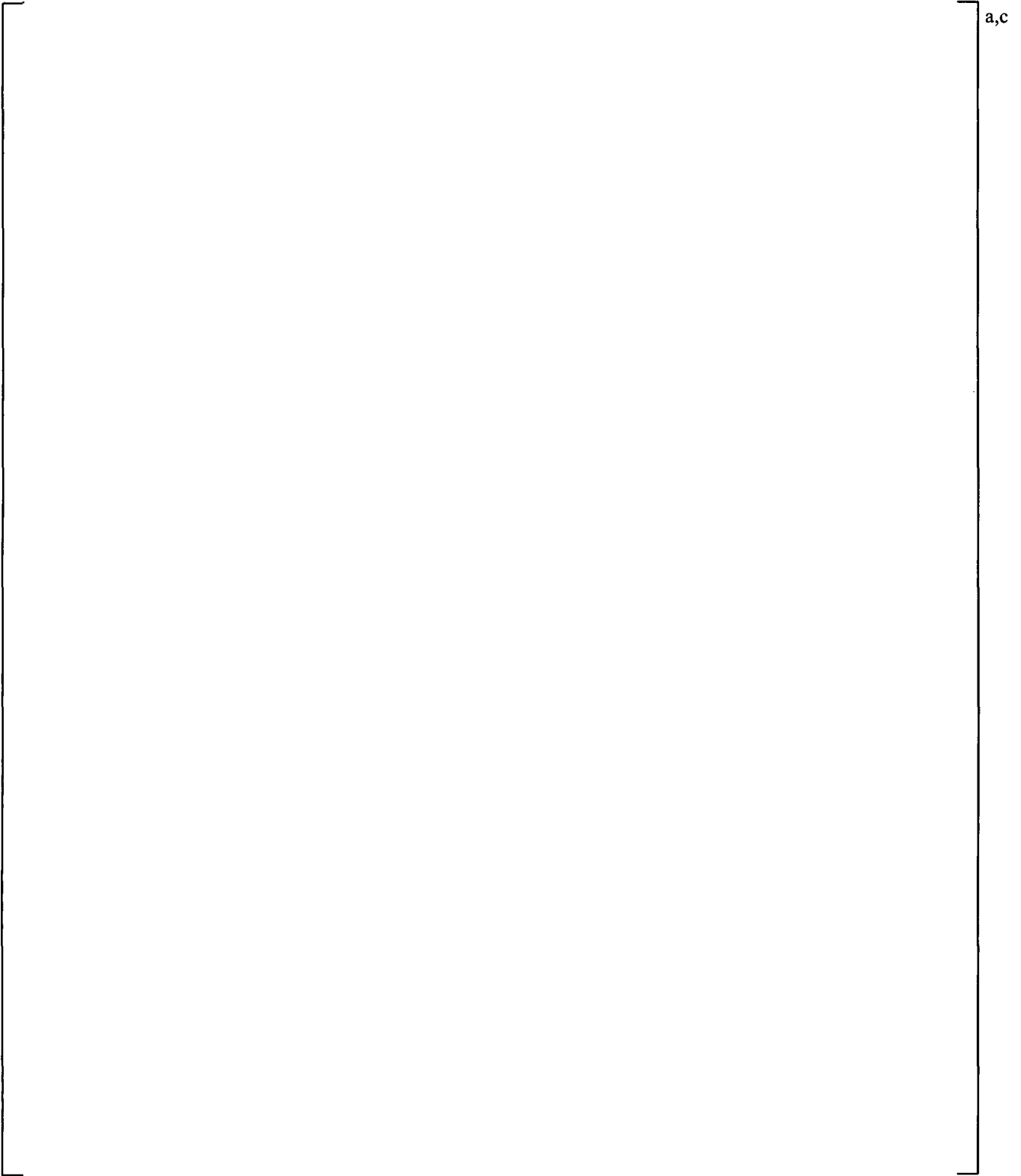
The corrosion model uncertainties were determined as a function of predicted thickness in order to cover 95% of the data over the entire measurement range. The actual uncertainty equation bounds more than 95% of the calibration data set.

In the FSLOCA methodology, [

] <sup>a,c</sup>



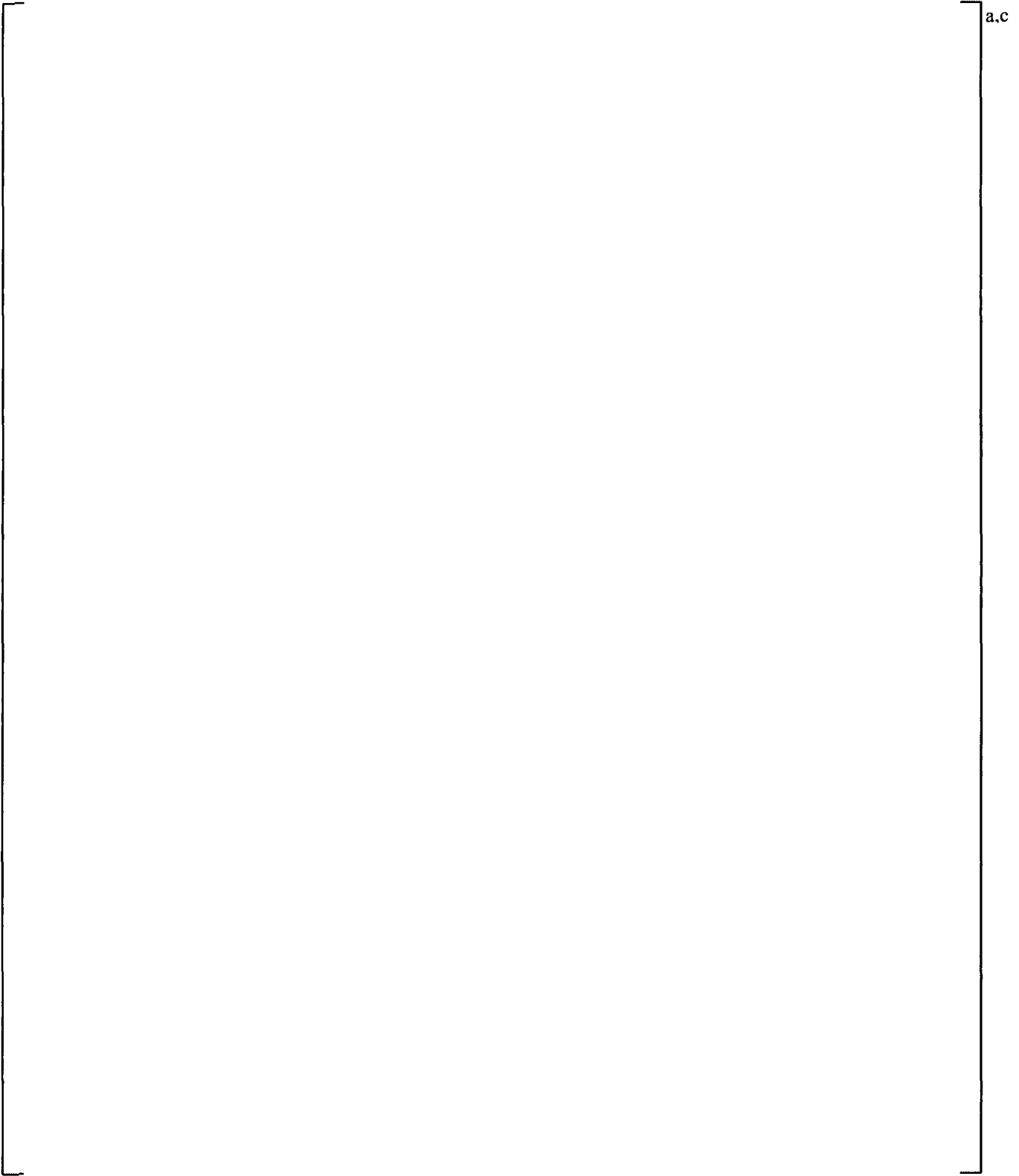




a,c

| **Figure 29.4.2-13** |

]<sup>a,c</sup>



a.c

**Figure 29.4.2-14** [

]<sup>a,c</sup>

**29.4.2.2 Initial Calibration of the Steady-State Condition for the Nuclear Rods**

The initial fuel temperature and rod internal pressure for Westinghouse PWRs are calibrated against the PAD5 fuel performance code (Crede et al., 2013). The calibration of initial fuel temperature is performed for  $J^{a,c}$  in FSLOCA.

The initial stored energy in the fuel is a direct function of the pellet average (radial) fuel temperature which we call TFUEL. The initial fuel temperature is a function of the local linear heat rate and burnup.

[

[

[

$$J^{a,c} \left[ \right]_{a,c} \tag{29.4.2-8}$$

$$J^{a,c} \left[ \right]_{a,c} \tag{29.4.2-9}$$

$$J^{a,c}$$

[

] <sup>a,c</sup>

[ ] <sup>a,c</sup>

(29.4.2-10)

[

] <sup>a,c</sup>

[ ] <sup>a,c</sup>

(29.4.2-11)

[

] <sup>a,c</sup>

[

] <sup>a,c</sup>

## 29.5 EVALUATION MODEL BIASES AND UNCERTAINTY (EMDAP STEP 20)

According to the Regulatory Guide 1.203, a singular uncertainty statement on the overall uncertainty results can only be achieved when the individual uncertainty contributions are determined. The procedure used to obtain the convolution of such uncertainties is the subject of Section 30. The development of the individual uncertainty contributors, ranges, and probability density functions has been the objective of this section.

The uncertainty contributors are divided in two main categories:

1. The first main category is the uncertainty associated with the code capability of representing phenomena and processes identified as highly important by the PIRT. The capability is established by assessing the code against SET/IET experiments that were designed to simulate such processes. The combined uncertainty will reflect the degree to which the individual models, correlations and methods used within the code represent the physical phenomena, the uncertainty associated with the use of such models, and the uncertainty associated with the experimental data itself and applicability of the data to PWRs.
2. The second main category is the uncertainty associated with the input boundary and initial conditions and all those parameters that define the plant state at the time of the postulated LOCA event, as well as the uncertainty associated with the break location, break type and size, etc. This uncertainty is not the result of the code capability of simulating the LOCA event, but rather the uncertainty associated with the LOCA scenario event itself.

The purpose of this section is to summarize the methodology for the treatment of the uncertainty contributors contained mainly in the first category. This is in line with the intent of Step 20 of the EMDAP, which asks for the determination of the EM biases and uncertainty. Since the process started by identifying the important phenomena with the PIRT, it is useful here to structure the review following the PIRT (Section 2), by describing how each of the phenomena was considered in the uncertainty methodology.

### 29.5.1 Fuel Rod

#### Stored Energy

Uncertainties in the initial stored energy of the hot rod and hot assembly are large. There is a wide range of possible peaking factors and power distributions that are allowed by the Technical Specifications. For a given power distribution, [

] <sup>a,c</sup> have been considered in the uncertainty methodology by explicitly ranging them as part of the uncertainty methodology.

### Clad Oxidation

The metal-water reaction rate is ranged based on uncertainty estimates obtained from experimental data. This uncertainty is treated as a local uncertainty – see Table 29-3a for the numerical values.

[ ]<sup>a,c</sup>

### Decay Heat

The decay heat uncertainties from the American National Standards Institute/American Nuclear Society (ANSI/ANS) 5.1-1979 standard are applied as described in Section 9.7. [

] <sup>a,c</sup>

### Clad Deformation (Burst Strain, Relocation)

These processes were ranked [

] <sup>a,c</sup> The uncertainty on cladding burst strain and temperature are obtained from the data scatter. The fuel pellet fragments packing fraction after relocation is also identified as an uncertainty contributor. Numerical values are provided in Table 29-3a and Table 29-3b.

## 29.7 REFERENCES

1. Akimoto, et al., 1984, J. Nucl. Sci. & Tech., 21[6], pp. 450-465, June 1984.
2. Bajorek, S. M., et al., 1998, "Code Qualification Document for Best Estimate LOCA Analysis," WCAP-12945-P-A, Volume 1 Revision 2, and Volumes 2 through 5 Revision 1, and WCAP-14747.
3. Boyack, B., et al., "Quantifying Reactor Safety Margins," NUREG/CR-5249, (1989).
4. American Nuclear Society, 1979, "Decay Heat in Light Water Reactors," ANSI/ANS 5.1.
5. Anklam, T. M., et al., 1982, "Experimental Investigations of Uncovered Bundle Heat Transfer and Two-Phase Mixture Level Swell Under High Pressure Low Heat Flux Conditions," NUREG/CR-2456.
6. Baum, A. J., 1977, "A Study of Transition and Film Boiling From Vertical Surfaces," Ph. D. Thesis, Carnegie-Mellon University.
7. Bordelon, F. M. and Murphy, E. T., 1974, "Containment Pressure Analysis Code (COCO)," WCAP-8327 (Proprietary), WCAP-8306 (Non-Proprietary).
8. Broughton, J. M., 1981, "PBF LOCA Test Series, Test LOC-3 and LOC-5 Fuel Behavior Report," NUREG/CR-2073.
9. Burman, D. L., 1980, "Comparison of Westinghouse LOCA Burst Tests Results with ORNL and Other Program Results," Specialist Meeting on Fuel Behavior Under Accident Conditions, September 1 – 4, Helsinki, Finland.
10. Cathcart, J. V., and Pawel, 1977, "Zirconium Metal-Water Oxidation Kinetics IV – Reaction Rate Studies," ORNL/NUREG-17, Oak Ridge National Laboratory, Oak Ridge, TN.
11. Combustion Engineering, 1981, "C-E ECCS Evaluation Model – Flow Blockage Analysis – ECCS Analysis," Enclosure 1-P-A (Proprietary) and Enclosure 1-NP-A (Non-Proprietary) to LD-81-095.
12. Crede, T. M., et al., 2013, "Westinghouse Performance Analysis and Design Model (PAD5)," WCAP-17642-P (Proprietary), WCAP-17642-NP (Non-Proprietary).
13. Crane Co., 1988, "Flow of Fluids Through Valves, Fittings, and Pipes," Technical Paper No. 410.
14. Dhir, V. K., Duffey, R. B., and Catton, I., 1981, "Quenching Studies on a Zircaloy Rod Bundle," ASME J. Heat Transfer, Vol. 103, pp. 293-299.
15. Draper, N. and Smith, H., 1981, "Applied Regression Analysis, Second Edition," John Wiley and Sons.

16. Frepoli, C., 2007, "Assessment of Rod-to-Rod Thermal Radiation Heat Transfer Contribution During Reflood in PWR Fuel Assemblies," ICAPP 2007, Nice, France, May 13-18, Paper 7323.
17. Garde, A., et al., "Westinghouse Clad Corrosion Model for ZIRLO and *Optimized ZIRLO*," WCAP 12610-P-A & CENPD-404-P-A, Addendum 2-A (Proprietary), WCAP-14342-A & CENPD-404-NP-A, Addendum 2-A (Non-Proprietary), October 2013.
18. Ganic, E. and Rohsenow, W. M., 1977, "Dispersed Flow Heat Transfer," Int. J. Heat Mass Transfer, Vol. 20, pp. 855-866.
19. Henry, R. E., 1974, "A Correlation for the Minimum Film Boiling Temperature," AICHE Symposium Series, Vol. 138, pp. 81-90.
20. Holmes, B. J., 1991, "ISP 25 Comparison Report," AEA-TRS-1043.
21. Lanning, D. D., Beyer, C. E., Geelhood, K. J., 2005, "FRAPCON-3 Updates, Including Mixed-Oxide Fuel Properties," Pacific Northwest National Laboratory, NUREG/CR-6534, Vol. 4.
22. Loftus, M. J., et al., 1980, "PWR FLECHT-SEASET Unblocked Bundle Forced and Gravity Reflood Task, Data Report," WCAP-9699.
23. Morita, T., et al., 1974, "Power Distribution Control and Load Following Procedures," WCAP-8385-P-A.
24. MPR, 1990, "Summary of Results From the UPTF Downcomer Separate Effects Tests, Comparison to Previous Scaled Tests, and Application to U.S. Pressurized Water Reactors," MPR Associates, MPR-1163.
25. Nissley, M. E., et al., 2005, "Realistic Large-Break LOCA Evaluation Methodology Using the Automated Statistical Treatment Of Uncertainty Method (ASTRUM)," WCAP-16009-P-A and WCAP-16009-NP-A.
26. Powers, D. A. and Meyer, R. O., 1980, "Cladding Swelling and Rupture Models for LOCA Analysis," NUREG/CR-0630.
27. Roe, J., 1998, "NRC Information Notice 98-29: Predicted Increase in Fuel Rod Cladding Oxidation."
28. Schueren, P., 2006, "Optimized ZIRLO™," WCAP-12610-P-A & CENPD-404-P-A, Addendum 1-A.
29. Shumway, R., 1985, "Return to Nucleate Boiling," ANS Proceedings National Heat Transfer Conference, Denver, CO, pp. 372-388.
30. Spier, E. M., et al., 1988, "Evaluation of Nuclear Hot Channel Factor Uncertainty," WCAP-7308-L-P-A.

31. Tasaka, K., et al., 1988, "The Results of 5% Small Break LOCA Tests and Natural Recirculation Tests at the ROSA-IV LSTF," Nuclear Engineering and Design, 108.
32. Tregoning, Abramson, Scott, and Chokshi, "LOCA frequency evaluation using expert elicitation," Nuclear Engineering and Design 237 (2007) 1429-1436.
33. Vijaykumar, R. and Dhir, V. K., 1992, "An Experimental Study of Sub-cooled Film Boiling on a Vertical Surface – Hydrodynamic Aspects," ASME J. Heat Transfer, Vol. 114, pp. 161-178.
34. Wong, S. and Hochreiter, L. E., 1981, "Analysis of the FLECHT-SEASET Unblocked Bundle Steam Cooling and Boiloff Tests," NRC/EPRI/Westinghouse-8.
35. Yoder, et al., 1982, "Dispersed Flow Film Boiling in Rod Bundle Geometry – Steady-State Heat Transfer Data and Correlation Comparisons," NUREG/CR-2435, ORNL-5822.

**Updates to Sections 30.1, 30.4, 30.5, 30.6 and 30.7 of**

**WCAP-16996-NP**

**“Realistic LOCA Evaluation Methodology Applied to the Full**

**Spectrum of Break Sizes**

**(FULL SPECTRUM LOCA Methodology)”**

## 30 TECHNICAL BASIS OF STATISTICAL PROCEDURES APPLIED IN FULL SPECTRUM LOCA UNCERTAINTY METHODOLOGY

### 30.1 STATISTICAL METHODOLOGY ROADMAP

A realistic (best-estimate) safety analysis asks for the assessment of uncertainties associated with physical models, data uncertainties, and plant initial and boundary condition variability. The current safety regulations of the United States Nuclear Regulatory Commission (US NRC) are stipulated in 10 CFR Part 50, Section 50.46. Based on the 10 CFR 50.46 rule, an emergency core cooling system (ECCS) design is required to satisfy prescriptive criteria. The regulation identifies the following five criteria:

1. Peak cladding temperature (PCT) shall be less than 2200°F
2. Maximum local oxidation (MLO) shall be less than 17%
3. Core-wide oxidation (CWO) shall be less than 1% (to limit the maximum amount of hydrogen generated)
4. The core shall maintain a coolable geometry
5. Long term cooling shall be demonstrated

NRC Information Notice 98-29 (Roe, 1998) provides further clarification that the 10 CFR 50.46(b)(2) MLO criterion “includes both pre-accident oxidation and oxidation occurring during a LOCA.” In the FSLOCA uncertainty methodology, therefore, ‘MLO’ results are the sum of the two.

Code Scaling, Applicability, and Uncertainty (CSAU) Element 3, the sensitivity and uncertainty analysis element, aims to provide a simple Best-Estimate Plus Uncertainty (BEPU) statement (Boyack, et al. 1989) that satisfies the first three criteria above. To accomplish this objective, the effects of the important uncertainty contributors are determined. The uncertainty statement is based on the combined effect of the contributors.

The objective of a LOCA analysis is to address criteria (b)(1), (b)(2) and (b)(3) of 10 CFR 50.46, the determination of peak cladding temperature (PCT), maximum local oxidation (MLO) and core-wide oxidation (CWO). Typically the last two criteria (coolable geometry and long-term cooling), are satisfied outside the LOCA analysis once the LOCA calculation is demonstrated to be in compliance with the first three criteria. [

] <sup>a,c</sup>

Regarding the treatment of uncertainties within the CSAU framework, the most straightforward approach is to combine the uncertainties with a direct Monte Carlo simulation. The procedure is designed to generate a sample of the short term LOCA ‘population,’ and then non-parametric statistical inference procedures are used to develop probabilistic statements that show compliance with the 10 CFR 50.46 criteria.

The code (WCOBRA/TRAC-TF2) is the 'black-box' which receives as input a set of random values, one for each uncertainty parameter, and outputs the three values that characterize a specific LOCA scenario (PCT, MLO and CWO). [

] <sup>a,c</sup>

Several cases (scenarios) are executed until the sample size is large enough to represent the population and stabilize the estimates of the key parameters of interest. The issue is how results are interpreted to demonstrate compliance with the 10 CFR 50.46 requirements.

10 CFR 50.46 states that "[...] uncertainty must be accounted for, so that, when the calculated ECCS cooling performance is compared to the criteria set forth in paragraph (b) of this section, there is a high level of probability that the criteria would not be exceeded." Paragraph (b) of 10 CFR 50.46 contains the list of the acceptance criteria. 10 CFR 50.46 does not explicitly specify how this probability should be evaluated or what its value should be.

Additional clarification as to the US NRC expectations on the acceptable implementation of the "high probability" requirement is provided in Section 4 of Regulatory Guide 1.157 (Best-Estimate Calculations of Emergency Core Cooling System Performance) that states: "a 95% probability is considered acceptable to the NRC staff [...]." Further, Regulatory Guide 1.157 introduced the concept of confidence level as a possible refinement to the uncertainty treatment, but did not expand further on this concept.

As statistical methods are implemented to perform LOCA safety analyses, a statistical statement which estimates or bounds the 95th quantile of the population with a 95% confidence level has been suggested by the NRC as acceptable to demonstrate the required "high probability." In the previous approved methodology (ASTRUM, WCAP-16009-P-A) the 95th quantile of the joint-distribution of PCT, MLO and CWO is bounded with at least 95% confidence level. The Safety Evaluation Report (SER) of the Westinghouse Best-Estimate Large Break LOCA methodology (ASTRUM) states the following: "*the staff determined that a 95th percentile probability level based on best approximations of the constituent parameter distributions and the statistical approach used in the methodology is appropriately high for this application.*"

Consistently with the previously approved methodology, the 95/95 criterion is also considered for the FULL SPECTRUM LOCA (FSLOCA) methodology.

One key difference between the previous LBLOCA methodology (ASTRUM, WCAP-16009-P-A) and FSLOCA is that the FSLOCA methodology extends the break area spectrum considered in the analysis to cover the full range from what is historically defined as Small Breaks (SB) to Large Breaks (LB) including break sizes typically not analyzed and classified as Intermediate Breaks (IB).

As discussed in Section 29.4, a simple extension of the ASTRUM approach to smaller break sizes was considered not appropriate because SBLOCA would not be properly considered in the sample by simply

extending a uniform probability distribution of the split break sizes in the SB region. A more balanced approach has been developed and was discussed in Section 29.4.

[

] <sup>a,c</sup>

30.4 [

] <sup>a,c</sup>

[

] <sup>a,c</sup>

[

] <sup>a,c</sup>

[

] <sup>a,c</sup>**30.5 OVERVIEW OF FULL SPECTRUM LOCA STATISTICAL PROCEDURE**

Sections 30.3 and 30.4 provided the theoretical basis for the various statistical procedures needed to:

1. Generate a representative sample of the LOCA scenarios population;
2. Analyze the results and infer figures of merit that can satisfy compliance with the 10 CFR 50.46 design criteria.

[

] <sup>a,c</sup>

[

] <sup>a,c</sup>

[

] <sup>a,c</sup>

### 30.6 CONCLUSIONS ON COMPLIANCE WITH 10 CFR 50.46 ACCEPTANCE CRITERIA

The previous Sections described the statistical theory used to determine the number of cases required to bound the 95th percentile of [ ]<sup>a,c</sup> with a joint probability of 95% confidence. This assures that there is a high probability that the first two acceptance criteria are met, consistent with the Code of Federal Regulations (CFR) 10 CFR 50.46 requirements and Regulatory Guide 1.157 guidance. Further insights on the full compliance with the 10 CFR 50.46 criteria are described below.

#### 30.6.1 [ ]<sup>a,c</sup>

[

] <sup>a,c</sup>

#### 30.6.2 [ ]<sup>a,c</sup>

[

] <sup>a,c</sup>

[

] <sup>a,c</sup>

### 30.7 REFERENCES

1. Boyack, B., et al., "Quantifying Reactor Safety Margins," NUREG/CR-5249, (1989).

2. [

] <sup>a,c</sup>

3. Guba, A., et al., "Statistical Aspects of Best Estimate Method-I," Reliability Engineering and System Safety, 80, (2003), pp. 217-232.

4. Montgomery, D. C., "Design and Analysis of Experiments," 5<sup>th</sup> Edition, 2000.
5. Press, W. H., et al., "Numerical Recipes in FORTRAN: The Art of Scientific Computing," 2<sup>nd</sup> Edition, Cambridge University Press, 1992, Chapter 7.
6. Roe, J., "NRC Information Notice 98-29: Predicted Increase in Fuel Rod Cladding Oxidation," August 3, 1998.
7. Wald, A., "An Extension of Wilks' Method for Setting Tolerance Limits," Annals of Mathematical Statistics, Vol. 14 (1943), pp. 45-55.
8. Wilks, S. S., "Determination of Sample Sizes for Setting Tolerance Limits," The Annals of Mathematical Statistics, Vol. 12 (1941), pp. 91-96.

**Updates to Sections 32.1, 32.2 and 32.4 of WCAP-16996-NP**

**“Realistic LOCA Evaluation Methodology Applied to the Full**

**Spectrum of Break Sizes**

**(FULL SPECTRUM LOCA Methodology)”**

## 32 METHODOLOGY SUMMARY

In this section, the FULL SPECTRUM LOCA (FSLOCA) evaluation model is assessed against applicable regulatory criteria and guidance.

### 32.1 COMPLIANCE WITH 10 CFR 50.46

1. (i) – This part briefly outlines the requirements for an acceptable evaluation model, and requires that demonstration be provided that the limits of the Code of Federal Regulations (CFR) 10CFR50.46 be met with a high degree of probability. Additional details concerning these requirements are spelled out in Regulatory Guides (RG) 1.157 (US Nuclear Regulatory Commission (NRC), 1989) and 1.203 (US Nuclear Regulatory Commission, 2005). Compliance of the best-estimate methodology with these requirements is addressed in detail in the next section.
2. Peak Cladding Temperature – The peak cladding temperature (PCT) is verified to remain below the limit of 2,200°F for loss-of-coolant accidents (LOCAs) of all break sizes, using the methods described in Section 30. A demonstrative application of the method is discussed in Section 31.
3. Maximum Cladding Oxidation – The maximum cladding oxidation (MLO) is verified to remain below the regulatory limit of 17 percent of cladding thickness, using the procedure described in Section 30. Consistent with NRC Information Notice 98-29 (Roe, 1998), MLO is taken as the sum of pre-accident oxidation and the oxidation occurring during the LOCA. A demonstrative application of the method is discussed in Section 31.
4. Maximum Hydrogen Generation – The hydrogen generated in the core, as determined by estimating the total volume of cladding oxidized for the limiting conditions, is verified to be less than the regulatory limit of 0.01 times the maximum theoretical amount, using the procedure described in Section 30. A demonstrative application of the method is discussed in Section 31.
5. Coolable Geometry – Westinghouse reload cores are analyzed using plant-specific or bounding seismic and LOCA loads to confirm that the core remains coolable during the LOCA. This acceptance criteria is met by compliance with acceptance criteria (b)(1), (b)(2), and (b)(3), and showing that grid crush due to combined seismic and LOCA loads does not extend to the in-board assemblies. Specific calculations are performed if grid crushing occurs in the in-board assemblies to assess the effects of the grid crush (Section 25.1).
6. Long-Term Cooling – Long-term cooling is dependent on the demonstration of continued delivery of cooling water to the core. The actions, automatic or manual, that are currently in place at these plants to maintain long-term cooling remain unchanged.

The NRC has initiated the formal process to revise the ECCS acceptance criteria in § 50.46 via issuance of an Advance Notice of Proposed Rulemaking (FR 40765). In its current form, the FSLOCA EM shows compliance with the current 10 CFR 50.46 criteria. Changes to the method will be required to address the 10 CFR 50.46c rulemaking, with the expectation that the Maximum Cladding Oxidation criterion will be replaced with an allowable Equivalent Cladding Reacted (ECR) limit that is based on cladding hydrogen

content (along with other considerations). Appendix A of this report describes how the FSLOCA EM will comply with known elements of the 10 CFR 50.46c rulemaking when the rulemaking process is complete.

### **32.2 COMPLIANCE WITH REGULATORY GUIDE 1.203**

The FULL SPECTRUM LOCA Evaluation Model (FSLOCA EM) has been developed consistently with Regulatory Guide (RG) 1.203 which represents an evolution and extension to the 1989 RG 1.157. RG 1.203 provides guidance on the Evaluation Model Development and Assessment Process (EMDAP). RG 1.203 extends on the regulatory positions of RG 1.157 which has been the basis of previously approved methodologies (2004 ASTRUM EM, WCAP-16009-P-A and 1996 CQD, WCAP-12945-P-A).

The EMDAP is the process utilized to define the function requirements of the EM and to guide through its assessment such that a decision on the EM adequacy for the purpose of LOCA safety analysis can be made. The EMDAP comprises 4 Elements and a total of 20 Steps which represent the Regulatory Position on the matter.

The mapping of the FSLOCA EM to the EMDAP was already provided in Section 1.2. The purpose of this section is to summarize main conclusions relative to compliance with regulatory guide RG 1.203 and aspect of RG 1.157 that are not already considered in RG 1.203.

## 32.4 REFERENCES

1. Bajorek, S. M., et al., 1998, "Code Qualification Document for Best Estimate LOCA Analysis," WCAP-12945-P-A, Appendix C (Proprietary).
2. Nissley, M. E., et al., 2005, "Realistic Large Break LOCA Evaluation Methodology Using Automated Statistical Treatment of Uncertainty Method (ASTRUM)," WCAP-16009-P-A, Revision 0, and WCAP-16009-NP-A, Revision 0 (Non-Proprietary).
3. NRC, 1989, "Best-Estimate Calculations of Emergency Core Cooling System Performance," Regulatory Guide 1.157.
4. NRC, 2005, "Transient and Accident Analysis Methods," Regulatory Guide 1.203.
5. Roe, J., "NRC Information Notice 98-29: Predicted Increase in Fuel Rod Cladding Oxidation," August 3, 1998.